In the Name of God

Journal of
Information Systems & Telecommunication
Vol. 2, No. 3, July-September 2014, Serial Number 7

Acknowledgement

Table of Contents

Latent Feature Based Recommender System for Learning Materials Using Genetic Algorithm

Mojtaba Salehi*
Department of Industrial Engineering, K. N. Toosi University of Technology, Tehran, Iran
mojtaba.salehi@kntu.ac.ir

Abstract

With the explosion of learning materials available on personal learning environments (PLEs) in the recent years, it is difficult for learners to discover the most appropriate materials according to keyword searching method. Recommender systems (RSs) that are used to support activity of learners in PLE can deliver suitable material to learners. This technology suffers from the cold-start and sparsity problems. On the other hand, in most researches, less attention has been paid to latent features of products. For improving the quality of recommendations and alleviating sparsity problem, this research proposes a latent feature based recommendation approach. Since usually there isn't adequate information about the observed features of learner and material, latent features are introduced for addressing sparsity problem. First preference matrix (PM) is used to model the interests of learner based on latent features of learning materials in a multidimensional information model. Then, we use genetic algorithm (GA) as a supervised learning task whose fitness function is the mean absolute error (MAE) of the RS. GA optimizes latent features weight for each learner based on his/her historical rating. The method outperforms the previous algorithms on accuracy measures and can alleviate the sparsity problem. The main contributions are optimization of latent features weight using genetic algorithm and alleviating the sparsity problem to improve the quality of recommendation.

Keywords: Collaborative Filtering; Hybrid Recommendation; E-Learning; Learning Materials; Sparsity Problem.

1. Introduction

The information available on the internet is increasing exponentially and it is necessary to create technologies which can assist learners to discover the most valuable information to them from all available information. To help users deal with information overload and provide personalized recommendations, recommender systems have become an important research area since the first paper on collaborative filtering in the mid-1990s [1]. The task of delivering personalized e-learning material is often framed in terms of a recommendation task in which a system recommends items to an active learner [2]. Several educational recommender systems have been proposed in the literature which most of them focus on recommending suitable materials or learning activities [3].

In recent years, recommender system is being deployed in more and more e-commerce entities to best express and accommodate customer's interests. According to their strategies, recommender systems can be divided into three major categories: content-based, collaborative, and hybrid recommendation [1].

Majority of researches have used collaborative filtering as a recommendation strategy in recommender systems. The main idea of collaborative filtering is grouping like-minded users together. These systems which are also called clique-based systems, assume users who had similar choices before will make the same selection in the future. Initial hints of relating collaborative filtering to education have appeared in early

relevant papers [4], but this strategy has been developed by other researchers [5-10]. Soonthornphisaj et al. [11] used collaborative filtering for material recommendation. First, the weights between the target learner and all the other learners are calculated by Pearson correlation. Then, n learners with the highest similarity to the active learner are selected as the neighborhoods. Finally, using the weight combination obtained from the neighborhood, the rating prediction is calculated. Bobadilla et al. [7] incorporated the learners score (obtained from a test) in the calculations by a new equation in collaborative filtering for item (material) prediction. Their experiment showed that the method obtained high item-prediction accuracy. Some of the (or some researchers) researchers used hybrid approaches for material recommendation. Liang et al. [12] implemented the combination of content-based filtering and collaborative filtering to make personalized recommendations for a courseware selection module. At first, a learner u enters some keywords on the portal of courseware management system. Then, the courseware recommendation module finds the k courseware with the same or similar keywords that others within the same learner interest group as learner u, choose. A relevance degree will be calculated for each k courseware by multiplying the degree of trust between learner u and other learners and evaluation of courseware by learner u. Finally the top five recommended courseware is outputted according to the recommendation degree. Their experiment revealed that the algorithm

which they have used can reflect learners' preferences with high efficiency.

While the collaborative filtering algorithms try to address the information overload and personalization problem, with growing number of users and items tremendously, these algorithms will suffer from serious sparsity problems [13]. In addition, most traditional recommendation algorithms have been developed for e-commerce applications which cannot cover some necessary requirements of e-learning environments. One of these drawbacks is that most traditional algorithms only consider user's rating information and cannot take the contextual information of user and item such as their features into account. These algorithms assume that there are sufficient historical data for measuring similarity between items or users. However, most of the time this assumption is not held in e-learning environments, where we do not have adequate information about learners and also new e-learning materials are added to the system every day. However, by considering leaner's features and learning materials for the recommendation process, we can get better recommendations in learning environment. Therefore, it is necessary to consider features of materials and learners to improve the quality and accuracy of recommendations in learning environment. In our previous research, we introduced an adaptive hybrid recommender framework that considers features of materials and learners and also learners' dynamic interests in the unified model [14]. We used learner preference matrix that can model leaners' interest based on attributes of materials using historical rating of accessed materials by learners. In addition, a new adaptive strategy was used to model dynamic preference of learners. Unfortunately, in most cases we cannot find appropriate features and collect the corresponding data because some data are involved people's privacy and some features could not be described and coded formally. It leads towards low accuracy of prediction based only on the limited observed features [15]. Therefore, in this research, latent features that are extracted by factorization technique and are optimized by genetic algorithm using historical rating of users to alleviate sparsity problem, are introduced. Therefore, in the previous approach we had used observed features of learner and material but in this approach, we used latent feature of learner and material by matrix factorization technique.

An appropriate recommendation technique can be chosen according to pedagogical reasons. These pedagogical reasons are derived from specific demands of lifelong learning [16]. Therefore, some recommendation techniques are more suitable for specific demands of lifelong learning than others. One way to implement pedagogical decisions into a recommender system is to use a variety of recommendation techniques in a recommendation strategy. Therefore, this research combines results of feature-based techniques with traditional recommendation techniques. such new method employs the history rating data to get the optimized latent features

weight for learners and materials using genetic algorithm and then uses these weight to generate recommendation.

The rest of the paper is organized as follows, at first the concept of latent features is described in section 2. In section 3, Methodology of research is described step by step. The empirical evaluations of the proposed approach are showed in section 4 and conclusion and review of the approach are presented in Section 5.

2. Latent Features

Collaborative filtering is the most successful technology for building recommender systems and is extensively used in many commercial recommender systems. this algorithms assumes that there are sufficient historical data for measuring similarity between items or users. However, this assumption is not held in various application domains such as e-learning environments where new learning materials are introduced every day and also adequate information about learners is not accessible. To address this drawback especially in e-learning environment, we introduce latent features of user and item that can be discovered by genetic algorithm and incorporated in the recommendation process to improve recommendation results and alleviate the sparsity problem.

Let U be the set of all users and let I be the set of all possible items. U_i denotes user i, and I_j denotes item j. Both user and item have their features, assuming the number of user's features is p and the number of features for items is q, features vectors define the user and item as: $U_i = (w_{i1}, w_{i2}, \ldots, w_{ip})$, $I_j = (e_{j1}, e_{j2}, \ldots, e_{jg})$. These features describe users and items in two high-dimensional spaces: Item space I and User space U. Collaborative filtering uses the rating matrix which is the result of interaction between two high-dimensional spaces in order to find the relationships between them. According to collaborative filtering assumption, the user's historical ratings are the results of the interaction between features of the user and items, thus the hidden (unknown) ratings should also depend on the features of user and items too. Therefore, by discovering these features and also establishing the relationship between the ratings and these features, we can predict the rating of unrated items.

Interaction between users and items makes a rating matrix. Each cell can be illustrated as a triple set $H = \{(U_i, I_j, r_i^j)\}$ which represents user's historical preferences, where r_i^j is a user preference and it usually is represented by a rating, and can be obtained explicitly by the user or implicitly by some measures such as the frequency of user accesses to the corresponding item.

Since ratings depend on the characteristics of users and items, the rating prediction function could be denoted as $= (M, U_i, I_j)$, M is a prediction model which is learned from the historical rating data H; U_i and I_j are features of the user i and the item j, respectively. Because the selection of suitable features for user and item in a CF

problem is almost an impossible mission, which needs a lot of prior expert knowledge in the art fields rather than technology, unfortunately, in most cases we cannot apply the mentioned method directly. Even if the feature set is chosen, it is approximately impossible to collect the corresponding data because some data are privacy information of people or some features could not be coded formally. It leads towards low accuracy of prediction based only on the limited observed features [15].

However, we can use the historical rating data in a user-item matrix for discovering some valuable features of user and item that are called reflected characteristics of latent features of items and users. The predication models built based on the observed features plus latent features should relatively have higher prediction accuracy.

On the other hand, we can assume that users are grouped by their interests e.g., users in a group will prefer some kind of items and also item are grouped by the rating mode e.g., items in a group will have similar rating values to some kind of users. Then, to explain our approach we assume that the probabilities which belong to user groups could be seen as latent features for users, and the probabilities which belong to item groups could also be seen as a latent feature for items. Therefore, the main problem will be selecting suitable methods to find the probability which belongs to a user or an item in one of these groups. In this research, we proposed a genetic algorithm based method that can optimize this probability using the historical rating. in fact, each probability indicates value of one dimension in the latent features space of users or items [15].

Let U^L; I^L denote latent feature space for users and items, respectively; let the vectors $U_i^L = (w_{i1}^L, w_{i2}^L, ..., w_{ik}^L)$ and $I_j^L = (e_{j1}^L, e_{j2}^L, ..., e_{jk}^L)$ represent user and item latent attributes, respectively. The prediction function could be denoted as $\varphi' = (M, U_i, I_j, U_i^L, I_j^L)$ and the historical rating data could be converted to $H' = \{(U_i, I_j, U_i^L, I_j^L, r_i^j)\}$. This research uses Nearest Neighborhood as prediction model and also uses Genetic Algorithm to discover latent features.

Genetic algorithm is used because with tremendously growing number of learners and materials for learning environments, recommendation algorithms will suffer serious scalability problems. This happens because computational materials are going beyond practical or acceptable levels rapidly. In the features space, different people may place different emphases on the interrelated features. The goal of GA is to find the relationship between the overall rating and the underlying features ratings for each learner. More specifically, given the ratings data of a learner, GA computes his/her preference model in terms of feature weights.

3. Methodology

As mentioned before, information acquisition is a challenging problem in many real-world applications since collecting information about features of users and items is often very expensive or even not possible at all.

Therefore to predict rating of users, we use latent features instead of observed features. Latent factor models which aim at mapping users and items to a common latent space by representing them as vectors in that space, were used to find latent features of users and items. dimensions of this space are called the factors. Here we should mention that we usually do not know the exact meaning of these factors and we are just interested in the correlation between the vectors in that space. Matrix factorization technique belongs to the family of latent factor models. We thoroughly describe this technique in the reminder of this section in order to describe the scientific base of our approach.

3.1 Matrix factorization technique

We presented a hybrid model in [17] that uses a preference matrix (PM) which can model the interests of a learner based on explicit attributes of learning materials in a multi-dimensional information model. In that research, fitness function used rating of users directly. to improve recommendation accuracy in this paper, we use matrix factorization to approximate a rating matrix $R \in S^{|U| \times |I|}$ which is the product of two smaller matrices U^L and I^L, i.e.

$$R \approx U^L.(I^L)^T \tag{1}$$

Where $U^L \in S^{|U| \times |K|}$ is a matrix where each row u is a vector containing K latent factors describing the user u, and $I^L \in S^{|I| \times |K|}$ is a matrix where each row i is a vector containing K latent factors describing the item i.

Let w_{iK}^L and e_{jK}^L be the elements of U_i^L and I_j^L in the vectors of U^L and I^L, respectively. The rating $r_x^{x'}$ given by a learner x to a material x' is predicted by Eq. (2):

$$p_x^{x'} = \sum_{k=1}^{K} w_{xk}^L.e_{x'k}^L = U_x^L.I_{x'}^L \tag{2}$$

The main issue of this technique is to find optimal values of the parameters U^L and I^L by a criterion such as Root Mean Squared Error (RMSE), which is determined by Eq. (3):

$$RMSE = \sqrt{\frac{\sum_{(x,x') \in D^{test}} (p_x^{x'} - r_x^{x'})^2}{|D^{test}|}} \tag{3}$$

Where D^{test} denotes the test data.

3.2 Optimization of latent features weight

In order to find optimal weight of the latent features of each user and item, $U_i^L = (w_{i1}^L, w_{i2}^L, ..., w_{ik}^L)$, $I_j^L = (e_{j1}^L, e_{j2}^L, ..., e_{jk}^L)$, we use genetic algorithms as a supervised learning task [18] whose fitness function is the Mean Absolute Error MAE of the RS. In this way (doing so), the population of our genetic algorithm becomes the set of different vectors of features weight. GA codes each possible latent features weight or solution candidate as a string, called chromosome. Each solution candidate is called individual, and the set of individual is called population. The population evolutes and a selection strategy are applied to choose better solution. While running our genetic algorithm, the successive population

generations tend to improve the MAE in the RS. Our genetic algorithm stops generating populations when MAE in the RS for a vector of features weight is lower than our threshold.

As usual, we use only a part of the whole rating data (training rating) in order to obtain optimal latent features weight. After obtaining the weights, we carry out our experiments to evaluate the feature weights using the test rating only.

3.2.1 Coding strategy

As usual, individuals of populations are represented in binary form as strings of 0s and 1s. Chromosome scheme which has been shown in the Fig. 1 represents the latent features weights for learners and materials where the N first rows indicate latent features weights for N learners or $U^L = (U_1^L, U_2^L, ..., U_N^L)$. The remaining rows indicate latent features weights for M learning materials or $I^L = (I_1^L, I_2^L, ..., I_M^L)$. Each component, w_{ik}^L or e_{jk}^L, in the latent features weight vectors, $U_i^L = (w_{i1}^L, w_{i2}^L, ..., w_{ik}^L)$ or $I_j^L = (e_{j1}^L, e_{j2}^L, ..., e_{jk}^L)$, will be represented by 10 bits.

The value of latent features weight is continuous and also between 0 to 1. in order to express these values with 1/1000th precision, because $512 = 2^9 < 1000 < 2^{10} = 1024$, 10 binary bits were used. Therefore, the number of columns in a chromosome will be $K \times 10$. by applying Eq. (4), These 10-bit binary numbers are transformed into decimal floating numbers, ranging from 0 to 1

$$x' = \frac{x}{2^{10} - 1} = \frac{x}{1023} \qquad (4)$$

Where x is the decimal number of each latent feature weight binary code. For example, the binary code for the weight of the 1st feature of *user 1* in Fig. 1 is $(1110000100)_2$. The decimal value is $(900)_2$ and it is interpreted as $x' = \frac{900}{2^{10}-1} = 0.8797653 \approx 0.880$.
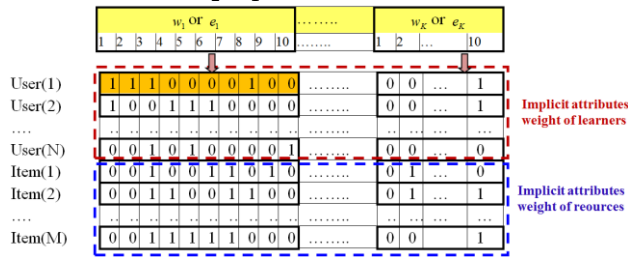
Fig. 1. Representation of latent features weight vectors in a chromosome

GA begins the process with a random population of chromosomes. Each chromosome is assigned alternately and tested by the fitness function. The fitness function measures the prediction accuracy of the rating using weights as defined in the current chromosome.

3.2.2 Fitness function

Two latent features weight matrixes, I^L and U^L which indicate latent features weight vectors for N learners and M materials respectively become the optimization targets. In our proposed genetic algorithm, the fitness function

will be the MAE of the RS (indeed we only use the training rating since we are trying to find two optimal latent features weight matrixes) for particular matrixes, I^L and U^L.

The MAE is obtained by comparing the real ratings with the predicted ratings made according to the matrixes. In order to calculate the MAE of the RS for particular matrixes I^L and U^L, which have been generated in one of itterations of GA, we need to follow the next steps:

Obtaining the set of H neighbors of user x, H_x (the H most similar users to a given user x) and also the set of H neighbors of item x', $H_{x'}$ through latent features weight matrixes, U^L and I^L using Eq. (5) and Eq. (6):

$$sim(u_x, u_y) = \frac{\sum_{i=1}^{K} w_{xi}^L . w_{yi}^L}{\sqrt{\sum_{i=1}^{K}(w_{xi}^L)^2} . \sqrt{\sum_{i=1}^{K}(w_{yi}^L)^2}} \qquad (5)$$

$$sim(i_{x'}, i_{y'}) = \frac{\sum_{i=1}^{K} e_{x'i}^L . e_{y'i}^L}{\sqrt{\sum_{i=1}^{K}(e_{x'i}^L)^2} . \sqrt{\sum_{i=1}^{K}(e_{y'i}^L)^2}} \qquad (6)$$

Predicting the rate of item x' by user x, $P_x^{x'}$ is obtained through the Deviation From Mean (DFM) as an aggregation approach. First, the rate is predicted according to user-based similarity (Eq. (7)), $sim(u_x, u_y)$, and item-based similarity (Eq. (8)), $sim(i_x, i_y)$, separately and then results of both methods are unified by linear combination (Eq. (9)):

$$p_x^{x'}(u) = \bar{r}_x + \frac{\sum_{y \in H_x} sim(u_x, u_y) \times (r_y^{x'} - \bar{r}_y)}{\sum_{y \in H_x} sim(u_x, u_y)} \qquad (7)$$

Where $P_x^{x'}(u)$ is the predicted rate of item x' by user x according to user-based similarity and $\bar{r}_x$ is the average of ratings made by the user x.

$$p_x^{x'}(i) = \overline{r^{x'}} + \frac{\sum_{y' \in H_{x'}} sim(i_{x'}, i_{y'}) \times (r_x^{y'} - \overline{r^{y'}})}{\sum_{y' \in H_{x'}} sim(i_{x'}, i_{y'})} \qquad (8)$$

Where $P_x^{x'}(i)$ is the predicted rate of item x' by user x according to item-based similarity and $\overline{r^{x'}}$ is the rating average of item x' by the users.

$$p_x^{x'} = \lambda . p_x^{x'}(u) + (1-\lambda) . p_x^{x'}(i) \qquad (9)$$

Where $P_x^{x'}$ is the predicted rate of item x' by user x and λ is the weight parameter of the unifying process.

Once every possible prediction is calculated by the unified method of item-based and user-based similarity, we obtain the MAE of the RS as in Eq. (10):

$$fitness(U^L, I^L) = MAE = \frac{1}{\#N} \sum_{x=1}^{N} \frac{\sum_{x'=1}^{M_i} |p_x^{x'} - r_x^{x'}|}{\#M_i} \qquad (10)$$

Where $r_x^{x'}$ is the real rating of item x' by user x. When running the genetic algorithm, $\#N$ and $\#M_i$ represent the number of users and the number of training items rated by the user i respectively. It must be noted that since we only

use the training rating in the learning stage of model, some of rated items by each user are selected as the training set and the remaining items are considered as the test set. When $fitness(U^L, I^L)$ is lower, the rating prediction accuracy would be higher.

3.2.3 Genetic operators

common operators are used in our genetic algorithm: selection, crossover (recombination) and mutation. We have not used other possible operators like migration, regrouping or colonization-extinction because, we have obtained satisfactory results using these three classical operators. features of our operators are as follows.

Selection: fitness proportional selection is used for selection so that the selection probability of an individual depends on its fitness level. The selection probability of each string is calculated by Eq. (11):

$$p_c(U^L, I^L) = 1 - \frac{f_c(U^L, I^L)}{\sum_{C=1}^{PS} f_C(U^L, I^L)} \tag{11}$$

Where $f_c(U^L, I^L)$ denotes the value of fitness function for chromosome c, PS is the number of individuals in the population or population size and $P_c(U^L, I^L)$ denotes the selection probability of chromosome c. Since the sum of fitness in a population is constant, an individual with lower fitness (rating prediction accuracy) has larger probability to be chosen.

Crossover: One-point crossover is used to produce offspring. The crossover probability is set to 0.9. This operator is implemented for each row of chromosome as presented in Fig. 1 (each latent feature weight) separately.

Mutation: A single point mutation technique is used in order to introduce diversity. The mutation probability is set to 0.1.

3.3 Recommendation

After training the model, we use the optimized latent features weights to generate recommendations. The top-N materials with largest $P_x^{x'}$ are regarded as the top-N materials recommendations for learner x. Therefore, equation (9) gives us the recommendation score in the proposed latent-feature based method. Since similarity in this method is based on features of items and users, other than depending only on ratings of user, we hope this method alleviates sparsity problem.

4. Implication

Experiments are carried out for the evaluation of the proposed approach. In this section, we introduce the performance metrics and analyze the experiment results to evaluate the effectiveness of our proposed recommendation approach.

4.1 Experiment environment and data set

Learning records of a real-world dataset are applied in our experiments. The learning records dataset origins from the usage data of the course management system, Moodle[1]. Moodle is a free source e-learning software platform, also known as a Course Management System designed using pedagogical principles, to help educators by creating effective online learning communities. Moodle stores detailed records of students' activities and the educator can access summarized reports about these activities according to the categories specified by the Moodle system. The summery of dataset is presented in Table 1. The used dataset contains 40445 lending records from 1980 learners on 2931 books where each record contains timestamp and rating information (as the ratio of certain lending time segment to maximum lending time segment). In order to increase the number of records in the test set as much as possible and to eliminate the effect of accidental factors, the top 60% access records of each learner in the ordered dataset are used as the training set and the remnant 40% access records are used as the test set.

Table 1. The characteristics of the dataset used in the experiments

Number of users	Number of items	Number of transactions	Density
1980	2931	40445	0.698%

There are four approaches for evaluation of recommender systems including: a real environment, an evaluation environment, the logs of the system and a user simulator. By using an evaluation environment, we let a set of users to interact with the system over a period of time. In this approach, usually, the results are not reliable enough because the users often know the purpose of the evaluation. A few systems use simulated users to evaluate their performance. This approach can enable large-scale experiments to be implemented quickly repeatedly and perfectly controlled. However, the main drawback of this system is that it cannot simulate the real behavior of a user. Users are too complicated to predict and also their feelings, their emotions, and therefore, their actions change dynamically. Analysis of the log files of real users obtained in a real or evaluation environment is also a common technique for evaluation of recommender systems. In this method, the cross-validation technique is often used for evaluation of recommender system. Results obtained in a real environment with real users are the best way to evaluate a recommender system. But the main problem of the real and the evaluation environments is repetition of the experiments. Therefore, in this research we use log files of real environment that enables us to repeat the experiments and implement the cross-validation technique.

4.2 Evaluation metrics

In this paper, the evaluation metrics of recommendation algorithm are divided into two categories:

Classification Accuracy Metrics: these metrics assume the prediction process as a binary operation, either items are predicted (good) or not (bad). The precision and

---

[1] Modular Object-Oriented Dynamic Learning Environment

the recall are the most popular metrics in this category. They have been used by various researchers [19,20]. When referring to recommender systems, the recall and precision can be defined by Eq. (12) and Eq. (13):

$$Recall = \frac{tp}{tp + fp} \tag{12}$$

$$Pr\,ecision = \frac{tp}{tp + fn} \tag{13}$$

Where tp stands for true positive, fp stands for false positive, and fn stands for false negative. The threshold for determining true positive is set to 3.5 meaning that if an item is rated 3.5 or higher, it is considered to be accepted by the user.

Since increasing the size of the recommendation set leads to an increase in the recall but at the same time a decrease in the precision, we can use F_1 measure [21,22] that is a well-known combination metric with the following Eq. (14):

$$F_1 = 2.\frac{Pr\,ecision.Recall}{Pr\,ecision + Recall} \tag{14}$$

Predictive Accuracy Metrics: these metrics measure how close predicted ratings of the recommender system are to the true user ratings. We use the MAE, a statistical accuracy metric [23] in this category which is computed with the following Eq. (15):

$$MAE = \frac{\sum_{x=1}^{x=N} \left| r_x^i - p_x^i \right|}{|N|} \tag{15}$$

Where P_x^i is the predicted rating for material i by learner x, r_x^i is real rating for material i by learner x, and N is the total number of learners.

4.3 Parameters setting

In the proposed feature-based recommendation method, we must run a set of experiments for adjusting parameters. The main parameters in GA comprise population size (PS), number of generations (NG), crossover probability (CP) and mutation probability (MP).

Since the results of genetic algorithms have stochastic nature, we have developed the experiments in a way that each set of parameters has been run for 50 times to reach a reliable conclusion. In this stage, we consider number of recommendation, RN=20, number of latent features, K=8, minimum number of rating required for test learners, M=100 and the number of learner, N=800.

Population size (PS): To be able to compare the effect of changing the initial size of the population on genetic algorithm efficiency and results, all of the parameters are fixed except the population. crossover probability would be set to (CP)=0.9 and mutation probability to (MP)=0.1. Generation numbers are chosen from 0 (initial generated data without running the algorithm) to 800 generations with the step size of 50 generations. The algorithm has been run 50 times for each population size and each generation value. Fig. 2 shows the results. This Figure compares only the average of best found solutions (in population).
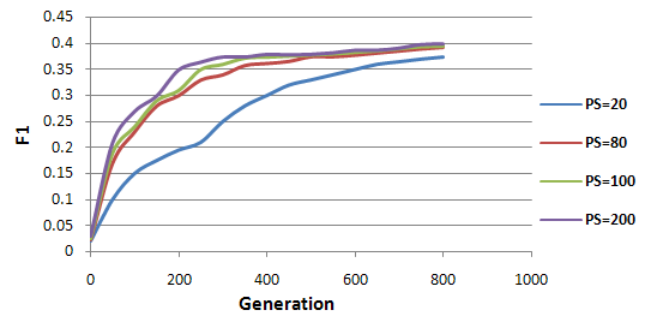
Fig. 2. Performance of the proposed method with respect of population Size

Results show that higher population size provides a high diversity and as a result, converging to better solutions happens sooner than smaller population sizes. On the other hand, higher population size needs more time for the algorithm to run. In this experiments, the population size of 20 lost diversity before reaching an acceptable solution. However, a population size of 200 does not provide much benefit over the population size of 100. Therefore, we will use a population size of 100 in our experiments.

Mutation probability (MP) and crossover probability of (CP): The optimal values of crossover and mutation probabilities are problem specifics that often are obtained by trial and error. Table 2 indicates the amount of F_1 for different value of MP and CP while NG=500, PS=100 and other parameters are similar to the previous experiment. According to experiment, CP=0.9 and MP=0.1 lead to good result for our problems.

Table 2. Performance of the proposed method with respect of MP and CP

MP	CP	F1
0	1	0.362
0.05	0.95	0.375
0.1	**.9**	**0.381**
0.15	.085	0.379
0.2	0.8	0.371
0.3	0.7	0.368
0.4	0.6	0.301

A Final parameter that must be adjusted is number of latent features. Fig. 3 shows the results obtained for the feature based approach with different number of latent features while NG=500, PS=100, CP=0.9 and MP=0.1. It can be seen that the performance improves steadily with increasing the number of features. To have high efficiency in the computation, we set K=8.
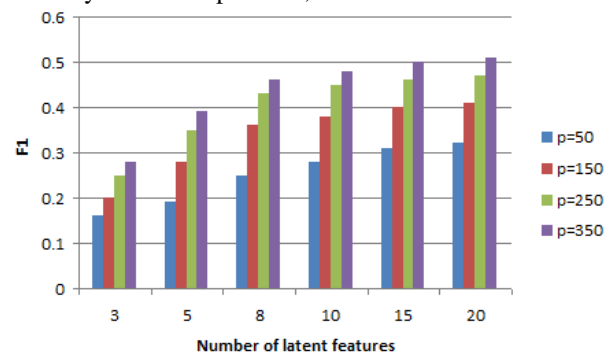
Fig. 3. Performance of the proposed method with respect of K

4.4 Comparative studies

4.4.1 Comparison of proposed method with Other algorithms

Table 3 presents a comparative study on recommendation quality between the proposed method and optimal state of five different algorithms in order to probabilistic recommendations: user-based CF using Pearson correlation with default voting (DV) [24], item-based CF using adjusted cosine similarity [25], two hybrid recommendation algorithms used by Pazanni [26] and Melville et al. [27], the personality diagnosis algorithm [28]. Comparisons were produced for N=800 learners with the average number of ratings equal to 100, M=80, CP=0.9, MP=0.1, NG=400 and PS=100.

As can be seen, linear combination of the proposed method (feature based method) with item based recommendation method generates better recommendations than other algorithms. Unlike individual feature based or item based method, the weighted method applies the results which are generated from two methods together and generates more qualified recommendation results.

Table 3. A comparison of prediction accuracy of various methods

System	Recall	Precision	F1
Linear combination of FBR with item based	0.377	0.623	0.470
FBR	0.373	0.583	0.447
User-based with DV	0.354	0.561	0.434
Item-based	0.321	0.53	0.400
Pazzani [24]	0.3622	0.601	0.452
Melville et al. [25]	0.373	0.619	0.465
Personality diagnosis	0.353	0.602	0.445

4.5 Performance evaluation for different sparsity levels

To illustrate that the proposed method can alleviate the sparsity problem, we increased the sparsity level of the training set by dropping some randomly selected entries. However, we kept the test set unchanged for each sparse training set. The performance of the proposed method algorithm was compared with other algorithms. Fig. 4 shows that the performance does not degrade rapidly in the case of proposed algorithm. It is because; features of an item can still be used for finding similar

items. Furthermore, this algorithm enriches item and user profiles with combining latent features in recommendation process.
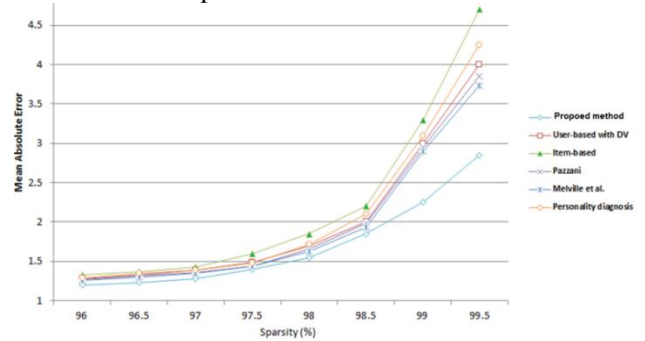
Fig. 4. Performance of algorithms under different sparsity levels

5. Conclusions

One of the most important applications of recommendation systems in the learning environment is personalization and recommendation of e-learning materials. However, since the repository of learning materials is very massive and these materials have several features, when applying the existing recommendation algorithms, there are some problems such as sparsity. To address sparsity problem and have better recommendations for learners, a hybrid recommender system is proposed to recommend learning items in users' learning processes. The proposed method discovers and optimizes latent features by GA and generates recommendation using collaborative filtering. The experiment results show that the proposed approach performs better than traditional approaches in the terms of accuracy measures measurements and also can alleviate sparsity problem. The main contribution of this paper is improving the quality of recommendations and addressing sparsity problem by considering latent features. For future researches, we can combine latent features with observed features to make a hybrid recommendation approach. In addition, we can make a comparison between meta-heuristic approaches for latent features optimization.

References

[1] G. Adomavicius, and A. Tuzhilin, "Toward the Next Generation of Recommender Systems: A Survey of the State-of-the-Art and Possible Extensions", IEEE Transactions on Knowledge and Data Engineering, Vol. 17, No. 6, pp. 734-749, 2005.

[2] B. Mobasher, Data Mining for Personalization. In: Brusilovsky, P., Kobsa, A., Nejdl, W. (eds.) The Adaptive Web: Methods and Strategies of Web Personalization, pp. 1–46, 2007.

[3] N. Manouselis, H. Drachsler, R. Vuorikari, H. Hummel, and R. Koper, Recommender systems in technology enhanced learning, Recommender Systems Handbook, pp. 387–415, 2011.

[4] L. Terveen, W. Hill, B. Amento, D. McDonald and J. Creter, "PHOAKS: a system for sharing recommendations" Communications of the ACM 40, pp. 59–62, 1997.

[5] T. Kerkiri, A. Manitsaris and A. Mavridou, "Reputation Metadata for Recommending Personalized learning

resources," Second International Workshop on Semantic Media Adaptation and Personalization, 2007, pp. 110–115.

[6] D. Lemire, H. Boley, S. McGrath and M. Ball, "Collaborative Filtering and Inference Rules for Context-Aware Learning Object Recommendation," International Journal of Interactive Technology and Smart Education, Vol. 2, No. 3, pp. 1–11, 2005

[7] J. Bobadilla, F. Serradilla, and A. Hernando, "Collaborative filtering adapted to recommender systems of e-learning." Artificial Intelligence (AI) in Blended Learning, Vol. 22, No 4, pp. 261–265, 2009.

[8] O.C. Santos, and J.G. Boticario, Recommendation strategies for promoting eLearning performance factors for all. In The 6th workshop on intelligent techniques for web personalization & recommender systems, 2008, pp. 89–98.

[9] N. Soonthornphisaj, E. Rojsattarat, and S. Yim-ngam, Smart E-learning using recommender system. Proceedings of the 2006 international conference on Intelligent computing, 2006, pp. 518–523.

[10] D. Aijuan, and W. Baoying, Domain-based recommendation and retrieval of relevant resources in e-learning. In IEEE international workshop on semantic computing and applications, 2008, pp. 103–108.

[11] N. Soonthornphisaj, E. Rojsattarat, and S. Yim-ngam, "Smart E-learning using recommender system", In Computational intelligence, Vol. 4114, pp. 518–523, 2006.

[12] G. Liang, K. Weining and L. Junzhou, "Courseware recommendation in e-learning system", In Advances in web based learning, pp. 10–24, 2006.

[13] X. Su and M. Khoshgoftaar, A Survey of Collaborative Filtering Techniques, Hindawi Publishing Corporation Advances in Artificial Intelligence, Volume 2009, Article No. 4, 19 pages, 2009.

[14] M. Salehi, I. Nakhai Kamalabadi M. B. Gaznavi Goushchi, A New Adaptive Hybrid Recommender Framework for Learning Material Recommendation, Vol. 5, No. 3, pp. 25-33, 2013.

[15] J. Zhong and X. Li, Unified collaborative filtering model based on combination of latent features, Expert Systems with Applications, Vol. 37, pp. 5666–5672, 2010.

[16] H. Drachsler H. G. K. Hummel, and R. Koper, "Personal recommender systems for learners in lifelong learning: requirements, techniques and model", International Journal of Learning Technology, Vol. 3, No. 4, pp. 404-423, 2008.

[17] M. Salehi, M. Pourzaferani, S. A. Razavi, Hybrid attribute-based recommender system for learning material using genetic algorithm and a multidimensional information model, Egyptian Informatics Journal, Vol.1, No. 14, pp. 67-78, 2013.

[18] D.E. Goldberg, Genetic algorithms in search, optomization, and machine learning. Reading, MA: addison-wesley, 1989.

[19] M. Pazzani, D. Billsus, Content-based recommendation systems. The adaptive web, pp. 325–341, 2007.

[20] J.L. Herlocker, J.A. Konstan, L.G. Terveen, J. Riedl, "Evaluating Collaborative Filtering Recommender Systems", ACM Transactions on Information Systems 22(1) (2004) 5-53.

[21] Y.Y. Shih and D.R. Liu, "Product recommendation approaches: Collaborative filtering via customer lifetime value and customer demands", Expert Systems with Applications, Vol. 35, No. (1–2) pp. 350–360, 2008.

[22] Y.H. Cho, J.K. Kim, "Application of Web usage mining and product taxonomy to collaborative recommendations in e-commerce", Expert Systems with Applications, Vol. 26, pp. 233–246, 2004.

[23] P. Symeonidis, A. Nanopoulos, A.N. Papadopoulos, Y. Manolopoulos, Collaborative recommender systems: Combining effectiveness and efficiency. Expert Systems with Applications, 34(4) (2008) 2996–3013.

[24] J.S. Breese, D. Heckerman and C. Kadie, Empirical analysis of predictive algorithms for collaborative filtering, UAI'98 Proceedings of the Fourteenth conference on Uncertainty in artificial intelligence, pp. 43–52, 1998.

[25] B. Sarwar, G. Karypis, J. Konstan and J. Reidl, "Item based collaborative filtering recommendation algorithms", in Proceedings of the 10th international conference on World Wide Web., pp. 285–295, 2001.

[26] M.J. Pazzani, "A framework for collaborative, content-based and demographic filtering", Artificial Intelligence Review, Vol. 13, No. 5–6, pp. 393–408, 1999.

[27] P. Melville, R.J. Mooney and R. Nagarajan, "Content boosted collaborative filtering for improved recommendations". in Eighteenth National Conference on Artificial Intelligence, pp. 187–192, 2002.

[28] D. Pennock, E. Horvitz, S. Lawrence and C. Giles, "Collaborative filtering by personality diagnosis: A hybrid memory and model-based approach", in Proceedings of the 16th Conference on Uncertainty in Artificial Intelligence, pp. 473–480, 2000.

Mojtaba Salehi received his B.Sc. degree from Shahid Bahonar University in 2004, M.Sc. degree from Tehran University in 2006 and Ph.D. degree from Tarbiat Modares University in 2013. During 2012, he was a researcher in Eindhoven University of technology in Netherlands, mathematics and computer science department. He was selected as the top student in Iran at 2012. He has about 20 journal papers. He is currently working as an Assistant Professor of K.N. Toosi University of Technology (KNUT). His research areas of interest include applied operation research, soft computing, data mining and recommender systems.

High I/Q Imbalance Receiver Compensation and Decision Directed Frequency Selective Channel Estimation in an OFDM Receiver Employing Neural Network

Abolfazl Falahati*
Department of Electrical Engineering, Iran University of Science and Technology, Tehran, Iran
afalahati@iust.ac.ir
Sajjad Nasirpour
Department of Electrical Engineering, Iran University of Science and Technology, Tehran, Iran
sajjadnassirpour@elec.iust.ac.ir

Abstract

The disparity introduced between In-phase and Quadrature components in a digital communication system receiver known as I/Q imbalance is a prime objective within the employment of direct conversion architectures. It reduces the performance of channel estimation and causes to receive the data symbol with errors. This imbalance phenomenon, at its lowest still can result very serious signal distortions at the reception of an OFDM multi-carrier system. In this manuscript, an algorithm based on neural network scenario, is proposed that deploys both Long Training Symbols (LTS) as well as data symbols, to jointly estimate the channel and to compensate parameters that are damaged by I/Q imbalanced receiver. In this algorithm, we have a tradeoff between these parameters. I.e. when the minimum CG mean value is required, the minimum CG mean value could be chosen without others noticing it, but in usual case we have to take into account other parameters too, the limited values for the aimed parameters must be known. It uses the first iterations to train the system to reach the suitable value of GC without error floor. In this present article, it is assumed that the correlation between subcarriers is low and a few numbers of training and data symbols are used. The simulation results show that the proposed algorithm can compensate the high I/Q imbalance values and estimate channel frequency response more accurately compared with to date existing methods.

Keywords: I/Q Imbalance; OFDM; Zero-IF; Direct Conversion; Neural Network; Channel Estimation, Frequency Selective Channel.

1. Introduction

Fig. 1 depicts a direct conversion receiver, normally called zero-IF architecture that is usually employed over an Orthogonal Frequency Division Multiplexing (OFDM) based wireless communication system.
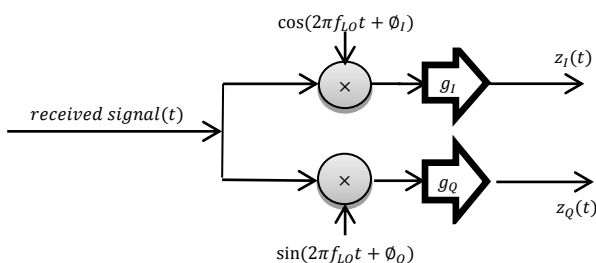
Fig.1. Generic model of an I/Q imbalance receiver

The direct conversion is a suitable approach that is deployed to decrease the complexity of an OFDM receiver. The receiver I/Q imbalance are observed by imperfect matching of the employed analog components in the In-phase (I) and the Quadrature (Q) branches which normally extinguishes the performance of the OFDM

system (Fig. 1). Hence, the estimation of such ambiguous parameters becomes an imperative necessity to digitally compensate I/Q imbalance behaviors for the design of a high performance receiver. Two sets of techniques are introduced in the previous published papers to estimate the I/Q imbalance process. The first technique is based upon the received training symbols [1-4]. Their method of deploying the received training symbols are not affected by mutual interference between the pairs of symmetric subcarriers. Indeed, within such approach, the single OFDM training symbols must be somehow modified. The second method proposed by [5] uses the uncorrelated transmitted subcarriers to provide a blind estimation. Since the adopted estimation technique is based on statistical analysis, a large number of received data symbols are required otherwise an error floor arises even at high SNRs.

In [6], Traverso *et al*. introduced an algorithm that compensated I/Q-imbalance feature of the OFDM receivers and estimated the channel frequency response jointly. Their method deployed both training symbols and pilot symbols for the OFDM receiver to reach the system strongly against the high I/Q-imbalance feature and their proposed system require the two different LTS to estimate

* Corresponding Author

imbalance parameters (K_1, K_2) at the OFDM-receiver, but by employing the neural network the receiver could compensate the imbalance parameters deploying only one LTS to train the neural network.

In this present article, it is assumed that the correlation between subcarriers is low and a few number of training and data symbols are used. The proposed system employs a neural network scheme to compensate the parameters of the high I/Q imbalance receiver with a high-order modulation and it is sensitive to I/Q imbalance characteristics. The proposed system employs uniform distribution function to estimate initial value of training phase of neural network and then using multilayer perceptron to parallel-process distribution to achieve suitable values of I/Q imbalance receiver. It deploys decision-directed scheme too, similar to the existing methods, to improve the performance of an OFDM receiver.

2. I/Q Imbalance Receiver Model of an OFDM System

Fig. 1 depicts an I/Q imbalance receiver due to a gain mismatch g and a phase mismatch $\emptyset$. The gain mismatch is produced by unequal gain in I and Q receiver branches. The phase mismatch is occurred by asynchronous oscillators that are employed in the receiver architecture. The I/Q imbalance parameters [1] can be written as:

$$K_1 = [e^{-j\emptyset_I}g_I + e^{-j\emptyset_Q}g_Q]/2 \qquad (1)$$
$$K_2 = [e^{+j\emptyset_I}g_I - e^{+j\emptyset_Q}g_Q]/2 \qquad (2)$$

where $\emptyset_I$ and g_I show the mismatch phase and gain parameters of RF in-phase branch respectively and $\emptyset_Q$ and g_Q show the mismatch phase and gain parameters of RF quadrature-phase branch. In the proposed system, the received signal [12] is given as follows:

$$R_k(n) = T_k(n)H_kK_1 + T_{-k}^*(n)H_{-k}^*K_2 = T_k(n)\alpha_k + T_{-k}^*\beta_k$$
$$\text{for } k \in \pm\left[1; \frac{N_{DFT}}{2} - 1\right] \qquad (3)$$

where $R_k(n)$ is the received signal of kth subcarrier at the nth symbol and $\alpha_k \triangleq H_kK_1$ and $\beta_k \triangleq H_{-k}^*K_2$. $T_k(n)$, N_{DFT} and H_k show the sender transmitted symbols, the Discrete Fourier Transform block size and the frequency response of transmission channel that are not damaged by imbalance receiver respectively. By using (3), the received symbols are formulated [6] as follows:

$$R = A1 \times H \times T \qquad (4)$$

Where

$$R = \begin{bmatrix} R_k(n) \\ R_{-k}^*(n) \end{bmatrix}, \ A1 = \begin{bmatrix} K_1 & K_2 \\ K_2^* & K_1^* \end{bmatrix}$$
$$H = \begin{bmatrix} H_k & 0 \\ 0 & H_{-k}^* \end{bmatrix}, \ T = \begin{bmatrix} T_k(n) \\ T_{-k}^*(n) \end{bmatrix} \qquad (5)$$

Note that, K_1^* and K_1^* are the conjugate of K_1 and K_2 respectively. In this case, the frequency offset between

local oscillators is not studied and it is assumed that its value is Negligible. Algorithms that are employed in [15], [5] can be used to cancel the effect of frequency offset in I/Q imbalance receivers.

In this section, it is explained that when sender transmits two different Long length Training Symbols (LTS), to compensate the parameters of I/Q imbalance receiver and to estimate the frequency response of transmission channel together, are not impossible objectives. By dividing the received LTS (P_{rk}) by the corresponding LTS (P_{tk}) that is transmitted by sender, the estimate value of channel C_k can be calculated. Note that the received LTS (P_{rk}) and transmitted LTS (P_{tk}), both are known at the OFDM receiver. In this case, P_{rk} and P_{tk} represent the powers of R_k and T_k respectively. By using (1), when sender transmits two LTSs that are different, two channel estimations $C_k(1)$ and $C_k(2)$ have to be available at the destination that are damaged by imbalance receiver. These channel estimations have linear relations [6] as follows:

$$C_k(1) = \frac{P_{r_k}(1)}{P_{t_k}(1)} = \alpha_k + L_k(1)\beta_k$$
$$C_k(2) = \frac{P_{r_k}(2)}{P_{t_k}(2)} = \alpha_k + L_k(2)\beta_k \qquad (6)$$

where $L_k(1) = P_{t_{-k}}^*(1)/P_{t_k}(1)$ and $L_k(2) = \frac{P_{t_{-k}}^*(2)}{P_{t_k}(2)}$ are parameters that the receiver has the knowledge of [17]. If the condition C defined by [6] is satisfied, by using the condition $K_1 + K_2^* = 1$ and known parameters α_k and β_k, the frequency response of transmission channel [17] is calculated as follows:

$$H_k = \alpha_k + \beta_{-k}^* \qquad (7)$$

By using (7) and $\alpha_k = H_kK_1$, the I/Q imbalance parameters is obtainable [6] as follows:

$$K_1 = \frac{\alpha_k}{\alpha_k + \beta_{-k}^*}, \qquad (8)$$
$$K_2 = 1 - K_1^*. \qquad (9)$$

At first, the estimation value of channel response and parameters of imbalance receiver are calculated and then by employing the matrix A_1 in (4), the transmitted data symbols are obtained.

3. OFDM Standard Employ a Single LTS

In many OFDM receivers, the LTSs are equal [6] and thus, the condition C [6] is not satisfied and previously adapted approaches are not suitable. In this part, a new algorithm is proposed to compensate the I/Q imbalance parameters by using the neural network with a single LTS as well as channel response and data symbols.

In the proposed iterative algorithm, primarily, the $\widehat{K_1}$ parameter is estimated by using the neural network and the single LTS and then the $\widehat{K_1}$ to estimate the channel frequency response and data symbols.

3.1 Algorithm with neural network

The four following steps are performed to establish the neural network algorithm:

1) Direct-decisions on data symbols: using the channel estimation C_k to estimate the sending data symbols $T_k(n)$ even in the absence of I/Q imbalance receiver.

2) Estimation of the I/Q imbalance parameters K_1 and K_2: it is known that, the best case is when the K_1 is unity and K_2 is zero. Considering neural network scenario, α_k and β_{-k}^* are as inputs to the network and K_1 is defined as network output.
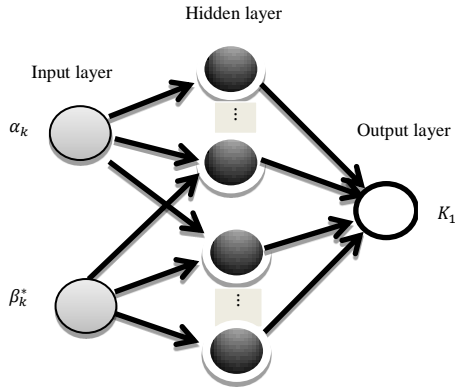

Fig.2. The neural network schematic to compensate the K_1 parameter

$$\widehat{K_1} = \frac{\widehat{\alpha_k}}{\widehat{\alpha_k} + \widehat{\beta_{-k}^*}} \qquad (10)$$

where $\widehat{K_2}$ is the imbalance parameter that is calculated by $\widehat{K_2} = 1 - \widehat{K_1^*}$.

3) Compensate the data symbols of the proposed OFDM system: By using K_1 and K_2 that are estimated in step 2 and the invert form of the matrix A_1 given in (4), the data symbols are obtained as follows:

$$\widehat{D_k}(n) = \frac{\widehat{K_1^*} R_k(n) - \widehat{K_2} R_{-k}^*(n)}{|\widehat{K_1}|^2 - |\widehat{K_2}|^2} \qquad (11)$$

4) Compensation of the channel estimation response: To estimate coefficients of channel response, the proposed algorithm employs independent LTS for each transmitted packet. To achieve this matter, in different bits and at different times the transmitted data and the received data are considered approximately independent. The estimate values $\widehat{H_k}$ resulted from $\widehat{H_k} = \widehat{\alpha_k} + \widehat{\beta_{-k}^*}$ are not good approximation for the following reasons; $\widehat{H_k}$ is severely damaged by errors that occur in step 1 since there is no averaging over the frequency range. But, because the estimation values of I/Q imbalance parameters with neural network are reliable, the I/Q imbalance compensation of the rough channel estimation C_k provides a good estimation of H_k employing step 3:

$$H_k = \frac{\widehat{K_1^*} C_k - L_k \widehat{K_2} C_{-k}^*}{|\widehat{K_1}|^2 - |\widehat{K_2}|^2}. \qquad (12)$$

After four steps are performed, (4) can be written as follows:

$$\begin{bmatrix} \widehat{D_{1k}}(n) \\ \widehat{D_{1-k}^*}(n) \end{bmatrix} = \widehat{A_1}^{-1} A_1 \begin{bmatrix} H_k & 0 \\ 0 & H_{-k}^* \end{bmatrix} \begin{bmatrix} T_k(n) \\ T_{-k}^*(n) \end{bmatrix} \qquad (13)$$

where $\widehat{A_1}$ is the estimation compensation matrix of the I/Q imbalance receiver. If the estimation compensation of the I/Q imbalance parameters is perfect, then $A_2 = \widehat{A_1}^{-1} A_1$ would be the identity matrix. Therefore, the data symbol and I/Q imbalance matrix are perfectly compensated. However, in most cases, the hard decision is erroneous, so the algorithm estimates I/Q imbalance parameters imperfectly. From $K_1 + K_2^* = 1$ and $\widehat{K_1} + \widehat{K_2^*} = 1$, it follows that after using the neural network by some hidden layers. And, using the α_k and β_{-k}^* as inputs to the network as well as K_1 is defined as network output, the value of $\widehat{K_1}$ would be compensated and $\widehat{D_{1k}}(n) = H_k T_k(n)$ can be used as the compensated data symbol at the receiver.

4. Simulation Results

In this section, the performance of the proposed algorithm is assessed in terms of compensation and the performance enhancement of the I/Q imbalance receiver and channel estimation. The data subcarriers of the system are modulated by a 64-QAM (Quadrature Amplitude Modulation). For each transmitted packet an independent channel realization of the Channel C [14], is assumed. The curves are the result of averaging over 100 received packets by I/Q imbalance receiver in the direct conversion OFDM system.

The algorithms have three parameters: the number of iterations i, the number of data symbols N and the Conversion Gain (CG) mean value. In this algorithm, we have a tradeoff between these parameters. I.e. when the minimum CG mean value is required and the other parameters are not important, the minimum CG mean value could be chosen without others noticing it, but in usual case we have to take into account other parameters too, the limited values for the aimed parameters must be known.

A good criterion to choose these parameters is minimize the number of iterations i with suitable value of the conversion gain defined as the power of the undesired complex down-conversion divided by the power of the desired complex down-conversion [12].The conversion gain of the compensated signal after the ith iteration [6] is defined by:

$$GC_{comp} = \left| \frac{\widehat{K_{2i}}}{\widehat{K_{1i}}} \right|^2 \qquad (14)$$

where $\widehat{K_{1i}}$ and $\widehat{K_{2i}}$ are the remaining I/Q imbalance parameters after using neural network in the ith iteration. This system is used under condition that the packet error rate does not exceed 10%,
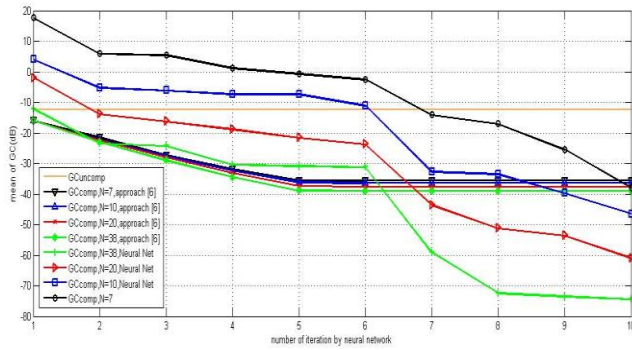
Fig.3. The conversion gain means versus the number of iterations for different values of N using the neural network

In the case that the energy per bit to noise ratio (E_b/N_0) is 25 dB, for the system without I/Q imbalance, the uncoded BER is 2×10^{-4} (Fig. 5). Hence, we have to define the optimal number of data symbols N, iterations i and the conversion gain for the compensated signal at $E_b/N_0 = 25$ dB.

4.1 System performance

The parameters that are chosen to perform I/Q imbalance conversion are $\emptyset_I = 0$, $g_I = 1$, $g_Q = 1.5$ and $\emptyset_Q = 15°$. Fig. 3 shows the mean of GC_{comp} versus the number of iterations for different values of N where $g_Q = 1.5$ and $\emptyset_Q = 15°$ with $E_b/N_0 = 25$ dB deploying neural network. The GC_{uncomp} is defined as the conversion gain of the uncompensated data symbols. Fig. 3 shows both approaches, the Traverso et al. [6] approach and the approach employed here, to decrease the GC. As Fig. 3 shows the curves for the approach where the system uses data from the fifth iteration to train the network and then uses the trained network to decrease the GC, to reach to a suitable GC without limitation. The best tradeoff between complexity and performance is also obtained for $i = 6$ and $N = 10$. Fig. 4 shows the mean of GC_{comp} versus the number of iterations for $N = 38$ and for different values of I/Q imbalance parameters. All curves show that as I/Q imbalance parameter values are increased, the absolute value of GC is decreased.
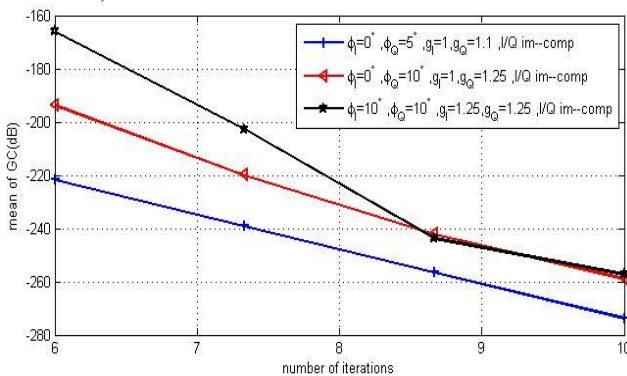
Fig.4. The conversion gain mean versus the number of iterations for different values of I/Q imbalance parameters with neural network.

Fig. 5 compares the performance of the mentioned algorithm with the performance of a system with no I/Q imbalance as well as the performance of a system with I/Q imbalance but without any compensation mechanism with the uncoded BER curves versus E_b/N_0 for $N = 64$, $\emptyset_I = 0$, $g_I = 1$, $g_Q = 1.5$ and $\emptyset_Q = 15°$.
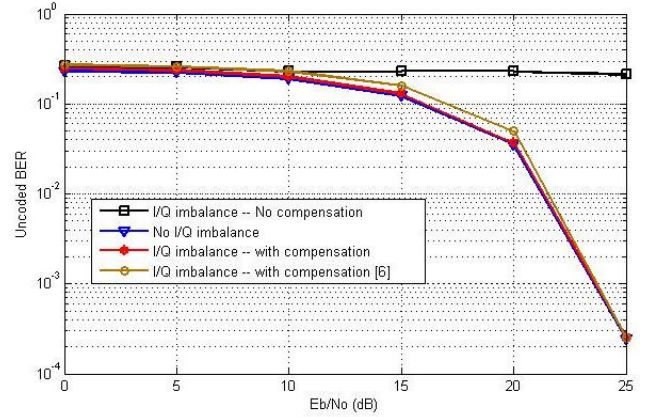
Fig.5. The uncoded BER performance for the receiver with no compensation, for the receiver using the proposed algorithm and for the receiver with no I/Q imbalance, as well as the receiver employed by [6] for comparison

As Fig. 5 shows, the BER of the proposed algorithm is very close to the BER curve of a system without I/Q imbalance even for high I/Q imbalance.

5. Conclusions

As it is known, it is impossible to match I and Q branches at the OFDM receiver in the analog domain perfectly. The I/Q imbalance affects the receiver performance. It reduces the performance of channel estimation and causes to receive the data symbol with errors. We propose an algorithm with neural network for joint channel estimation and I/Q imbalance compensation in OFDM receivers. The proposed algorithm uses the training and data received OFDM symbols in a decision-directed scheme. It provides a good improvement in the performance of I/Q imbalance receiver. It uses the first iterations to train the system to reach the suitable value of GC without error floor.

Furthermore, to employ the proposed system over a time-varying multipath channel, a memory device of about 100Mbytes which are commonly available in today's systems, is required to save few number of received data bits for such a neural network evaluations.

References

[1] J. Tubbax, A. Fort, L. bet Van der Perre, S. Dannay, M. Engels, M. Moonen and H. De Man, "Joint compensation of IQ imbalance and frequency offset in OFDM systems", IEEE Global Communications Conference (GLOBECOM 03), Dec. 2003.

[2] J.Y. Yu, M. F. Sun, T. Y. Hsu, and C.-Y. Lee, "A novel technique for I/Q imbalance and CFO compensation in OFDM systems", IEEE International Symposium on Circuits and Systems (ISCS), May 2005, pp. 6030-6033.

[3] P. Rabiei, W. Namgoong and N. Al-Dhahir, "Reduced-complexity joint baseband compensation of phase noise and I/Q imbalance for MIMO-OFDM systems", IEEE Trans. On Wireless Communications, Vol. 9, No. 11, pp.3450-3460, Nov 2010.

[4] Zh. Zhu, X. Huang and H. Leung, "Blind compensation of frequency-dependent I/Q imbalance in direct conversion OFDM receivers", IEEE Communications Letters, Vol. 17, No. 2, Feb. 2013.

[5] T. Y. Hsu, W. C. Lai and T. Y. He "Frequency-dependent I/Q imbalance compensator for 2x2 MIMO-OFDM systems", Congress on Engineering and Technology (S-CET), May 2012.

[6] S. Traverso, M. Ariaudo, I. Fijalkow, J. L. Gautier and C. Lereau, "Decision- directed channel estimation and high I/Q imbalance compensation in OFDM receivers", IEEE Trans. On Communications, Vol. 57, No. 5, May 2009.

[7] N. Moghaddam and A. Falahati, "An improved ICI reduction method in OFDM communication system in presence of phase noise", the 18th Annual IEEE international symposium on personal, indoor and mobile radio communications (PIMRC'07), Sept. 2007.

[8] R. K. McPherson, J. Schroeder, "Frequency-selective I/Q imbalance compensation for OFDM receivers using decision-feedback adaptive filtering", 46th Conf. Signals systems and computers (ASILOMAR), Nov. 2012.

[9] A. Tarighat, R. Bagheri, and A. H. Sayed, "Compensation schemes and performance analysis of IQ imbalances in OFDM receivers," IEEE Trans. Signal Processing, Vol. 53, No. 8, pp. 3257 - 3268, Aug. 2005.

[10] A. Schuchert, R. Hasholzner and P. Antoine, "A novel IQ imbalance compensation scheme for the reception of OFDM signals", IEEE Trans. Consumer Electron., Vol. 47, No. 3, pp. 313318, Aug. 2001.

[11] M. Windisch and G. Fettweis, "Preamble design for an efficient I/Q imbalance compensation in OFDM direct-conversion receivers", 10th International OFDM Workshop, Sept. 2005.

[12] M. Windisch, and G. Fettweis, "Standard-independent I/Q imbalance compensation in OFDM direct-conversion receivers", 9th International OFDM Workshop, Sept. 2004, pp. 5761.

[13] Wireless LAN Medium Access Control (MAC) and Physical Layer (PHY) Specifications: High-Speed Physical Layer in the 5 GHz Band, IEEE standard 802.11a-1999 - part 11 Std.

[14] Channel Models for HiperLAN2 in Different Indoor Scenarios, European Telecommunication Standard Institute (ETSI) Broadband Radio Access Networks (BRAN) Std., Mar. 1998. Authorized licensed.

[15] F. Yan, W.-P. Zhu, and M. O. Ahmad, "Carrier frequency offset estimation and I/Q imbalance compensation for OFDM systems," EURASIP J. Advances in Signal Processing, Vol. 2007, pp. 453–464, 2007.

[16] T. Tsuji, N. Bu, O. Fakuda, M. Kaneko, "A Recurrent Log-Linearized Gaussian Mixture Network", IEEE Trans. Neural Networks, Vol. 14, No. 2, pp. 304-316, March 2003.

[17] F. Rahman, M.H.R., R. Devanathen, Z. Kuanyi, "Neural Network Approach For Linearizing Control Of Nonlinear Process Plants", IEEE Trans. Industrial Electronics, Vol. 47, No. 2, pp. 470-477, April 2000.

[18] Asad A. Abidi, "Direct-conversion radio transceivers for digital communications", IEEE J. Solid-State Circuits, Vol. 30, No. 12, pp. 13991410, Dec. 1995.

[19] Behzad Razavi, "Design considerations for direct-conversion receivers", IEEE Trans. Circuits Syst. II, Vol. 44, No. 6, pp. 428435, June 1997.

[20] F. E. Churchill, G. W. Ogar and B. J. Thompson, "The correction of I and Q errors in a coherent processor", IEEE Trans. Aero sp. Electron. Syst., Vol. 17, pp. 131 137, Jan. 1981.

[21] M. Valkama, M. Renfors, and V. Koivunen, "Advanced methods for I/Q imbalance compensation in communication receivers", IEEE Trans. Signal Processing, Vol. 49, Oct. 2001.

Abolfazl Falahati is an Associate Professor at the University of Science and Technology in Tehran, he is graduated from UK and spent 4 years doing his post-doctorate in RAL Lab(Oxford-UK), his research interests are in the areas of digital communication systems mainly in Coding and Cryptography.

Sajjad Nasirpour, bachelor's degree from shiraz university in communication engineering course at 2011, master degree from iran university of science and technology in secure communication engineering at 2014.

Target Tracking in MIMO Radar Systems Using Velocity Vector

Mohammad Jabbarian Jahromi

Department of Electrical and Electronic Engineering, Malek Ashtar University of Technology, Tehran, Iran

jabbarian@iust.ac.ir

Hossein Khaleghi Bizaki*

Department of Electrical and Electronic Engineering, Malek Ashtar University of Technology, Tehran, Iran

bizaki@ee.iust.ac.ir

Abstract

The superiority of multiple-input multiple-output (MIMO) radars over conventional radars has been recently shown in many aspects. These radars consist of many transmitters and receivers located far from each other. In this scenario, the MIMO radar is able to observe the targets from different directions. One of the advantages of these radars is exploitation of Doppler frequencies from different transmitter-target-receiver paths. The extracted Doppler frequencies can be used for estimation of target velocity vector so that, the radar can be able to track the targets by use of its velocity vector with reasonable accuracy. In this paper, two different processing systems are considered for MIMO radars. First one is the pulse Doppler system, and the second one is continuous wave (CW) system without range processing. The measurement of the velocity vector of the target and its counterpart errors are taken into account. Also, the extended Kalman target tracking by using its velocity vector is considered. Besides, its performance is compared with those of MIMO target tracking without using the velocity vector and conventional radars. The simulation results show that the MIMO radars using velocity vector have superior performance over other above-mentioned radars in fast maneuvering target tracking. Since the range processing is ignored in CW MIMO radar systems, the complexity of this system is much lower than that of Pulse Doppler MIMO radar system, but has lower performance in tracking fast maneuvering target.

Keywords: MIMO Radar; Continuous Wave Radar; Pulse-Doppler Radar; Extended Kalman Filter; Target Tracking; Velocity Vector.

1. Introduction to MIMO Radar Systems

While the idea of Multistatic Radar is not new, Multiple Input Multiple Output (MIMO) radar is very different from it in some aspects. In design of detectors in MIMO radar, it is desired to estimate unknown parameters, such as Radar Cross-Section (RCS), as a part of detection algorithm [1, 2]. One of the specifications of MIMO radars is that the transmitted signals should be orthogonal or highly uncorrelated. We consider two different orthogonal signals for two different MIMO radar systems. The different carrier frequencies with arbitrary narrowband modulations are good candidate for CW radar systems. On the other hand, the Direct Sequence (DS) signaling can be a good candidate in pulse Doppler radars due to its security and easy implementation.

The various properties of DS codes have discussed in many references, for example [3]. The length of desired DS code depends on hardware capabilities. It is clear that more processing gain can be attained with longer DS code, but its implementation constraints the code length from being long. These codes are good candidate for Pulse-Doppler radars so that, each pulse is multiplied in special code sequence and then transmits. Figure 1 shows a block diagram of typical pulse Doppler MIMO radar. In this configuration it is shown that the signal of each transmitter can be separated in each receiver by passing the signal from match filter banks. After integrating K pulses, the intended signals are passed from FFT block and finally they arrive to detection and Doppler estimation unit. In this unit, the target is detected in the cell of under test so that, the location and its various Doppler frequencies are extracted, too. The output of this block which consists of the estimated target location passes through the extended Kalman filter in order to track the target.

The main contribution of this paper compared to previous works is to use the velocity vector in fast target tracking for two different MIMO radar systems. The velocity vector is obtained from various Doppler frequencies extracted from different transmitter-target-receiver paths. We will show that target tracking using velocity vector outperform that of conventional target tracking in MIMO radar systems especially in tracking fast maneuvering target.

In Figure 1, it is assumed that the MIMO radar consists of 2 Transmitters (TXs) and 2 Receivers (RXs) which are located at different positions. The transmitted waveform consists of two orthogonal signals as C1 and C2 (two DS codes) so that, these signals can be separated in each receiver easily by use of orthogonal property. Thus, every receiver can be able to extract two transmitted signals, appropriately. Hence, this configuration is equal to four virtual Bistatic Radars [2]. According to figure 1, the received signals from four virtual radars are processed in central processing unit. In this architecture, the task of

---

* Corresponding Author

control unit is to inform the exact frequency and timing of each TX to each RX, so it uses a pulse amplifier in TXs and accurate frequency synthesizer in both TXs implemented in each coherent pulse interval.

The operation of CW MIMO radar is somewhat different from Figure 1. In this system, it is assumed that the separation among carrier frequencies is sufficiently large so that the received signals from different transmitters are extracted easily. Then, the Doppler processing will be done on each extracted signal. In this paper, it is assumed that the CW MIMO radar does not have the range processing, thus the system complexity is much lower compared to pulse Doppler MIMO radar system. Furthermore, CW MIMO radar does not need synchronization among receivers and transmitters. The localization in this system is done based on transmit and receive angles.

In [4], the superiority of target tracking in MIMO radar compared to conventional and phased array radar is taken into account. Its authors use the maximum likelihood estimator for target location and velocity, but they have not considered the effect of Doppler frequencies estimation in target tracking. Target localization for MIMO radar using Doppler frequencies is considered in [5] and [6], but they use grid search method to find target location which has high computational cost. Our paper tries to show the superiority of MIMO radars over conventional and bistatic radars in fast manoeuvring target tracking by using velocity vector. The paper is organized as follows: the signal processing in MIMO radar is discussed in section 2. In section 3 the relation between target velocity and its various Dopplers are considered. Target tracking using extended Kalman filter is devoted in section 4. The simulation is run in section 5 to show that the performance of proposed processing algorithm in MIMO radar against conventional methods and finally, the paper ends with conclusions.
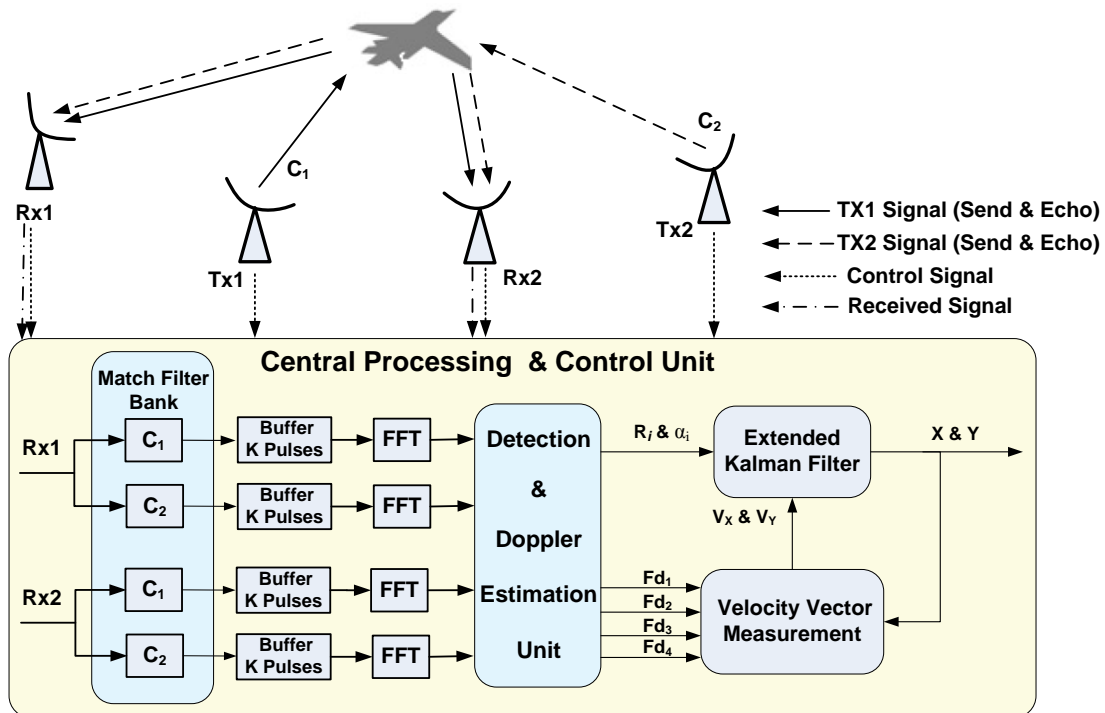
Fig. 1. Configuration of pulse Doppler MIMO Radar

2. Signal Processing in MIMO Radar Systems

The extraction of various Doppler frequencies of target from different paths between TXs-target-RXs with proper accuracy is one of the important aims of signal processing in MIMO radar. These Doppler frequencies are used in velocity vector calculation in section 3. This paper considers two different types of systems; the pulse-Doppler MIMO radar, and CW MIMO radar. We explain these two systems in following subsections.

2.1 Signal model for pulse Doppler MIMO radar

One of the good specifications of the pulse-Doppler system is its capability to obtain various Doppler frequencies of target. It means that pulse Doppler radars are good candidate to attain Doppler frequencies without any ambiguity. In these radars, the Doppler spectrum is periodic with a period equal to the Pulse Repetition Frequency (PRF) where, only the main period $[-\frac{PRF}{2} \quad \frac{PRF}{2}]$ is needed [7]. The receiver's noise is considered to be uniformly distributed over the whole spectrum. Clutter occupies a portion of spectrum which contains only low frequencies around the

DC. Therefore, Doppler processing can be used to separate the target and clutter signals in the frequency domain. In order to obtain the sign of Doppler (plus or minus), two channel I & Q are used. The transmitted signals from TX1 and TX2 are considered as:

$$S_{t1} = \sqrt{\frac{E}{T_P}} C_1 Cos(2\pi f_c t)$$

$$S_{t2} = \sqrt{\frac{E}{T_P}} C_2 Cos(2\pi f_c t)$$

(1)

where C1 and C2 are two DS codes, $\|C_1\|^2 = 1$, $\|C_2\|^2 = 1$, f_c, is carrier frequency and $E/2$ is the energy of singnal, and T_P is pulse duration. The received signals in RX1 and RX2 can be written as:

$$S_{r1} = \alpha_{11}\sqrt{\frac{E}{T_P}} C_1 Cos\left(2\pi f_c\big(t - \tau_{11}(t)\big)\right)$$
$$+\alpha_{12}\sqrt{\frac{E}{T_P}} C_2 Cos\big(2\pi f_c(t - \tau_{12}(t))\big) + n_1(t)$$

(2)

$$S_{r2} = \alpha_{21}\sqrt{\frac{E}{T_P}} C_1 Cos\left(2\pi f_c\big(t - \tau_{21}(t)\big)\right)$$
$$+\alpha_{22}\sqrt{\frac{E}{T_P}} C_2 Cos\big(2\pi f_c(t - \tau_{22}(t))\big) + n_2(t)$$

where, $\alpha_{ij}, i, j = 1,2$ models target fluctuations and assumed to be random variable with uniform distribution, $n_i(t), i = 1,2$ is the additive white Gaussian noise, i.e, $n \sim N(0, \sigma_n^2)$, $\tau_{ij}(t)$, $i, j = 1,2$, is equal to delay of echo signals of different paths.

Delay of τ can be modelled in various types, but linear model is one of the practical models. Linear model of delay can be described as [8]:

$$\tau_{ij}(t) = \tau_0 + \frac{R_{ti}(t) + R_{rj}(t)}{C}$$
$$= \tau_0 + \frac{V_{ti}(t) + V_{rj}(t)}{C} t \quad i, j = 1,2$$

(3)

where, τ_0 is initial delay, $V_{ti}(t)$ is the radial velocity between TXs and target, $V_{rj}(t)$ is the radial velocity between RXs and target and C is the velocity of wave.

As shown in figure 1, the K echo pulses from target integrated in the buffer and are then fed to the FFT block. Therefore, the spectrum of the signal including the Doppler frequencies of the target can be exploited.

2.2 Signal model for CW MIMO radar

In this system, it is assumed that the transmitted signals are the different carrier frequencies with arbitrary narrowband modulations. Therefore, the transmitted signal from two TX1 and TX2 are considered as:

$$S_{t1} = \sqrt{\frac{E}{T_P}} A_1(t)Cos(2\pi f_1 t)$$

$$S_{t2} = \sqrt{\frac{E}{T_P}} A_2(t)Cos(2\pi f_2 t)$$

(4)

where $A_1(t)$ and $A_2(t)$ are arbitrary narrowband modulations with $\frac{1}{T_P}\int_{T_P}^1 |A_1(t)|^2 dt = 1$ and $\frac{1}{T_P}\int_{T_P}^1 |A_2(t)|^2 dt = 1$, f_1 and f_2 are carrier frequencies and $E/2$ is the energy of signal, and T_P is time duration for signal processing. The received signals in RX1 and RX2 can be written as:

$$S_{r1} = \alpha_{11}\sqrt{\frac{E}{T_P}} A_1(t) Cos\left(2\pi f_1\big(t - \tau_{11}(t)\big)\right)$$
$$+\alpha_{12}\sqrt{\frac{E}{T_P}} A_2(t) Cos\big(2\pi f_2(t - \tau_{12}(t))\big) + n_1(t)$$

(5)

$$S_{r2} = \alpha_{21}\sqrt{\frac{E}{T_P}} A_1(t) Cos\left(2\pi f_1\big(t - \tau_{21}(t)\big)\right)$$
$$+\alpha_{22}\sqrt{\frac{E}{T_P}} A_2(t) Cos\big(2\pi f_2(t - \tau_{22}(t))\big) + n_2(t)$$

These two signals are passed through the band pass filters which their center frequencies are f_1 and f_2. Therefore, the received signals from different transmitters are extracted easily. The Doppler frequency of each extracted signal can be obtained by FFT processing.

3. Relation between Target Velocity and Various Doppler Frequencies

The locations of TX, RX and target for a typical scenario for bistatic radar in which 1 transmitter and 1 receiver located far from each other are shown in figure 2.

The imposed Doppler frequency at receiver can be calculated as follows [9]:

$$f_d = \frac{V_x}{\lambda}(Cos\alpha + Cos\beta) + \frac{V_y}{\lambda}(Sin\alpha + Sin\beta)$$

(6)

where, λ is the wavelength of transmitted signal, V_y and V_x are the elements of velocity vector in direction of Y axis and X axis, respectively.
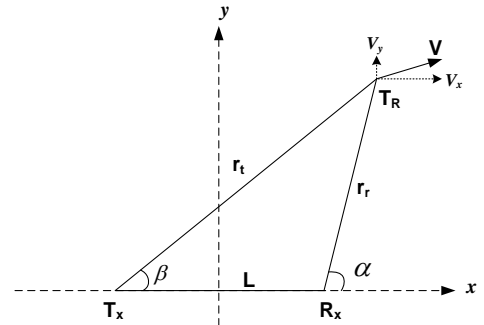

Fig. 2. A typical scenario for bistatic radar.

Now, we extend (6) for MIMO radar in which more than one transmitter and receiver exist. The MIMO radar that consists of M TXs and N RXs has MN various Doppler frequencies that can be obtained as follows:

$$\begin{bmatrix} f_{d1} \\ f_{d2} \\ \vdots \\ f_{dMN} \end{bmatrix} =$$

$$\frac{1}{\lambda} \begin{bmatrix} Cos\alpha_1 + Cos\beta_1 & Sin\alpha_1 + Sin\beta_1 \\ Cos\alpha_2 + Cos\beta_2 & Sin\alpha_2 + Sin\beta_2 \\ \vdots & \vdots \\ Cos\alpha_{MN} + Cos\beta_{MN} & Sin\alpha_{MN} + Sin\beta_{MN} \end{bmatrix} \begin{bmatrix} V_x \\ V_y \end{bmatrix} \quad (7)$$

Thus, the least square solution of velocity vector of target is abstained as:

$$V = (G^T G)^{-1} G^T f_d \qquad (8)$$

where, $V = [V_x \quad V_y]^T$ is velocity vector, and $f_d = [f_{d1} \quad \cdots \quad f_{dMN}]$ is Doppler vector. The matrix G is defined as follows:

$$G = \frac{1}{\lambda} \begin{bmatrix} Cos\alpha_1 + Cos\beta_1 & Sin\alpha_1 + Sin\beta_1 \\ Cos\alpha_2 + Cos\beta_2 & Sin\alpha_2 + Sin\beta_2 \\ \vdots & \vdots \\ Cos\alpha_{MN} + Cos\beta_{MN} & Sin\alpha_{MN} + Sin\beta_{MN} \end{bmatrix} \quad (9)$$

The obtaining target velocity vector can be used in target tracking, where is discussed in next section.

The error due to velocity vector computation is a function of three elements:

1. Error of location estimation.
2. Error of Doppler estimation.
3. Target position with respect to RXs and TXs positions.

Error of location estimation: Because α_i and β_i are a function of target position, computation of sine and cosine of α_i and β_i are influence of this error.

Error of Doppler estimation: This error is due to FFT resolution. The interpolation or other such techniques can be used in order to decrease this undesired effect.

Target position with respect to RXs and TXs positions: The final error of velocity vector influenced with this error severely. In section 5, this effect will be discussed in more details.

4. Target Tracking by Extended Kalman Filter

Kalman filter is a method that recursively minimizes the mean squared error. The important advantage of Kalman filter against other prediction methods is that, it considers the observation noise in its model [10]. This subject is important in target tracking because of observation noise that exists in manoeuvring target [11]. Since Kalman filter considers process noise, it has better performance than other methods practically. We use extended Kalman filter in both pulse Doppler and CW MIMO radar systems due to the nonlinearity of observation equations.

4.1 Target tracking in pulse Doppler MIMO radar

The observation equations in pulse Doppler MIMO radar are range estimates $R_i[n]$ and bearing estimates $\alpha_i[n]$ of ith receiver which are derived as following:

$$R_i[n] = \sqrt{(x[n] - x_i^r)^2 + (y[n] - y_i^r)^2}$$
$$\alpha_i[n] = \tan^{-1}\left(\frac{y[n] - y_i^r}{x[n] - x_i^r}\right) \qquad (10)$$

Where $(x[n], y[n])$ is the position of target at time n, and (x_i^r, y_i^r) is the position of ith receiver. Now, we choose the signal vector to be the target position and velocity components:

$$\mathbf{s}[n] = [x[n] \quad y[n] \quad V_x[n] \quad V_y[n]]^T \qquad (11)$$

In general terms the observation equation is:

$$\mathbf{p}[n] = \mathbf{h}(\mathbf{s}[n]) + \mathbf{w}[n] \qquad (12)$$

where $\mathbf{w}[n]$ is estimation error (or measurement noise) assumed to be Normal distribution with zero mean and covariance matrix:

$$\mathbf{C} = diag\left([\sigma_{R_1}^2 \quad \sigma_{\alpha_1}^2 \quad \cdots \quad \sigma_{R_N}^2 \quad \sigma_{\alpha_N}^2 \quad \sigma_{R_{Vx}}^2 \quad \sigma_{R_{Vy}}^2]\right) \quad (13)$$

$\mathbf{p}[n]$ and $\mathbf{h}(\mathbf{s}[n])$ for pulse Doppler MIMO Radar are obtained as:

$$\mathbf{p}[n] = [R_1[n] \quad \alpha_1[n] \quad \cdots \quad R_N[n] \quad \alpha_N[n] \quad V_x[n] \quad V_y[n]]^T \quad (14)$$

$$\mathbf{h}(\mathbf{s}[n]) = \begin{bmatrix} \sqrt{(x[n] - x_1^r)^2 + (y[n] - y_1^r)^2} \\ \tan^{-1}\left(\frac{y[n] - y_1^r}{x[n] - x_1^r}\right) \\ \vdots \\ \sqrt{(x[n] - x_N^r)^2 + (y[n] - y_N^r)^2} \\ \tan^{-1}\left(\frac{y[n] - y_N^r}{x[n] - x_N^r}\right) \\ V_x[n] \\ V_y[n] \end{bmatrix}_{(2N+2) \times 1} \quad (15)$$

The extended Kalman filter process is given in Table I [12].

The measurement matrix $\mathbf{H}$ is calculated as shown in (16). The process noise is assumed to be Normal distribution with zero mean and modified covariance matrix [13] as follows:

$$\mathbf{Q} = q \begin{bmatrix} \frac{T^3}{3} & 0 & \frac{T^2}{2} & 0 \\ 0 & \frac{T^3}{3} & 0 & \frac{T^2}{2} \\ \frac{T^2}{2} & 0 & T & 0 \\ 0 & \frac{T^2}{2} & 0 & T \end{bmatrix} \quad (17)$$

where T is sampling time, and q is a constant coefficient.

For considered model, the state transient matrix A can be given as:

$$\mathbf{A} = \begin{bmatrix} 1 & 0 & T & 0 \\ 0 & 1 & 0 & T \\ 0 & 0 & 1 & 0 \\ 0 & 0 & 0 & 1 \end{bmatrix} \quad (18)$$

The estimation of vectors velocity, V_y and V_x, by estimation of different Doppler frequencies is one of the main specifications of MIMO radar. Thus, the extended

Kalman filter that is used in this type of radar consists of two inputs: positions (R_i, α_i) and velocity (V_x, V_y). In order to demonstrate the fair comparison between MIMO radar and conventional radar in target tracking, we simulate them in the same condition. We show that the MIMO radar has better performance in target tracking against the conventional radars when it uses velocity vector in tracking filter. It should be noted that in conventional radars there is not target velocity in directions X and Y in order to estimate target position.

Table 1. Extended Kalman Filter Process

Initialization

1- $\mathbf{s}[0] = [x[0] \quad y[0] \quad V_x[0] \quad V_y[0]]^T$
2- $\mathbf{M}[0] = 10\mathbf{I}$

For $n = 1, \dots, N_{Sample}$
a) $\hat{\mathbf{s}}[n|n-1] = \mathbf{A}\hat{\mathbf{s}}[n-1|n-1]$
b) $\mathbf{M}[n|n-1] = \mathbf{A}\mathbf{M}[n-1|n-1]\mathbf{A}^T + \mathbf{Q}$
c) $\mathbf{K}[n] = \mathbf{M}[n|n-1]\mathbf{H}^T[n](\mathbf{C} + \mathbf{H}[n]\mathbf{M}[n|n-1]\mathbf{H}^T[n])^{-1}$
d) $\hat{\mathbf{s}}[n|n] = \hat{\mathbf{s}}[n|n-1] + \mathbf{K}[n](\mathbf{p}[n] - \mathbf{h}(\hat{\mathbf{s}}[n|n-1]))$
e) $\mathbf{M}[n|n] = (\mathbf{I} - \mathbf{K}[n]\mathbf{H}[n])\mathbf{M}[n|n-1]$

4.2 Target tracking in CW MIMO radar

The observation equations in CW MIMO radar are transmit angle estimates $\beta_j[n]$ of jth transmitter and bearing estimates $\alpha_i[n]$ of ith receiver which are derived as following:

$$\beta_j[n] = \tan^{-1}\left(\frac{y[n]-y_j^t}{x[n]-x_j^t}\right)$$
$$\alpha_i[n] = \tan^{-1}\left(\frac{y[n]-y_i^r}{x[n]-x_i^r}\right) \tag{19}$$

Where $(x[n], y[n])$ is the position of target at time n, and (x_j^t, y_j^t) and (x_i^r, y_i^r) are the positions of jth transmitter and ith receiver, respectively. The signal vector and the observation equation are the same as (11) and (12), respectively. The covariance matrix of measurement noise is considered as:

$$\mathbf{H}[n] = \left.\frac{\partial \mathbf{h}}{\partial \mathbf{s}[n]}\right|_{\mathbf{s}[n]=\hat{\mathbf{s}}[n|n-1]} = \begin{bmatrix} \frac{x[n]-x_1^r}{\sqrt{(x[n]-x_1^r)^2+(y[n]-y_1^r)^2}} & \frac{y[n]-y_1^r}{\sqrt{(x[n]-x_1^r)^2+(y[n]-y_1^r)^2}} & 0 & 0 \\ \frac{-(y[n]-y_1^r)}{(x[n]-x_1^r)^2+(y[n]-y_1^r)^2} & \frac{x[n]-x_1^r}{(x[n]-x_1^r)^2+(y[n]-y_1^r)^2} & 0 & 0 \\ \vdots & \vdots & \vdots & \vdots \\ \frac{x[n]-x_N^r}{\sqrt{(x[n]-x_N^r)^2+(y[n]-y_N^r)^2}} & \frac{y[n]-y_N^r}{\sqrt{(x[n]-x_N^r)^2+(y[n]-y_N^r)^2}} & 0 & 0 \\ \frac{-(y[n]-y_N^r)}{(x[n]-x_N^r)^2+(y[n]-y_N^r)^2} & \frac{x[n]-x_N^r}{(x[n]-x_N^r)^2+(y[n]-y_N^r)^2} & 0 & 0 \\ 0 & 0 & 1 & 0 \\ 0 & 0 & 0 & 1 \end{bmatrix} \tag{16}$$

$$\mathbf{H}[n] = \left.\frac{\partial \mathbf{h}}{\partial \mathbf{s}[n]}\right|_{\mathbf{s}[n]=\hat{\mathbf{s}}[n|n-1]} = \begin{bmatrix} \frac{-(y[n]-y_1^t)}{(x[n]-x_1^t)^2+(y[n]-y_1^t)^2} & \frac{x[n]-x_1^t}{(x[n]-x_1^t)^2+(y[n]-y_1^t)^2} & 0 & 0 \\ \vdots & \vdots & \vdots & \vdots \\ \frac{-(y[n]-y_M^t)}{(x[n]-x_M^t)^2+(y[n]-y_M^t)^2} & \frac{x[n]-x_M^t}{(x[n]-x_M^t)^2+(y[n]-y_M^t)^2} & 0 & 0 \\ \frac{-(y[n]-y_1^r)}{(x[n]-x_1^r)^2+(y[n]-y_1^r)^2} & \frac{x[n]-x_1^r}{(x[n]-x_1^r)^2+(y[n]-y_1^r)^2} & 0 & 0 \\ \vdots & \vdots & \vdots & \vdots \\ \frac{-(y[n]-y_N^r)}{(x[n]-x_N^r)^2+(y[n]-y_N^r)^2} & \frac{x[n]-x_N^r}{(x[n]-x_N^r)^2+(y[n]-y_N^r)^2} & 0 & 0 \\ 0 & 0 & 1 & 0 \\ 0 & 0 & 0 & 1 \end{bmatrix} \tag{23}$$

$$\mathbf{C} = diag([\sigma^2_{\beta_1} \quad \cdots \quad \sigma^2_{\beta_M} \quad \sigma^2_{\alpha_1} \quad \cdots \quad \sigma^2_{\alpha_N} \quad \sigma^2_{R_{V_x}} \quad \sigma^2_{R_{V_y}}]) \quad (20)$$

p[n] and h(s[n]) for CW MIMO Radar are obtained as:

$$\mathbf{p}[n] = diag([\hat{\beta}_1[n] \cdots \quad \hat{\beta}_M[n] \quad \hat{\alpha}_1[n] \quad \cdots \quad \hat{\alpha}_N[n] \quad V_x[n] \quad V_y[n]]) \quad (21)$$

$$\mathbf{h}(\mathbf{s}[n]) = \begin{bmatrix} \tan^{-1}\left(\frac{y[n]-y_1^t}{x[n]-x_1^t}\right) \\ \vdots \\ \tan^{-1}\left(\frac{y[n]-y_M^t}{x[n]-x_M^t}\right) \\ \tan^{-1}\left(\frac{y[n]-y_1^r}{x[n]-x_1^r}\right) \\ \vdots \\ \tan^{-1}\left(\frac{y[n]-y_N^r}{x[n]-x_N^r}\right) \\ V_x[n] \\ V_y[n] \end{bmatrix}_{(M+N+2)\times 1} \quad (22)$$

The measurement matrix **H** for CW MIMO radar is calculated as shown in (23).

5. Simulation and Results

Different configurations are proposed for RXs and TXs of MIMO radar in [14]. In this paper, we consider two different configurations for two different MIMO radar systems as in following subsections.

5.1 Pulse Doppler MIMO radar

For pulse Doppler MIMO radar, it is assumed that TXs are omni-directional and RXs are directional with stacked beam. By using of stacked beams that is processed digitally, it is possible to search the whole surveillance area simultaneously. In this case, the search time is substantially reduced, but the computational burden is so high.

The range cell of the proposed MIMO radar with two TXs, two RXs and the target trajectory are shown in Figure 3.
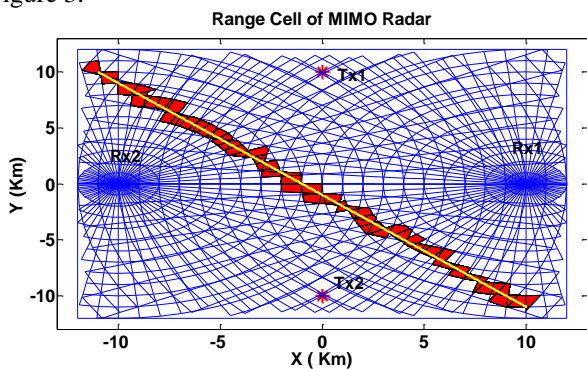
Fig.3. Configuration of Proposed pulse Doppler MIMO Radar

In pulse Doppler MIMO radar configuration, each range cell does not have any symmetric shape. Because it is obtained by subscription of several range cells that lead to smaller range cell. The parameters of system under simulation are considered as follows:

$f_c = 800MHz$	$T_c = 24.4nsec$	$N_C = 1024$
$PRF = 8kHz$	$N_P = 128$	$D.C = \%20$

Where f_c, T_c and N_C are carrier frequency, chip duty and code length, respectively. Also PRF, N_P and $D.C$ are pulse repetition frequency, number of integrated pulses and duty cycle, respectively. The carrier frequency and PRF are determined such a manner that there is not any ambiguity in Doppler and range calculation. We assume the maximum radial velocity is 800m/s, so that the maximum Doppler frequency will be 4kHz. In order to eliminate ambiguity in Doppler calculation, the PRF can be chosen 8 kHz. The number of integrated pulses is considered to be 128. Thus, in Doppler frequency spectrum computation, the FFT with 128 point can be used.

In this paper it is assumed that the target has fast maneuvering movement equations as follows:

$$X = 5000 + 100t + 300Cos(3\pi t)/(3\pi t)$$
$$Y = 3000 - 100t - 300Sin(3\pi t)/(3\pi t) \quad (24)$$
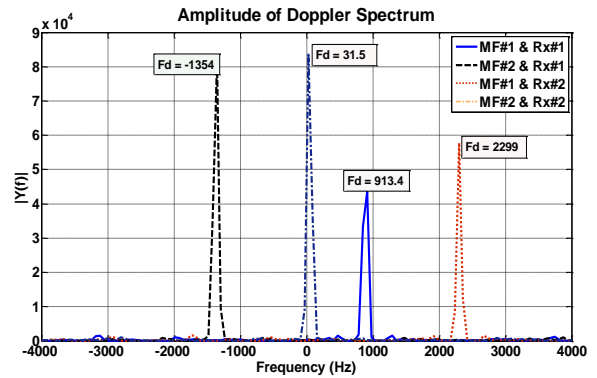
Fig. 4. Signals after FFT Computation
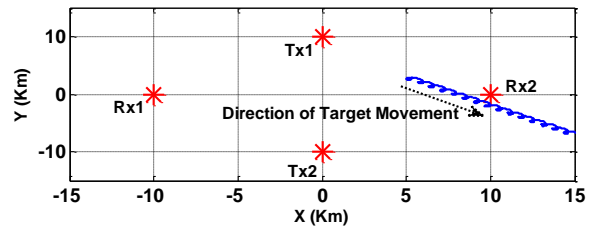
Fig. 5. The Path of moving target from the surveillance area of MIMO radar
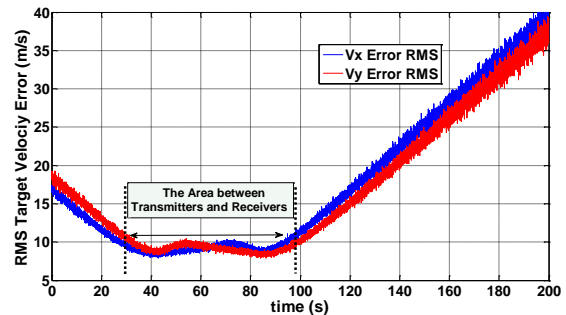
Fig. 6. RMS error of Velocity

The received signals after passing through matched filter and FFT block in RX1 and RX2 are shown in Figure

4. In this case, the signals are in frequency domain so that the Doppler frequencies of different paths can be obtained.

From Figure 4 it is observed that each TX-target-RX paths have different Doppler frequencies. It should be noted that the different amplitude of spectrum between channels is due to RCS fluctuations of target in which is considered in simulation.

In order to show the effect of target position relative to TX and RX antennas, we consider the target manoeuvre as Figure 5. In this case, the best target position relative to TX and RX antennas is obtained by minimum RMS in estimation of target velocity.

The RMS error of velocity is depicted in Figure 6. It is shown that when the target is located between RXs and TXs, the RMS error is less than other positions. This is due to the MIMO radar capability in different Doppler observation of target lead to target velocity be estimated accurately. As a result, The MIMO radar has its best performance when the target located between RXs and TXs antennas. After estimation the target velocity, it is possible to track the target by using of extended Kalman filter, accurately.

It should be noted that, we considered fast manoeuvring targets in target tracking to show that the MIMO radar outperforms in this scenarios. The initial conditions for extended Kalman filter are considered as follows:

$$\mathbf{s}[0] = [4950 \quad 2950 \quad 200 \quad -200]^T \tag{25}$$

$$T = 16 msec \qquad q = 10^6 \tag{26}$$

$$\sigma_{f_{d1}} = \sigma_{f_{d2}} = \sigma_{f_{d3}} = \sigma_{f_{d4}} = 50 Hz \tag{27}$$

$$\sigma_{R_1} = \sigma_{R_2} = 30m \qquad \sigma_{\alpha_1} = \sigma_{\alpha_2} = 0.1 rad \tag{28}$$

Target position estimations for extended Kalman filter in MIMO radar with and without using velocity vector and in conventional radar are demonstrated in Figures 7, 8, and 9, respectively. Clearly, it is observed that the designed extended Kalman filter by using velocity vector in MIMO radar has good performance in target tracking, but in the other cases, the result is not acceptable.
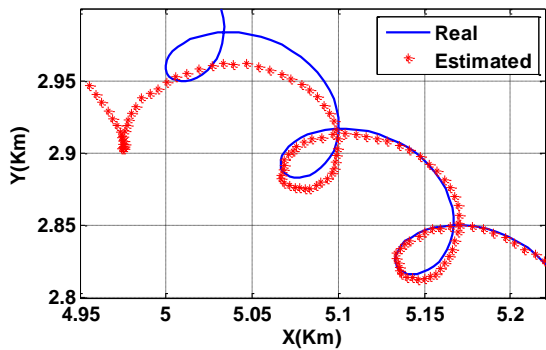
Fig. 7. Location Estimation in pulse Doppler MIMO Radar using velocity vector
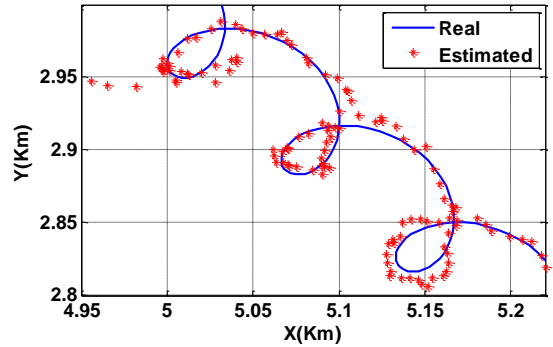
Fig. 8. Location Estimation in pulse Doppler MIMO Radar without using velocity vector
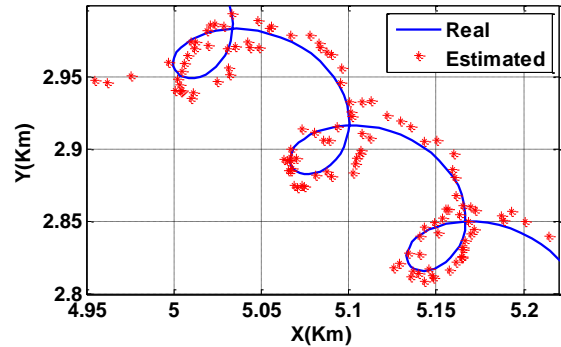
Fig. 9. Location Estimation in Conventional pulse Doppler Radar

The RMS error of target position for standard deviation of measurement noise $\sigma_{R_1} = \sigma_{R_2} = 30m$ and $\sigma_{\alpha_1} = \sigma_{\alpha_2} = 0.1 rad$, is shown in Figure 10. As observed from Figure 10, in conventional pulse Doppler radar, the RMS error decreases to 26m, and in pulse Doppler MIMO radar without using velocity vector it decreases to 19m but in pulse Doppler MIMO radar using velocity vector it decreases to 6m (Figure 10).
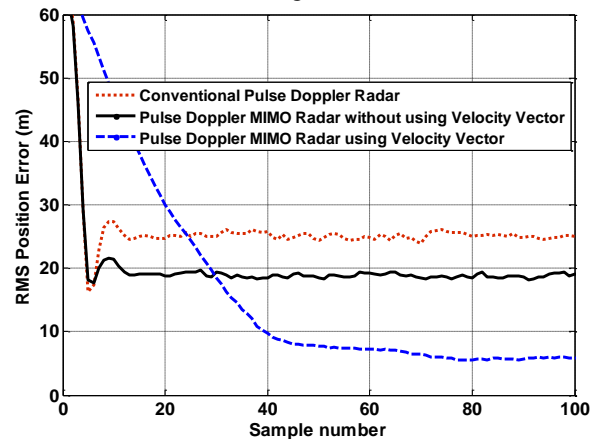
Fig. 10. RMS Error of Location Estimation

In figure 10, we see that the proposed method converges with more delay respect to the other methods. The reason is that in other methods we estimate the target velocity by obtaining difference between new and old estimated target positions and then divide by the sampling time. Due to the big difference between initial position

and estimated position at beginning, the value of velocity is big and causes the curve converges quickly. But in our method, target velocity is estimated by Doppler method, so its value is close to target velocity and it converges with more delay. To solve this problem, we can start tracking without using target velocity at several initial steps, then use target velocity vector in tracking filter.

5.2 CW MIMO radar

For CW MIMO radar, it is assumed that both TXs and RXs are directional. In this case, the angle of transmitted signal to target and received signals from target will be estimated. Then, EKF will track the target by using these angles and velocity vector. As mentioned in introduction, there is no range processing in this system, therefore the complexity of this system is much lower than MIMO radar system.

We compare this system with CW bistatic radar in which the angle of transmitted and received signal take part in EKF. Similar to CW MIMO radar, it is assumed that there is no range processing in CW bistatic radar. It should be noted that in bistatic radars, we cannot estimate target velocity in directions X and Y because there is only one equation, and two unknowns in (5). Therefore, this equation is underdetermined, and does not have unique solution.

Since the range processing is ignored in CW MIMO radar systems, they cannot track fast manoeuvring target as pulse Doppler MIMO radars can do. Therefore, we reduce the acceleration of target in movement equations as following:

$$X = 2000 + 100t + 300Cos(0.5\pi t)/(0.5\pi t)$$

$$Y = 6000 - 100t - 300Sin(0.5\pi t)/(0.5\pi t)$$

$$(29)$$

The initial conditions for extended Kalman filter are considered as follows:

$$\mathbf{s}[0] = [2900 \quad 6900 \quad 200 \quad -200]^T \qquad (30)$$

$$T = 16msec \qquad q = 10^7 \qquad (31)$$

$$\sigma_{f_{d1}} = \sigma_{f_{d2}} = \sigma_{f_{d3}} = \sigma_{f_{d4}} = 50Hz \qquad (32)$$

$$\sigma_{\beta_1} = \sigma_{\beta_2} = 0.1rad \qquad \sigma_{\alpha_1} = \sigma_{\alpha_2} = 0.1rad \qquad (33)$$
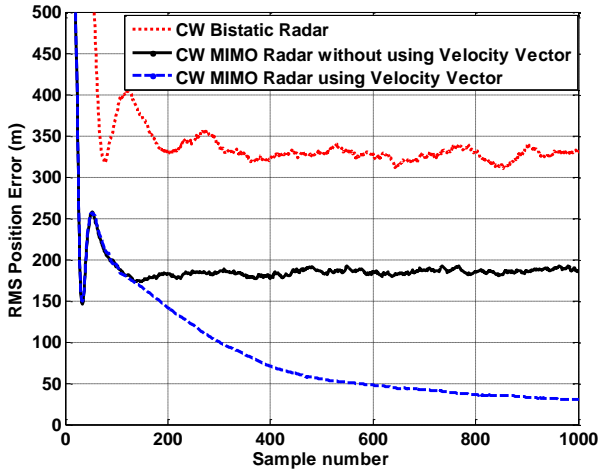
Figure 11 shows the RMS position error of different CW radars. For CW MIMO radar using velocity vector, we start tracking without using target velocity at 100 initial steps, then use target velocity vector in tracking filter. It makes this method converge with less delay. As seen in this figure, in CW bistatic radar, the RMS error decreases to 325m, and in CW MIMO radar without using velocity vector it decreases to 180m but in CW MIMO radar using velocity vector it decreases to 30m.

The above results show the superiority of MIMO radar in target tracking against to conventional radar when it uses velocity vector in tracking filter. The MIMO radar can reach to lower RMS error and track the target accurately when it uses velocity vector which is extracted from Doppler processing, and it is only possible in MIMO Radar with widely separated antenna. By using velocity vector in tracking, extended Kalman filter is able to track fast manoeuvring target.

6. Conclusions

In this paper, the problem of target tracking in MIMO radar by using velocity vector is considered. Also, two different types of processing system are taken into account; first on was pulse Doppler system, and the other was CW system. The result that is taken in simulations shows that target tracking by MIMO radar using target velocity is more accurate than that without using velocity vector in MIMO and conventional radar. Because of the MIMO radar capability to exploit the different Doppler frequencies of target, it can be able to estimate the velocity vector of target. By using of this vector and location of target, the radar can be able to track the target accurately. Also, the proposed MIMO radar with CW system without rang processing has lower performance in tracking fast maneuvering targets compared to pulse Doppler system which exploits range processing in target tracking.

Fig. 11. RMS Error of Location Estimation

References

[1] E. Fishler, A. Haimovich, R. Blum, L. Cimini, D. Chizhik, and R.Valenzuela, "Spatial Diversity in Radars—Models and Detection Performance," *IEEE Trans. Signal Processing*, vol. 54, pp. 823–838, Mar. 2006.

[2] A. Sheikhi, A. Zamani, "Coherent detection for MIMO radars", IEEE Radar Conf. 2007, Waltham, Massachusetts, USA, April 2007.

[3] R. L. Peterson, R. E. Ziemer, D. E. Borth, *Introduction to Spread Spectrum Communications*, Prentice Hall, 1995.

[4] R. Niu, R. S. Blum, P. K. Varshney, A. L. Drozd, "Target Localization and Tracking in Noncoherent Multiple-Input Multiple-Output Radar Systems", *IEEE Trans. Aerosp. Electron. Syst.*, vol. 48, pp. 1466–1489, Apr. 2012.

[5] Y. Kalkan, B. Baykal, "Target Localization and Velocity Estimation Methods for Frequency-Only MIMO Radars", IEEE Radar Conf. 2011, pp. 489–492.

[6] Y. Kalkan, B. Baykal, "MIMO Radar Target Localization by Using Doppler Shift Measurement", European IEEE Radar Conf. 2009, pp. 458–463.

[7] M. A. Richards, "*Fundamentals of Radar Signal Processing*". McGrow-Hill, 2005.

[8] I. V. Komarov, S. M. Smolskiy, "*Fundamentals of Short-Range FM Radar*", Artech House, 2003.

[9] M. Skolnik, "*Radar Handbook*", 2rd ed. New York: Mc-Graw-Hill, 1991.

[10] Mohinder s. Grewal & Angus p. Andrews, "*Kalman filtering, theory and practice using matlab*," second edition, John Wiley & Sons, Inc.

[11] S. Blackman, R. Popoli, "*Design and Analysis of Modern Traking Systems*", Artech House, 1999.

[12] S. M. Key, "*Fundamentals of Statistical Signal Processing: Estimation Theory*," Prentice Hall International, 1993.

[13] Y. Bar-Shalom, X. R. Li, and T. Kirubarajan, "*Estimation with Applications to Tracking and Navigation*", Hoboken, NJ; Wiley, 2001.

[14] A. Sheikhi and A. Zamani, "Temporal coherent adaptive target detection for multi-input multi-output radars in clutter," *IET Trans. Radar Sonar Navig*, Vol. 2, No. 2, April 2008.

Mohammad Jabbarian Jahromi received the B.S. degree in electrical engineering from Shiraz University, Shiraz, Iran, in 2005 and the M.Sc. degree from the Electrical and Electronic Engineering University Complex, Tehran, Iran, in 2008. He is currently working toward the Ph.D. degree in the School of Electrical Engineering, Iran University of Science and Technology. From 2009, he was a research staff in the Signal & System Modeling laboratory, IUST. His current research interests are in the areas of array signal processing, radar signal processing, and sparse reconstruction.

Hossein Khaleghi Bizaki received the Ph.D. degree in electrical engineering, communication system, from Iran University of Science and Technology (IUST), Tehran, Iran, in 2008. He has authored or coauthored more than 20 publications. His research interests include information theory, coding theory, wireless communication, MIMO systems, space-time processing, and other topics on communication system and signal processing.

Low Distance Airplanes Detection and Tracking Visually using Spectral Residual and KLT Composition

Mohammad Anvaripour*
Research Institute for ICT, ACECR, Tehran, Iran
anvaripour@ictrc.ir

Ramin Shaghaghi Kandovan
Research Institute for ICT, ACECR, Tehran, Iran
shaghaghi@ictrc.ir

Sima Soltanpour
Research Institute for ICT, ACECR, Tehran, Iran
simasoltanpour@yahoo.com

Abstract

This paper presents the method for detection and tracking airplanes which can be observed visually in low distances from sensors. They are used widely for some reasons such as military or unmanned aerial vehicle (UAV) because of their ability to hide from radar signals; however they can be detected and viewed by human eyes. Vision based methods are low cost and robust against jamming signals. Therefore, it is mandatory to have some visual approaches to detect airplanes. By this way, we propose spectral density for airplane detection and KLT algorithm for tracking. This approach is a hybrid of two distinct methods which have been presented by researchers and used widely in detection or tracking specific objects. To have accurate detection, image intensity would be adjusted adaptively. Correct detected airplanes would be achievable by eliminating some long optical flow trajectory in image frames. The proposed method would be analyzed and evaluated by comparison with state of the art approaches. The experimental results show the power of our approach in detection of multiple airplanes unless they become too small in presence of other objects and multiple airplanes. We make some test by implementing our approach on an useful database presented by some researchers.

Keywords: Airplane Detection; Spectral Density; KLT Method; Adaptive Image Adjusting.

1. Introduction

Nowadays visual aircraft detection is one of the interesting subjects in image processing projects because of the wide usage of low distance and low altitude airplanes. These kinds of airplanes are applied in military purposes, airplane industries and training. Unmanned Aerial Vehicle (UAV) is used for espy, mapping, taking picture, etc. and is utilized by many countries. Since keeping borders against unwanted imposition, study of constructed airplanes and monitoring their behaviors are necessary for industries and governments, many researchers spend their time on some subjects such as visual approach. The means of Visual approach are tracking and detection by some sensors which work as like as eyes, such as cameras. Images must be processed, analyzed and utilized by image processing and computer vision techniques. By this way, we can have some information about the object.

In this paper, spectral residual of image is applied to extract salient regions that indicate the most plausible regions of objects. Since the purpose of the paper is to track airplanes in sky we need to search for airplane features and track them. Blob analysis is common in tracking and is used for objects detection and clustering in video frames. Blobs are commonly extracted by morphological approaches that utilized in some researches such as [1]. In this research, blobs are extracted from salient regions extracted from spectral residual and analyzed by their aspect ratio. All of the probable regions for airplane existence are extracted and used for tracking by famous KLT (Kanade-Lucas-Tomasi) algorithm that has been discussed in [2]. All of the good features for tracking are extracted and tracked by KLT method and followed frame by frame in video sequence. The detection procedure, spectral density extraction and blob analysis, is repeated every 7 frame to find new airplanes and remove unwanted events because of noise, clouds, birds, etc. The diagram of the proposed approach was illustrated in Fig. 1.

We made a wide range of experiments and evaluated the method by comparing with state of the art method. For this reason, the aircraft database presented in [3] was used for experiments and comparisons.

The rest of the paper is summarized as follow. In the next subsection; related works, some methods are presented discussed before for detection and aircraft tracking. Section 2 is about proposed approach. Experimental Results are presented in section 3. The final section summarizes overall discussion.

---

* Corresponding Author

1.1 Related work

In literature, there are researches about tracking that state of the art survey has been reported in [4]. The common step for tracking is feature selection that has been received a lot of attention by researchers. Common features which are used for visual tracking are color, edges, optical flow, SIFT, HOG, and texture. In [5] edges were used for tracking. SIFT and HOG feature are described for object detection in [6,7] and were used by authors in [8,9] for tracking. Optical flow presented in [10] is very popular for tracking and has been proposed as the main feature for tracking in some literatures such as [11].
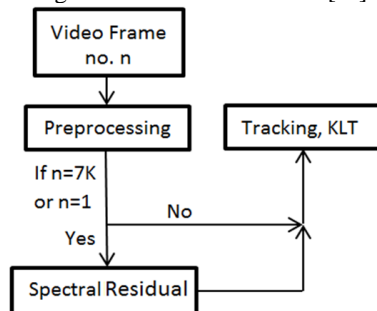

Fig. 1. Diagram of proposed approach.

Object detection is one of the basic concepts that can be introduced through tracking task. In this case the object is detected and localized in images. There are some researches in object detection that human detection and tracking is the main purpose of the authors [12]. In this case, HOG features were proposed with SVM classifier for human or pedestrian detection. In [13] color was proposed for face detection and tracking.

Airplane is favorite object that researchers pay attention on it. Radar signal cannot detect some low altitude flying objects but they can be observed by human eyes and tracked. Therefore, some visual approaches need to be investigated for tracking. In [9] optical flow discussed for image registration in stereo vision applications. Optical flow has a lot of application in tracking. In [2] a method has been described by authors, KLT, that optimizes the performance of optical flow. KLT uses good features for tracking extracted from corners. KLT method was used for tracking in [3]. Although optical flow and KLT method is good for tracking tasks, object tracking remains challenging when we face some unwanted events such as camera movements and illumination changes. Based on some efforts to overcome these failures, some techniques such as histogram equalization have been presented. Kalman Filter is a searching tool that has been presented to predict the interest object in video frame and has been used in [15]. However Kalman filter can detect and predict the object, it can be used for one target or object and will fail to track multiple objects. Mean Shift searching is a clustering algorithm which was proposed for tracking the interest object in [16]. The most problem in mean-shift algorithm is the time consuming process for clustering in each frame. Furthermore, the algorithm will be failed in presence of multiple objects near each other. Thus, blob analysis that is derived from background reduction and morphological processes is more

common [1]. Occlusions are uninteresting events that make tracking tasks too challenging, because, two or more objects will be counted as just one object. To have an accurate tracking and detection some patch based approaches have been suggested in [12]. Patches establish a dictionary or codebook that contains object features. This bag of features is classified and used for feature matching and searching. In some works, researchers' aims are to detect targets from aerial vehicles. In this case they are looking for interest objects by template matching [12]. The model of the object which has been stored is used for matching.

When all is said and done, there are some challenging events in tracking such as image blurring coming from camera movements, occlusion, luminance changes, and changing colors in different frames that researchers present techniques to compensate these flaws. In this paper an approach is tried to be presented to have a robust airplane detection and tracking.

2. Proposed Approach Steps

The aim of this section is to provide the proposed algorithm to detect and track airplanes visually in some steps. During the detection process we need to compensate unwanted events such as noise, occlusion and false positives to have an accurate detection. This section is divided in 3 subsections to cover authors' concept.

2.1 Preprocessing

The first step in most image processing and computer vision tasks is preprocessing. It is concluded with image enhancement, color transformation, image adjusting, filtering, etc. that prepares the image for further processes. In this paper we present an adaptive image adjusting that separate image objects based on their intensities. To remove noise from image median filter is applied and the resulting image would be sent to next step.
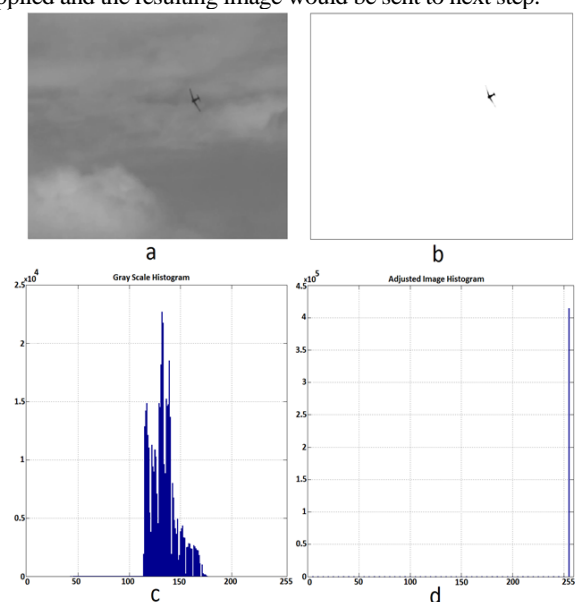

Fig. 2. Histograms of adjusted image. a) Gray scale original image,
b) adjusted image, c) histogram of the gray scale original image,
d) histogram of adjusted image

Image adjusting is stretching the desired range of image intensity histogram to new area or rang to highlight interesting regions and objects. Adaptive adjusting is proposed to achieve a good result in video frames. For this reason histogram of image intensity is extracted in each frame. Since airplanes in sky occupy a small part of images, airplane intensities cover small fraction of image. By this way, the histogram of the image contains with large amount of sky intensities and small amount for airplanes. Image adjusting would be useful for further process to segment airplane from background. As we know, airplanes are observed in sky with different intensities or color from background. By adjusting the image, the intensities of airplane would be distributed during all of the intensity range, [0 255], and rest of them will be concatenated in 255 or 0. If background intensity be higher than desired range they move to 255 otherwise they move to 0. Fig. 2 shows the histograms of the images intensities. This figure illustrates the original image in gray scale (a), adjusted image (b), histogram of gray scale (c) and histogram of adjusted images (d). As we can see from the figure, airplane has been bolded in adjusted image and background has been removed.

In most of the images some unwanted objects would be extracted. Noise causes these events. Although image adjusting shifts noise intensity to undesired range, some of them have intensities in the range of airplane intensities and would be appeared in image. According to speckle or salt and pepper noises in video images, median filter has a good performance for noise reduction. Therefore, in this paper two dimensions median filter is implemented to remove noises.

2.2 Spectral residual

The aim of the object detection is to find interest object and extract it from background. There are researches in object detection which use particular feature of targets such as edges [17], local appearance [18], etc. Since extracting these kinds of features is time consuming in video processing and training stage is needed to train object's information, general purpose saliency detection is required. Saliency detection is presented in this paper based on the efforts of Hou et al [19]. In [19] log spectrum has been presented for saliency map extraction.

$$L(f) = \log(A(f)) \tag{1}$$

In above equation, $A(f)$ is the amplitude of Fourier transform of image. According to the experiments in [19], average spectrum can be approximated by convoluting the input image:

$$Av(f) = h_n(f) * L(f) \tag{2}$$

Where $h_n(f)$ is an n×n matrix defined as below:

$$h_n(f) = \frac{1}{n^2} \begin{bmatrix} 1 & 1 & \dots & 1 \\ 1 & 1 & \dots & 1 \\ \vdots & \vdots & \ddots & \vdots \\ 1 & 1 & \dots & 1 \end{bmatrix} \tag{3}$$

Spectral residual $R(f)$ could be achieved by:

$$R(f) = L(f) - Av(f) \tag{4}$$

Saliency map would be available in spatial domain of image by Inverse Fourier Transform. Saliency map contains with specified areas which can be used to interpret expected portions of the image. Saliency map is illustrated by Eq. (5).

$$S(x) = F^{-1}\left(\exp(R(f) + P(f))\right)^2 \tag{5}$$

Where P denotes to phase or angle of Fourier transform, and F^{-1} is inverse Fourier transform. As discussed in [19], a threshold is applied to segment image and detect proto-objects in saliency map.

$$O(x) = \begin{cases} 1 & if S(x) > threshold \\ 0 & else \quad where \end{cases} \tag{6}$$

In our experiments, the threshold is set to 10×(average intensity).

Although saliency map and segmentation help us to remove background and extract most probable regions for object, some unwanted objects or false positives would be extracted because of clutters in natural images. To compensate this kind of faults we implemented aspect ratio of aircraft to extract them in image. Aspect ratio is defined as the ratio of length to width. The result of this operation would be an image containing the most probable regions of the object. Fig. 3 illustrates saliency map and segmented image after setting a threshold, and extracted the most probable regions by implementing aspect ratio. As the Fig. 3 shows, some undesirable regions are detected in segmented saliency map. This event is unavoidable because of the differences of intensities of objects with background.

2.3 Tracking

KLT (Kanade-Lucas-Tomasi) tracking algorithm is a common tracking algorithm that has been presented in [2] and is used widely in all of the tracking tasks. Optical flow which was discussed by Kanade-Lucas in [10] was optimized by Shi-Tomasi [2] by selecting good feature for tracking. The below equation is describing the motion between two consecutive frames in video.

$$I(x, y, t + \tau) = I(x - a, y - b, t) \tag{7}$$

In the equation, I represents the image intensity, t and τ are time and difference of time between two frames respectively, a and b are increments of dimensions in frame of time t. Images have some noises which they are imposed in frames and could be aggregated to Eq. (7).

Therefore, Eq. (7) can be calculated to minimize the noise (n).

$$n = \iint_{W} \left[I(x-a, y-b, t) - I(x, y, t+\tau) \right]^2 w(x, y) dx dy \tag{8}$$

In the above equation, w(x,y) indicates to weighting function and W is the window of searching. According to reports in papers [2, 3], we set the weight to unity. Since displacement is small relative to searching window, this equation can be rewritten by Taylor series approximation as below. Furthermore, we don't inter time symbols to formulas because displacements are needed for this reason.
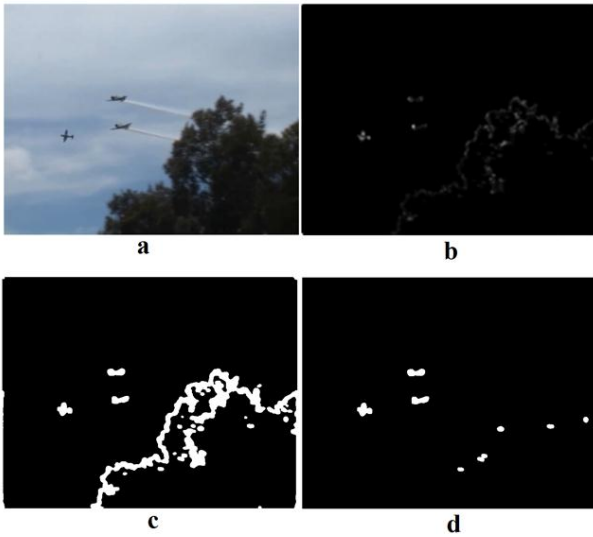
Fig. 3. Saliency map extraction using Spectral Residual. a) natural image, b) spectral residual, c) resulted image after threshold, d) resulted image using aspect ratio criteria.

$$I(x-a, y-b) \approx I(x, y) - a \frac{\partial I}{\partial x}(x, y) - b \frac{\partial I}{\partial y}(x, y), \tag{9}$$

$$g = \left[\frac{\partial I}{\partial x} \quad \frac{\partial I}{\partial y} \right]^T \tag{10}$$

$$I(x-a, y-b) \approx I(x, y) - g.D, \quad D = (a, b) \tag{11}$$

By substituting these approximated series, Eq. (8) would be rewritten as below.

$$n = \iint_{W} \left[I(x, y, t) - g.D - I(x, y, t+\tau) \right]^2 dx dy \tag{12}$$

$$n = \iint_{W} \left[F - g.D \right]^2 dx dy \tag{13}$$

$$F = I(x, y, t) - I(x, y, t+\tau)$$

To find displacement, D, the Eq. (13) must be differentiated respect to D and set to zero.

$$\iint_{W} \left[F - g.D \right] g \, dx dy = 0 \tag{14}$$

$$\iint_{W} gg^T D \, dx dy = \iint_{W} Fg \, dx dy \tag{15}$$

$$GD = H$$

$$G = \begin{bmatrix} \dfrac{\partial^2 I}{\partial x^2} & \dfrac{\partial^2 I}{\partial x \partial y} \\ \dfrac{\partial^2 I}{\partial x \partial y} & \dfrac{\partial^2 I}{\partial y^2} \end{bmatrix} \tag{16}$$

Fig. 4. Airplane Detection. Airplanes' contours and centers are shown by red color

Based on the Shi and Tomasi's definition in [2], if λ_1 and λ_2 are the eigenvalues of matrix G, the best features for tracking would satisfy the relation, $\min(\lambda_1$ and $\lambda_2)>\lambda_{th}$, which threshold is obtained from uniform intensity regions. By this way, corners and highly textured of image is extracted.

In this paper we suggest to extract and track good features by KLT algorithm from regions that are obtained from spectral residual stage. It is time saving for us to track and extract specific points and regions. Furthermore, detection would be more accurate. The probable problem comes from segmented salient map which some unwanted regions or objects are extracted as Fig. 3. To remove such clutters we suggest two solutions. As we know moving camera and stable camera are two strategies which used for tracking. In stable camera clutters and false positives are from flying objects, although some small camera movements can cause this event. To overcome camera movement fault we remove all of the small optical flow lower than threshold. In airplane tracking using moving camera the goal is to maintain the airplane in middle of the scene, therefore all false positive events come from static objects and have bigger optical flow thus, they can be eliminate by setting a threshold.

It can be seen from the Fig. 1 images are moved to tracking block after passing through preprocessing stage and spectral residual. In some conditions which two or more airplanes occlude each other, or new airplanes come to the scene, it is needed to have a detection stage to find and localize airplanes. Therefore, spectral residual is implemented to every 7 frame. We choose every 7 frame arbitrarily which based on our observation and experiments in the database, it is a significant choice to find coming airplane to the scene. Thus, based on the application or database, it can be changed. Other frames don't need any detection or spectral residual extraction process and airplanes would be tracked by KLT algorithm and their features are obtained from previous regions from segmented saliency map. By this way a fast, accurate, and reliable tracking process would be obtained.
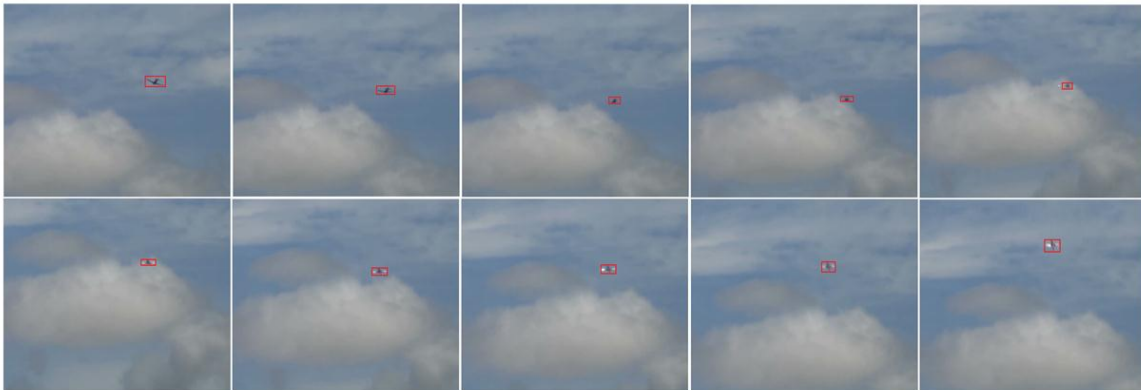
Fig. 5. Consecutive s step frames of an aerobatic airplane

3. Experimental Results

We examine our proposed approach by making some experiments on common database presented in [3], and compare it with state of the art methods and results show the acceptable performance of our approach in detection and tracking. Fig. 4 shows some example of the database. It can be seen from Fig. 4 that the database contains with variety scenes of airplanes such as occlusion, and multiple in various sizes.

The database has been collected in AVI format. All of them are at the rate of 25 frames per second and frame size of 720×576 pixels. 27 videos less than 1 minute and 4 sequences in low resolution 640×480 exist in the database. As mentioned before, several types of airplanes, jet, aerobatic, fighter, transport, and propeller with occlusion, pose variations, and multiple planes. All of them include the camera movements and optical zoom.

In this paper we specify the detected objects by their contours at every 7 frame. It is achievable because we use spectral residual for detection. Fig. 4 illustrates detected airplanes in various scenes. The centers of the detected objects are shown by a red plus sign. Good features are extracted from these regions and tracked by KLT algorithm. The tracked objects are shown by a rectangle such as Fig. 5.

We implemented our method by MATLAB using a Pentium dual core 32 bit PC with 2.60 GHz CPU and evaluated by experiments on all of the sequences in the database and compare with [3] that authors use KLT with Haar features, state of the art methods such as Kalman Filter using appearance model which was discussed in [13], Mean Shift clustering as presented in [16] and GMM model as like as [1]. These methods are used widely for tracking tasks. Table 1 shows the tracking results and process time and compares our method with them.

We used tracking accuracy to evaluate tracking performance. It means the number of correctly tracked airplanes per total number of airplanes in frames or sequences. Furthermore, frame would be considered as unsuccessful tracking process if some false positives be detected and tracked or airplanes are not detected. Therefore, tracking accuracy would count the total tracked airplane properly without any false positives. To achieve the best criteria for comparison, we compare our method with others with their optimum parameters and their best accuracies.

3.1 Comparisons

In many researches GMM is used and modeled based on the RGB space and extracts foreground from background. As it can be observed from table 1, Tracking Accuracy using GMM is not better than our proposed method and False Positive is relatively high. The high false positive is inevitable because GMM uses blob analysis mainly that is very sensitive to unwanted objects such as clouds, birds, and buildings in airplane database.

Kalman Filter is one of the famous approaches for tracking and estimating the most probable region of presence of the object such as approach in [13]. Kalman Filter is based on the Gaussian distribution and can support the single peak but it is modified by GMM to find more peaks and objects. As it can be seen from Table 1, it has an accuracy 79% . As aforementioned, it is obvious that Gaussian distribution and blob analysis is responsible for occurring false positives and making worse process.

Mean Shift clustering is used widely in tracking process [16]. It is working properly in some tasks that camera is stable and false positives can be removed by background subtraction. To achieve the reasonable accuracy some additional processes are needed to decrease the false positives. Then, the complexity and the process time would be increased. Table 1 shows that the process time of our method is reasonable.

In [3] the author is presenting an approach to track and detect airplane. In this paper Haar feature is used to detect object that is a famous feature in face detection tasks. KLT algorithm is used for tracking. Since the Haar feature use intensity of the object it makes mistake by extracting regions such as clouds or birds in some frames and causes false positives.

In our proposed approach, we use spectral residual and aspect ratio for object detection. Since moving camera tries to locate airplanes at middle of the screen, false positives are removed by eliminating high optical flows. Furthermore, detection is repeated every 7 frame as we mentioned in section 2-3, and all of the airplanes are detected and tracked. Process time and tracking accuracy of our approach are reasonable and better than other state of the art methods.

As Fig. 4 shows, top right airplane, our method has better accuracy than presented approach in [3] which uses this sequence as the challenging video. The paintings on the airplane caused some problems in detection and tracking in [3], although the airplane is detected and tracked accurately by our proposed method in most of the frames. Fig. 5 shows some consecutive frames of tracked airplane in one of the sequences. The airplane in this sequence has various positions and the cloud exists in sky. The airplane has different intensities in sequences which would be challenging for detection but image adjusting makes all of the parts and intensities belonging to the airplane more available and spectral residual make a reliable saliency map for detection.

3.2 Faults and limitations

We encounter some detection problems in the database. These faults come from very small or far airplanes, noises, occlusions or camera movements.

One of the limitations in our work is the camera movements. Camera movements are not very critical problem but in some cases it would have disruptive effects on. Since the data base contains with videos from moving camera we eliminate large optical flows during tracking process. Therefore, in some cases which the camera cannot follow the object some good points would be removed. As Fig. 6 illustrates, an airplane are divided in 3 parts and every part may be detected as an airplane. Another limitation is about the size of the object. Fig. 6 illustrates that our algorithm would not track successfully if the flying object is too far from the camera. This fault comes from the Spectral Residual and aspect ratio parameters for noise elimination.

Fig. 6. Two samples of fails of our proposed approach.

4. Conclusion

In this paper we proposed a method with several stages to track airplanes. They are image adjusting, spectral residual or saliency map extraction, and tracking using state of the art method KLT algorithm. Our method has the ability to detect multiple objects in several scales, accurate, with reasonable speed. We evaluated our method by making experiments by aircraft tracking dataset. In this research we faced problems which they affected the tracking and detection processes. They come from camera movements which cause multiple detection of an airplane, very far away airplanes that they are observed very small, and occlusions.

For future, we have a plan to overcome the discussed problems and have a more reliable technique for tracking. Some training approach such as SVM would be useful to have an accurate tracking in presence of occlusion and other unwanted events. Furthermore, some features such as HOG would be significance for object recognition. Furthermore, some matching approach can be utilized. Detecting and tracking small flying objects are other problem that would be in our next research proceedings.

Table 1. Comparing tracking Results

	Tracking Accuracy	Process Time Per Frame
Our Method	86%	0.09
[3]	82%	0.09
GMM	80%	0.1
Kalman Filter + Appearance	79%	0.09
Mean Shift Clustering	80%	0.12

References

[1] D. H. H. Santosh, P. Venkatesh, L. N. Rao, and N. A. Kumar, "Tracking Multiple Moving Objects Using Gauusian Mixture Model", International Journal of Soft Computing and Engineering (IJSCE), Vol. 3, Issue 2, May 2013.

[2] J. Shi, and C. Tomasi, "Good features to track", IEEE Conference on Computer Vision and Pattern Recognition, pages: 593-600, 1979.

[3] A. S. Mian, "Realtime Visual Tracking of Aircrafts", Digital Image Computing: Techniques and Applications, 2008.

[4] A. Yilmaz, O. Javed, M. Shah, "Object Tracking: A Survey", ACM Computing Surveys, Vol. 38, No. 4, December 2006.

[5] B. Wu, and R. Nevatia, "Simultaneous Object Detection and Segmentation by Boosting Local Shape Feature based Classifier", IEEE Conference on Computer Vision and Pattern Recognition, Pages: 1-8, June 2007.

[6] D. Lowe, "Distinctive image features from scale-invariant key points", International Journal of Computer Vision, Vol. 60, Issue 2, 2004.

[7] N. Dalal, and B. Triggs, "Histograms of oriented gradients for human detection", IEEE Conference Computer vision and Pattern Recognition, Vol. 1, 2005.

[8] R. Szeliski, "Computer Vision: Algorithms and Applications", 2010.

[9] T. Brox, and J. Malik, "Large displacement optical flow: descriptor matching in vibrational motion estimation", IEEE Transaction on Pattern Analysis and Machine Intelligence, 2011.

[10] B. Lucas, and T. kanade, "An iterative image registration technique with an application to stereo vision", Internation Joint Conference on Artificial Intelligence, Pages: 674-679, 1981.

[11] H. Badino, U. Franke, C. rabe, S. Gehrig, "Stereo Vision-Based Detection of Moving Objects Under Strong Camera Motion", 1st International Conference on Computer Vision Theory and Applications, February 2006.

[12] B. Wu and R. Nevatia, "Detection and Segmentation of Multiple, Partially Occluded objects by Grouping, Merging, assigning Part Detection Responses", International Journal of Computer Vision, Vol. 82, Pages: 185-204, 2009.

[13] H. T. Nguyen and A. W. M. Smeulders, "Fast Occluded Object Tracking by a Robust Appearance Filter", IEEE Transactions on Pattern Analysis and Applications, Vol. 26, No. 8, 2004.

[14] Q. Liu, and G. Z. Peng, "A robust skin color based face detection algorithm", 2nd International Asia Conference on Informatics in Control, Robotics, Pages: 525-528, March 2010.

[15] M. Isard, and A. Blake, "Consideration – conditional density propagation for visual tracking", International Journal of Computer Vision, Vol. 29, Issue 1, Pages 5-28, 1998.

[16] D. Comaniciu, V. Ramesh, and P. Meer, "Kernel-based object tracking", IEEE Transaction on Pattern Analysis and Machine Intelligence, Vol. 25, Pages: 564-575, 2003.

Mohammad Anvaripour received Bachelor of Science in electrical engineering, Telecommunication, from Shiraz University in June 2006 and was graduated from Master of Science in electrical engineering, communication systems, from Sahand University of Technology of Tabriz in October 2010. He gained Iran Telecommunication Research center grant for his MS thesis in image processing and computer vision. He has several journal and conferences. He is working as researcher in ICT research center currently, and was one of the R&D members of the PayaSoft Company. His research interests are pattern recognition, image processing, and computer vision. He is member of International Association for Pattern Recognition (IAPR), Iranian Society of Machine vision and Image Processing (MVIP), and Member of Computer Society of Iran (CSI).

Ramin Shaghaghi Kandovan received the B.S. degree in electronic engineering from Tehran University, Tehran, Iran, in 1990 and M.S. and Ph.D. degrees in communication engineering from Islamic Azad University, Tehran, Iran, in 1993 and 2002, respectively. He is currently an Associate Professor in Communication Engineering Department of Islamic Azad University-Shahre Rey Branch. His research interests include Higher Order Statistics, security in communication networks, signal processing.

Sima Soltanpour received Bachelor of Science in electrical engineering, Electronic, from Amirkabir University of Technology (Tehran Polytechnic) at July 2005, and was graduated from Master of Science in electrical engineering, communication systems, from Sahand University of Technology of Tabriz at October 2010. She has several journal and conferences. Her research interests are pattern recognition, image processing, Biometrics. She is member of International Association for Pattern Recognition (IAPR), Iranian Society of Machine vision and Image Processing (MVIP).

166

A Low-Jitter 20-110MHz DLL Based on a Simple PD and Common-Mode Voltage Level Corrected Differential Delay Elements

Sarang Kazeminia*
Microelectronics Research Laboratory, Urmia University, Urmia, West Azerbaijan, Iran
s.kazeminia@urmia.ac.ir
Khayrollah Hadidi
Microelectronics Research Laboratory, Urmia University, Urmia, West Azerbaijan, Iran
kh.hadidi@urmia.ac.ir
Abdollah Khoei
Microelectronics Research Laboratory, Urmia University, Urmia, West Azerbaijan, Iran
a.khoei@urmia.ac.ir

Abstract

In this paper, a 16-phases 20MHz to 110MHz low jitter delay locked loop, DLL, is proposed in a 0.35μm CMOS process. A sensitive open loop phase detector, PD, is introduced based on a novel idea to simply detect small phase differences between reference clock and generated delayed signals. High sensitivity, besides the simplicity reduces the dead zone of PD and gives a better jitter on output generated clock signals, consequently. A new strategy of common mode setting is utilized on differential delay elements which no longer introduce extra parasitics on output nodes and brings the duty cycle of generated clock signals near to 50 percent. Also, small amplitude differential clock is carefully transferred inside the circuit to considerably suppress the noise effect of supply voltage. Post-Layout simulation results confirm the RMS jitter of less than 6.7ps at 20MHz and 2ps at 100MHz input clock frequency when the 3.3Volts supply voltage is subject to 75mVolts peak-to-peak noise disturbances. Total power consumption reaches from 7.5mW to 16.5mW when the operating frequency increases from 20MHz to 100MHz. The proposed low-jitter DLL can be implemented in small active area, around 380μm×210μm including the clock generation circuit, which is proper to be repeatedly used inside the chip.

Keywords: Delay Locked Loop; Clock Generation; Low-Jitter Clock Distribution; Wide-Range DLL; Low-Jitter DLL.

1. Introduction

Delay locked loops, DLLs, are broadly used for low-jitter multiphase clock generation, [1], [2] and [3]. Multiple operations within multitask mixed signal applications are regularly scheduled using a digital switching strategy on a single hardware. Recently, for example, single-stage analog comparators are proposed to perform three operations (reset, pre-amplification and latch) in a single hardware, [6], [7] and [8]. Also, the switching strategy of sample and holds (S/H) in high speed and high resolution analog to digital converters (ADCs) should be strictly considered to meet the desired resolution and jitter specifications through sampling. In low jitter applications, although PLLs can considerably reject the input clock jitter due to generating a fresh and low jitter clock by the VCO, however, smaller area and lower power consumption introduce DLLs as a proper choice when they are repeatedly used inside the chip. Furthermore, PLLs are regularly used for generation of very high frequency clock signals due to the inherent abilities of ring and LC oscillators. Whereas, DLLs are usually utilized to generate multiple phases of a middle frequency reference clock signal, manually generated inside or transferred into the chip.

Frequency-Phase detectors (Phase Detectors), PFDs (PDs), are known as the main building blocks of PLLs (DLLs), [10], which dominantly determine the sensitivity of closed loop structure. Reducing the dead-zone of PD dominantly improves the RMS and peak-to-peak jitter of DLL because this makes the loop to response to small phase differences. Hence, employing a sensitive PD is one of the main challenges of DLL design. This is highlighted when DLL is used in jitter sensitive applications, such as high resolution ADCs, when the RMS jitter of generated clock directly affects the dynamic behavior, (e.g., SNDR). The conventional phase detectors, [2] and [5], are constructed from positive feedback NAND gates which opposes against changing stored values on output nodes. Hence, larger phase differences are required at PD's inputs to firstly remove the previous data and secondly develop the new charge on output nodes of PD. This means larger dead zone and smaller sensitivity. Also, non-differential or pseudo-differential delay cells are applied in [2] and [5], in which the power supply noise can directly emerge on generated clocks and consequently diminish the RMS jitter.

In this paper, a low jitter DLL is proposed based on fully differential delay cells to considerably alleviate the supply noise on output generated clocks. A sensitive PD is introduced in section II to reduce the jitter besides the simplicity. Compatible charge pump and delay cells are also proposed in this section. Moreover, a simple strategy of common mode (CM) level setting is proposed to bring the generated phases around the middle point of supply and ground voltages. This CM setting strategy, no longer introduces extra parasitic capacitances on the output nodes of delay elements, and yields a better duty cycle, near 50 percent, when the outputs of delay elements are used via simple inverters. The strategy of transferring small signal input clock and generating full range reference clock inside the chip is discussed in section III. The duty cycle adjuster circuits, as used in [4], are not required when the combination of CM setting strategy and clock transferring is applied. Simulation results are shown in section IV and finally, section V concludes the paper.

2. Building Blocks of the Proposed DLL

Building blocks of the proposed DLL are illustrated in Fig.1. Eight differential delay elements are employed to provide 16-phases. Input reference clock and its complementary, Clk and Clkb, are applied to a PD as reference clocks. Also, the 180° delayed clock, Clk_180°, which is generated on one of the output nodes of delay cells, is fed back to PD to form the close loop structure of DLL. PD produces a digital pulse with the width of phase difference between digital inputs. Namely, generated pulse of PD is modulated with the phase difference. An analog charge pump is required to translate the generated digital pulse to analog control voltage, V_C, to be prepared for the next use by delay cells.
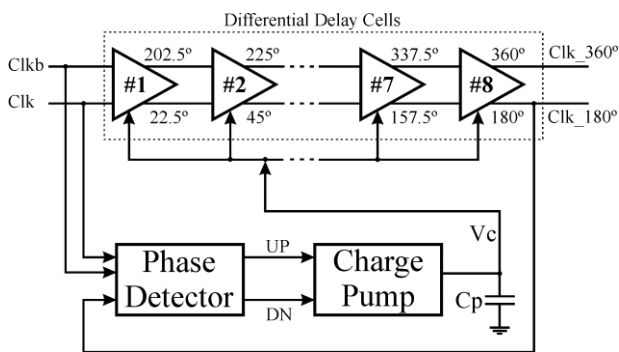
Fig. 1. Block Diagram of the Proposed DLL

V_C adjusts the delay of cells in close loop structure in such a way that no phase difference is remained on inputs of PD. Hence, 360° phase difference is expected through the cells. Propagating the same delays, 16 phases should be produced in 8 differential elements which means 22.5° phase shift between generated clocks in current and neighbor cells. To produce similar signal transitions on generated phases, equal capacitive loads are considered for all cells. Hence, dummy loads are required for other phases when Clk_180° is reused by PD.

2.1 Phase detector

The proposed phase detector is shown in Fig.2(a). Unlike the other similar works, three digital input signals are here used to detect the phase difference. PD can be divided into two main sections: the main core of phase detection which generates Q_2, and the pulse generator logic which provides UP and DN signals. As depicted in Fig.2(a), the main core of PD is constructed from two clocked inverters employed in master-slave configuration. Namely, Clk_180° is applied as input signal of a master-slave clocked buffer which is controlled by differential reference clocks, called Clk and Clkb. When the falling edge of Clk arrives before/after the falling edge of Clk_180°, high/low level of input voltage would be buffered to node Q_2. Signal transitions are also clarified in Fig.2(b).
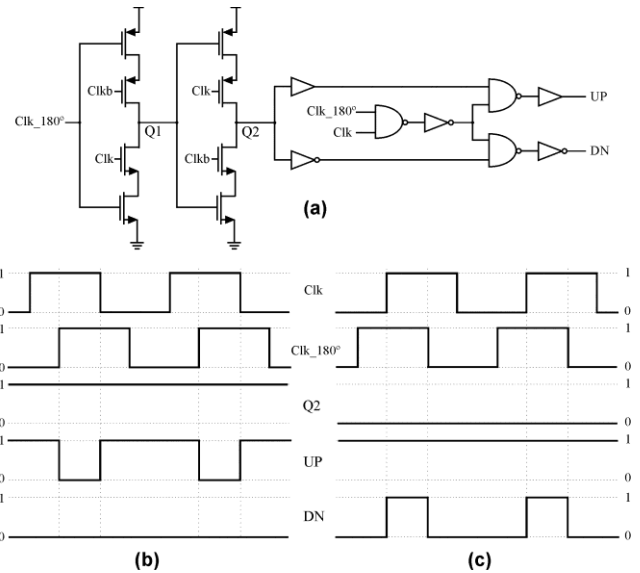
Fig. 2. (a) The Proposed Phase Detector, The Case of (b) Increasing and (c) Decreasing Delay

Hereafter, pulse generator generates narrow pulses of up and down operations. When Q_2 is set to high level voltage, pulls DN down to zero and produces the inverted overlap of Clk and Clk_180° at UP node. In the other case, as depicted in Fig.2(c), when Q_2 goes down to zero value, pulls the UP node up and produces the overlap of Clk and Clk_180° at DN output. The sensitivity of the proposed PD is only restricted by the required time for sampling in master clocked inverter as introduced as the main core in PD. In the other works, [2] and [5], where positive feedback structure is used for phase detection, a time portion should be allocated to overcome the positive feedback and remove the previous latched data.

2.2 Charge pump

The schematic of the compatible charge pump is illustrated in Fig.3 which provides the analog voltage based on generated pulses of PD, UP and DN. M_{p2} and M_{n2} are controlled by UP and DN signals. Detail description of charge pump behavior can be separately

surveyed for two cases of Fig.2(b) and 2(c). In the case (b), when the DN signal is set to zero, the discharge direction is closed and falling edges of UP signal opens the charge direction of the load capacitance through M_{p1} and M_{p2}. In the other case, when the falling edge of Clk_180° occurs before the falling edge of the sampling clock, Fig.2(b), UP goes up to high level voltage which disconnect the charging direction of the load capacitance. Furthermore, DN represents the overlap of Clk and Clk_180° which discharges the V_C via M_{n1} and M_{n2} when goes to high level. Decreasing V_C speeds up the delay elements.
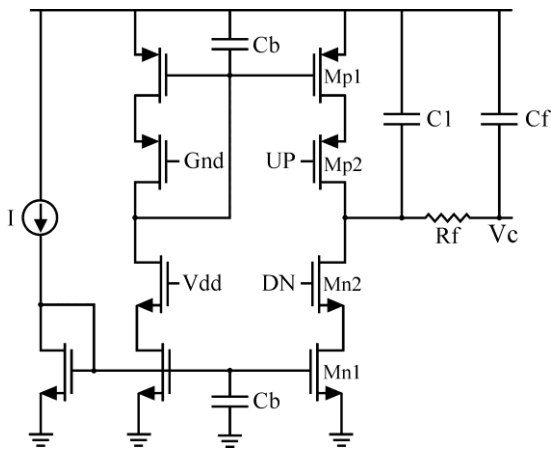
Fig. 3. Compatible Charge Pump and Low Pass Filter

2.3 Differential delay elements

Detail description of differential delay cells is shown in Fig.4 in which V_C determines the bias current. As depicted in Fig.4, increasing V_C slows down the delay elements due to decreasing the bias current. Bias adjusting is continued until the falling edge of reference Clock, Clk, corresponds on rising edge of Clk_180°, which means 180° phase shift. Due to the differential structure of delay elements in Fig.4, 360° phase shift is expected from Clk to Clk_360°. Differential structure of delay cells might encounter the problem of mismatch between up and down tail current sources. This might shift up or down the cross points of differential delayed signals from the middle of supply and ground voltages. If the outputs of delay elements are applied on inverter gates to drive other loads, the cross point should be adjusted near the threshold of a simple inverter gate. Otherwise, the duty cycle undesirably deviates from 50 percent at outputs of inverter gates. Hence, an internal feedback is required to adjust the cross points by compensating up and down tail current sources. The main concern of using regular common mode setting strategies is reducing the upper limit of operating speed due to introducing capacitive loads on output differential nodes. A new CM setting strategy is proposed which no longer introduce extra capacitive loads on output nodes. On the other hand, sensing the average value of differential outputs from output nodes of delay cells slows down the transitions of delayed clocks due to introducing extra parasitics. This

effect could be considered as an offset delay which restricts the speed of DLL.

Since the differential outputs of each cell are applied as the inputs of the next one, cross level is emerged on the average value of nodes X and Y due to the source follower combination of input devices in differential pair. Hence, the DC-level of each stage is sensed at the next one via two resistors, R_{CM}, and then is corrected by changing the up and down tail currents via M_{CMP} and M_{CMN}, as depicted in Fig.4. This means a simple averaging on generated clock signals without reducing speed. Considering a larger value for R_{CM}, however, a portion of tail current of differential pairs is inevitably used for CM level setting. M_{BN} and M_{BP} are employed to enhance the resolution of current mirror by providing the similar conditions for both bias and tail current sources.
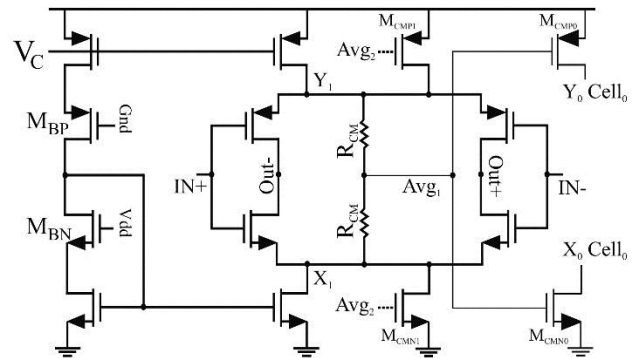
Fig. 4. Differential Delay Elements and DC-Level Setting Strategy

3. Generating Low-Jitter Reference Clock

Reference differential clocks, should be carefully transferred inside the chip. Hence, the circuit of Fig.5 is employed to alleviate the supply noise and generate low jitter reference clock. Ck and Ckb represent the smaller amplitude clock signals which should be transferred inside the chip and generate full range reference clocks, Clk and Clkb. The simple circuit of Fig.5(a) produces the filtered supply and ground, Vdd_FLTR and Gnd_FLTR, from noisy supply. M_1 and M_2 are NMOS and PMOS transistors which are selected in large size to play the role of low pass filter's capacitance along with R_1. The voltage drop across R_1 depends on the current drawn by the next devices which introduces a constraint on selecting R_1 value. M_3 and M_4 generate the threshold voltage of a simple inverter, TH, which is around the middle point of the differential supply range when M_3 and M_4 are properly scaled. Threshold voltages of the same size inverter gates are approximated to be identically varied at several corners. Hence, TH is also affected as the same as the threshold voltage of inverter gates at several corners to eliminate the dependency of the duty cycle to corner variations. This fact is here considered by generating TH through M_3 and M_4 and using as reference voltage. Hence, the duty cycle adjuster circuits, as used in [4], are not

required. As shown in Fig.5(b), a simple differential pair is applied to amplify the small amplitude of input differential clock around the DC-level which is set to threshold voltage of an inverter gate. M_5 and M_6 are also used as resistors to complete the DC-level setting strategy. Here, the filtered supply and ground are used as the differential supply of differential pair and inverters. Clk and Clkb are low jitter and full range reference clock signals which are generated in a reasonable duty cycle.
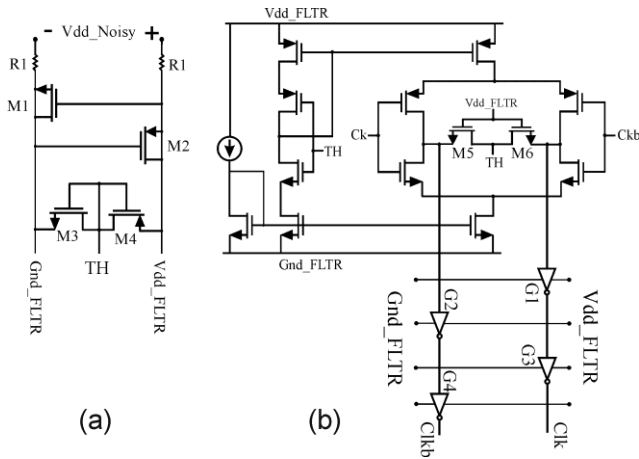
Fig. 5. Low-Jitter Reference Clock Generation via (a) Filtered Supply and Corner-Dependent Reference Generation, and (b) Full Range Recovery Circuit

4. Post-Layout Simulation Results

Layout pattern of the proposed DLL in a 0.35µm CMOS technology is illustrated in Fig.6 which confirms that the proposed 16-phases DLL could be implemented in about 380µm×210µm active area. The layout pattern of Fig.6 also includes the clock generator circuit of Fig.5.

Fig. 6. Layoutt Pattern of the Proposed DLL

Post-layout simulations of the proposed DLL are performed for the range of 20MHz to 110MHz operating frequencies. A peak-to-peak power supply noise of around 75mv is also constructed by a set of sinusoidal waveforms with different amplitudes and frequencies. Larger values of noise components are assigned to the amplitudes of the multiples of input clock frequency, to highlight the noise of clock coupling on the power supply lines. For example, amplitude of around 16mv, 10mv and 15mv are considered

for 20MHz, 40MHz and 60MHz frequencies, when the DLL is simulated at 20MHz. The noisy and the filtered supply of Fig.5(a) are illustrated in Fig.7(a) and 7(b). Settling behavior of the control voltage, V_C, is also depicted in Fig.7(c) at 20MHz operating frequency.
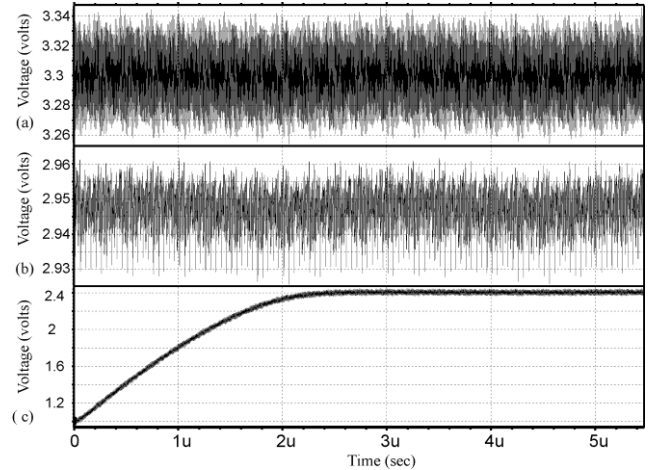
Fig. 7. (a) Noisy and (b) Filtered Vdd, (c) Control Voltage at 20MHz

After settling, 16 phases are generated through 8 differential delay cells as depicted in Fig.8 in which the delay time of generated phases differs from the neighbor one, equal to 1/16 of the period time of the reference clock. The generated phases at 20MHz are illustrated in Fig.8. which all are differed 22.5 degrees from each other.
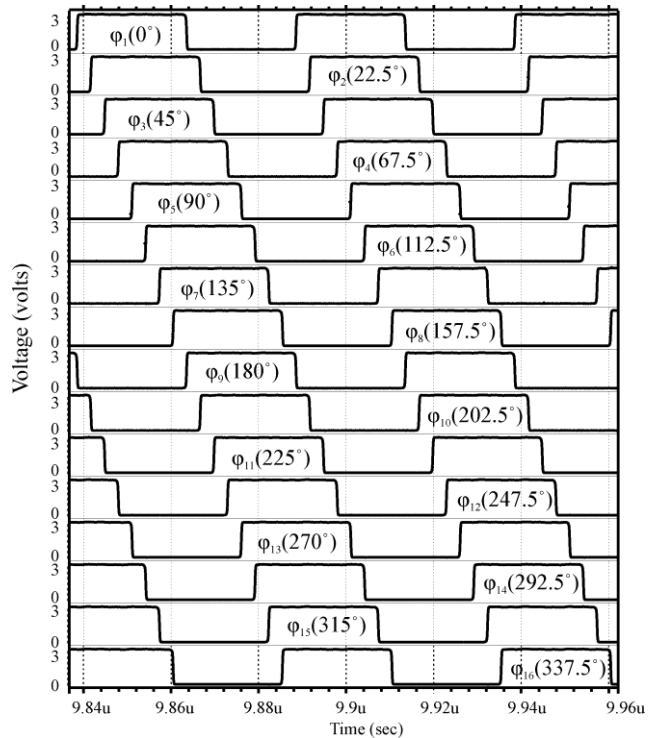
Fig. 8. All Generated Phases at 20MHz Operating Frequency

Settling behavior of V_C is also shown in Fig.9 at 100MHz operating frequency. As discussed earlier, V_C is expected to settle to smaller values when the operating frequency is increased.

Input clock jitter would not be eliminated in DLL's output, meanwhile, PLLs can suppress the input clock jitter due to providing a new and fresh clock on VCO's output. Firstly, a low-jitter input clock signal is utilized as reference clock to qualify the jitter of the proposed DLL when supply is subject to around 75mv peak-to-peak noise voltage. Noise harmonics are manually weighted at multiples of the fundamental clock frequency as expected in real test conditions. Firstly, the circuit of Fig.5(b) is simulated to qualify the jitter behavior of full-range clock inside the chip, in presence of 75mv peak-to-peak noise on supply voltage. The eye diagram of small amplitude clock, ck and ckb, and generated full range signals, clk and clkb, are illustrated in Fig.10 at 100MHz input clock frequency, when the supply voltage is subject to 75mv peak-to-peak noise. Jitter histogram of the generated full-range clock is also illustrated in which the peak-to-peak and RMS jitter of 10.4ps and 2.1ps are obtained, respectively.

Eye diagram and jitter histogram is evaluated for one of outputs at 100MHz operating frequency. Results are illustrated in Fig.11 which shows around 11ps and 2ps peak-to-peak and RMS jitter, respectively. Simple comparison between reference clock and generated outputs, clarifies that the RMS jitter of input clock would be similarly emerges on outputs in DLL loop structure.

To evaluate this claim, a manual peak-to-peak jitter of around 2.3ns is applied on reference input clock which represents the RMS jitter of around 58ps on small amplitude reference signals. As illustrated in Fig. 11 peak-to-peak jitter of output generated clock is similarly increased when the reference clock is encountered to jitter disturbances. Hence, suppressing the supply noise is the main challenge of designing low-jitter DLLs.
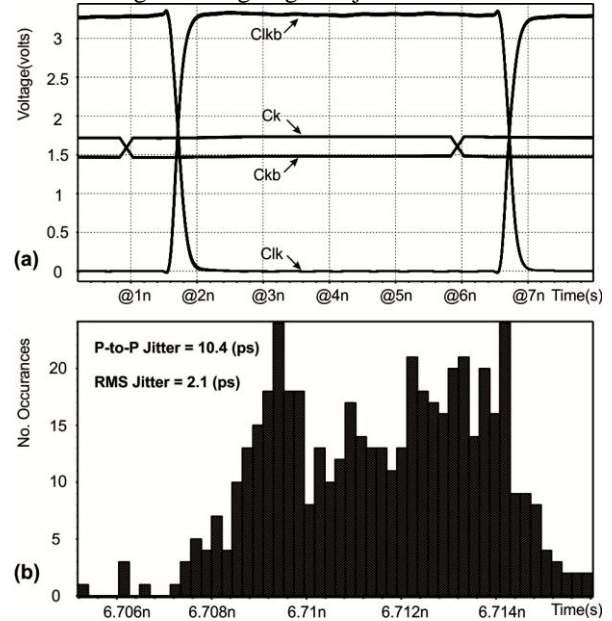
Fig. 10. (a) Eye diagram of Small Amplitude Input and Generated Full-Range Reference Clock (b) Jitter Histogram of Full-Range Reference Clock. @100MHz in Presence of 75mv Peak-to-Peak Supply Noise

Fig. 9. The Control Voltage and Generated Phases at 100MHz
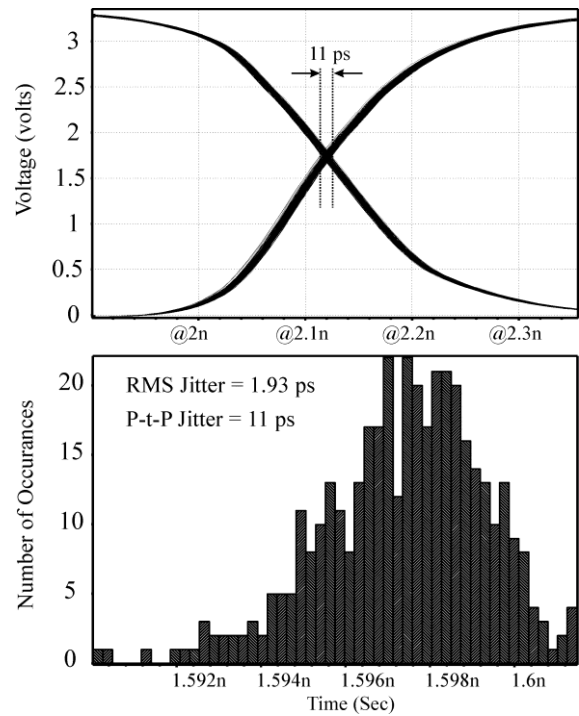
Fig. 11 Eye Diagram and Jitter Histogram of Differential Output Clocks at 100MHz Operating Frequency in Presence of 75mv peak-to-peak Supply Noise
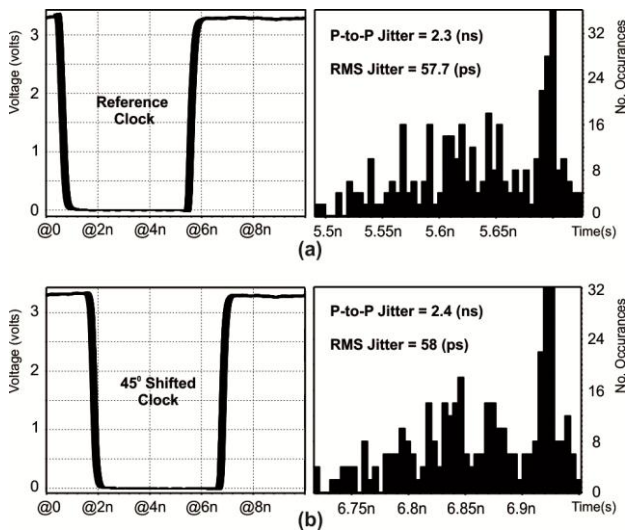
Fig. 12. Eye Diagram and Jitter Histogram of (a) Input Jittery Reference Clock (b) 45º Generated Clock, in Presence of 75mv Peak-to-Peak Supply Noise and 2.3ns Peak-to-Peak Jitter on Input Reference Clock

Table 1 summarizes the DLL specifications for 20MHz, 50MHz, 80MHz and 100MHz operating frequencies when the supply is subject to 75mv peak-to-peak noise. As shown, the value of V_C is decreased for higher operating frequencies.

Table 1. DLL Specifications at Different Operating Frequencies

	20 MHz	50 MHz	80 MHz	100 MHz
RMS Jitter (ps) @75mv p-t-p Supply Noise	6.7	5	4.5	2
Power Consumption (mW)	7.6	10.5	14.2	16.5
Control Voltage, V_C (volts)	2.4	2.1	1.85	1.45

5. Conclusions

A low-jitter 20MHz-110MHz DLL is proposed based on a simple and sensitive open loop phase detector. Also, a simple strategy of cross couple setting is introduced on differential outputs to provide 50% duty cycle digital signals. Hence, the duty cycle adjustment block is not required. The strategy of transferring low-noise reference clock signals inside the chip has been also discussed.

Table 2 compares the proposed DLL with other similar works. Small Active area and power consumption, introduces the proposed DLL as a proper choice when the DLL should be repeatedly used inside a chip. Furthermore, the maximum operating frequency is reversely proportional to the number of delay cells in closed loop structure. Namely, smaller delay values are expected from each delay cell, when the loop is constructed from further number of delay elements in similar conditions. Hence, the maximum operating frequency is reduced in this work.

Table 2. Comparison Table

	[2]	[4]	[5]	This work
Process (µm)	0.5	0.25	0.6	0.35
Maximum Operating Frequency (GHz)	1	0.4	0.22	0.11
Supply (volts)	2	2.5	3.3	3.3
No. Phases	9	8	15	16
PtP Jitter (ps) @Supply Noise	20 N.A	54 Quiet	49 N.A	11 @75mv
RMS Jitter (ps) @ Supply Noise	3.2 N.A	6.7 Quiet	6.4 N.A	2 @75mv
Power(mW)	33	60	33	16.5
Area (mm²)	0.6	0.13	0.45	0.08

References

[1] X. Gao and et Al., "Advantages of Shift Registers Over DLLs for Flexible Low Jitter Multiphase Clock Generation", IEEE Transaction on Circuits and Systems-II, Vol. 55, No. 3, March 2008.

[2] D. J. Foley and et Al., "CMOS DLL-Based 2-V 3.2-ps Jitter 1-GHz Clock Synthesizer and Temperature Compensated Tunable Oscillator", IEEE Journal of Solid-State Circuits, Vol. 36, No. 3, March 2001.

[3] G. Dehng and et Al., "Clock-Deskew Buffer Using a SAR-Controlled Delay-Locked Loop", IEEE Journal of Solid-State Circuits, Vol. 35, No. 8, August 2000.

[4] Y. Jung and et Al., "A Dual-Loop Delay-Locked Loop Using Multiple Voltage-Controlled Delay Lines", IEEE Journal of Solid-State Circuits, Vol. 36, No. 5, May 2001.

[5] J. Kim and et Al., "A Low-Jitter Mixed-Mode DLL for High-Speed DRAM Applications", IEEE Journal of Solid-State Circuits, Vol.35, No.10, October 2000.

[6] S. Kazeminia, M. Mousazadeh, Kh. Hadidi and A. Khoei, "High-speed low-power Single-Stage latched-comparator with improved gain and kickback noise rejection", IEEE Asia Pacific Conference on Circuits and Systems, APCCAS 2010. Page(s): 216 – 219

[7] S. Kazeminia, M. Mousazadeh, Kh. Hadidi and A. Khoei, "A 500MS/s 600µW 300µm2 Single-Stage Gain-Improved and Kickback Noise Rejected Comparator in 0.35µm 3.3v CMOS Process", IEICE Transactions on Electronics, Vol. E94.C, No. 4, April 2011, pp. 635-640

[8] S. Kazeminia, O. Shino, E, Haghighi and Kh. Hadidi, "Improved Single-Stage Kickback-Rejected Comparator for High Speed and Low Noise Flash ADCs", 21th European Conference on Circuit Theory and Design, ECCTD 2013, Accepted and wild be published on Sep. 2013.

[9] S. Kazeminia, Kh. Hadidi, A. Khoei, "A Low Jitter 110MHz 16-Phase Delay Locked Loop Based on a Simple and Sensitive Phase Detector", 21th Iranian Conference on Electrical Engineering, ICEE, May 2013.

[10] B. Razavi, "Design of Analog CMOS Integrated Circuits", Boston, MA: McGraw-Hill, 2001, Chapter 11, pp: 377-389.

Sarang Kazeminia was born in 1982, Tonekabon, Iran. He received BS degree in Electrical engineering from Isfahan University of Technology, (IUT), Isfahan, Iran, 2004, MS degree in Electrical engineering from Urmia University, Urmia, Iran, 2007. He is currently working on high speed and high resolution A/D converters, towards the Ph.D. degree in electrical engineering at Microelectronics Research Laboratory of Urmia University. His research interests are high speed high resolution digital to analog and analog to digital converter design, low jitter clock generation, DLL, PLL and Bandgap reference Design.

Khayrollah Hadidi received his BS degree from Sharif University of Technology in Tehran, Iran, his MS degree from polytechnic University, New York, and his Ph.D. degree from University of California, Los Angeles, all in electrical engineering. His research interests are high speed high resolution data converter design, wideband integrated filter design, and nonlinearity analysis and improvement in analog circuits. He is currently with Electrical Engineering Department and Microelectronics Research Laboratory in Urmia University, Urmia, Iran. He holds one US patent (issued), and one US plus 12 Japanese patents (pending).

Abdollah Khoei was born in Urmia , Iran. He received BS, MS and Ph.D. degrees in electrical engineering from North Dakota State University, USA, in 1982, 1985, 1989, respectively. His research interests are analog and digital integrated circuit design for fuzzy and neural network applications, fuzzy based industrial electronics, and DC-DC converters for portable applications. He is currently with Electrical Engineering Department and Microelectronics Research Laboratory in Urmia University, Urmia, Iran..

Enhancing Efficiency of Software Fault Tolerance Techniques in Satellite Motion System

Hoda Banki
Department of Electrical and Computer Engineering, University of Kashan, Isfahan, Iran
banki@grad.kashanu.ac.ir

Seyed Morteza Babamir
Department of Electrical and Computer Engineering, University of Kashan, Isfahan, Iran
babamir@kashanu.ac.ir

Azam Farokh
Department of Electrical and Computer Engineering, University of Kashan, Isfahan, Iran
farokh@grad.kashanu.ac.ir

Mohammad Mehdi Morovati*
Department of Electrical and Computer Engineering, University of Kashan, Isfahan, Iran
morovati@grad.kashanu.ac.ir

Abstract

This research shows the influence of using multi-core architecture to reduce the execution time and thus increase performance of some software fault tolerance techniques. According to superiority of N-version Programming and Consensus Recovery Block techniques in comparison with other software fault tolerance techniques, implementations were performed based on these two methods. Finally, the comparison between the two methods listed above showed that the Consensus Recovery Block is more reliable. Therefore, in order to improve the performance of this technique, we propose a technique named Improved Consensus Recovery Block technique. In this research, satellite motion system which known as a scientific computing system is consider as a base for our experiments. Because of existing any error in calculation of system may result in defeat in system totally, it shouldn't contains any error. Also the execution time of system must be acceptable. In our proposed technique, not only performance is higher than the performance of consensus recovery block technique, but also the reliability of our proposed technique is equal to the reliability of consensus recovery block technique. The improvement of performance is based on multi-core architecture where each version of software key units is executed by one core. As a result, by parallel execution of versions, execution time is reduced and performance is improved.

Keywords: Software Fault Tolerance; Multi-core; Parallel Execution; Consensus Recovery Block; N-version Programing; Acceptance Test.

1. Introduction

Nowadays the influence of software on different domains such as economics, medicine, aerospace and so on is quite sensible. One of the main requirements of these systems is safety and reliability of software. According to the importance of software reliability, demand for using fault tolerance techniques in software development have increased significantly. Design diversity is one of the fault tolerance methods which needs to run multiple versions of the program [1]. software fault tolerance techniques increase software reliability, on the other hand by increasing number of versions of the program, execution time increases at the same time and this will reduce the performance. by taking advantages of distributed and parallel processing systems, the efficiency is increased and thus the cost of using these systems will be acceptable. Using the multi-core architecture is a good idea for taking advantage of parallel processing.

Based on the idea of software fault tolerance, for some software key units in a system, N versions can be developed separately with similar functionality [2]. The purpose of design diversity is constructing independent modules as many as possible and minimizing occurrence of identical errors in these modules [3]. All versions are executed with identical initial conditions and inputs. Output of all versions is given to a decision module and the decision module selects a unique result as a correct output.

The paper continues as follow: section 2 introduces N-version programming and recovery block and their derivative techniques. Section 3, introduces satellite motion system as a case study. Section 4, discusses the usage of multi-core architecture in fault tolerance techniques. Implementation results are reviewed in Section 5 .the proposed method is presented in Section 6 and finally in Section 7 conclusions are discussed.

2. Software Fault-Tolerance Techniques

In this section some fault tolerance techniques are introduced.

---

* Corresponding Author

2.1 N-version programing technique

Using different algorithms and designs, Most program functions can be performed in various ways. A program version denoting a separate implementation of a program function is called a variant. Each variant has a varying degree of efficiency in terms of memory management and utilization, execution time, reliability, and other criteria.

N-version programming (NVP) technique is one of the main techniques of software fault tolerance. In this technique, N different versions of a module are implemented and executed concurrently (simultaneously). Then the results will be presented to a decision module and this module selects the correct result [3]. The decision module examines the results and selects the "best" one if exists. There are other available alternative decision mechanisms. For example one decision mechanisms is majority voter. The NVP algorithm technique is shown in Fig. 1.

```
run Version 1, Version 2, …, Version n
if (Decision Mechanism (Result 1, Result 2, …, Result n)
        return Result
else failure exception
```

Fig. 1. N-version programming technique algorithm

Other augmentations, enhancements, and combinations have been made to the NVP techniques. These are typically given an entirely new name rather than being called an extension to the NVP technique. Some of these techniques are described in the following.

2.2 N-version programing-Tie broker technique

In order to improve the performance of NVP technique, N-version programming-Tie Broker (NVP-TB) technique has been developed whose strategy is to synchronize the versions. In this technique, assuming that three versions of software key unit are developed, when the results of two faster versions are produced, it does not wait for the slowest version anymore. In other words, when the two faster versions, complete their execution, their results will be compared and one of the results is returned as a correct result if they match, otherwise, it waits for the result of slowest version and then the correct result is determined by decision mechanism [4]. The algorithm of this technique is represented in Fig. 2.

```
run Version 1, Version 2, Version 3
if (Comparator (Fastest Result 1, Fastest Result 2) )
        return Result
else Wait ( Last Result)
            if (Voter (Fastest Result 1, Fastest Result 2, Last Result) )
                return Result
else error
```

Fig. 2. N-version programming-Tie broker technique algorithm

2.3 N-version programing-Acceptance test technique

To reduce the probability of selecting an incorrect result, Tai and his colleagues added an acceptance test to the NVP technique. In this technique, after the decision mechanism selects one of the results as the correct one, this result is passed to the acceptance test for checking its correctness in order to increase the reliability [4]. The N-version programing-Acceptance test technique is represented in Fig. 3.

```
run Version 1, Version 2, Version 3
if (Voter (Result 1, Result 2, Result 3) )
        If (Acceptance Test (Result))
            return Result
else error
```

Fig. 3. N-version programming-Acceptance test technique algorithm

2.4 N-version programing-Tie broker- Acceptance test technique

Because the two modified NVP techniques are complementary, N-version programming-Tie Broker-acceptance test (NVP-TB-AT) technique has been developed to concentrate on both reliability and performance. Actually, this technique is a combination of NVP-TB technique and acceptance test. Acceptance test is used to increase the reliability which will cause the execution time to increase and thus the performance will be reduced. But by using the Tie-broker technique, reduction of performance is compensated. As a result, not only this technique has higher performance than NVP-AT, but also has reliability equal to NVP-AT[5]. The N-version programing-Tie broker Acceptance test is explained in Fig. 4.

```
run Version 1, Version 2, Version 3
if (Comparator (Fastest Result 1, Fastest Result 2) )
        return Result
else Wait ( Last Result)
            if (Voter (Fastest Result 1, Fastest Result 2, Last Result) )
                If (Acceptance Test (Result))
                    return Result
else error
```

Fig. 4. N-version programming-Tie broker-Acceptance test technique algorithm

2.5 Recovery block technique

Recovery block (RcB) technique is one of the main techniques of software fault tolerance. This technique works in a way that different versions are prioritized in order of their importance; then they is run in order of their preferences. In other words, RcB incorporates these variants such that the most efficient module is located first in the series, and is called the primary alternate or primary try block. Acceptance or rejection of each version is identified by acceptance test module. At first, the overall situation of system is stored. if no versions can successfully pass the acceptance test, the system is returned to the saved state and then the next module will run [3]. If no alternates are successful, an error occurs. The algorithm of RcB technique is shown in Fig. 5.

```
ensure              Acceptance Test
by                  Primary Alternate
else by             Alternate 2
else by             Alternate 3
…
else by             Alternate n
else failure exception
```

Fig. 5. Recovery block technique algorithm

2.6 Distributed recovery block technique

Distributed recovery block (DRB) technique, is the distributed version of RcB technique in which several recovery blocks are implemented in several systems. the only difference between these blocks is the priority of modules [6].

The basic DRB technique consists of a primary node and a shadow node, each cooperating with each other and running an RcB scheme. In DRB, the recovery blocks are concurrently executed on both nodes. The initial primary node executes the primary algorithm and the initial shadow node executes the alternate alternative one. First, the technique attempts to ensure that the primary algorithm on node 1's results passes the AT (i.e., produces a result which passes the test. If this result fails the AT, then the DRB tries the result from the alternate algorithm on node 2. If neither passes the AT, then backward recovery is used to execute the alternate on Node 1 and the primary on Node 2. The results of these executions are checked to ensure the AT. If neither of these results passes the AT, then an error occurs. If any of the results are successful, the result is passed on to the successor computing station.

2.7 Consensus recovery block technique

The consensus recovery block (CRB) technique is a combination of NVP and RcB., at first NVP runs and if it fails to produce the correct result, recovery Block runs and produces the correct result[3]. The consensus recovery block technique is represented in Fig. 6.

```
Run Ranked Version 1, Ranked Version 2, …, Ranked Version n
If (Decision Mechanism (Result 1, Result 2, …, Result n ) )
            return Result
else
        ensure              Acceptance Test
        by                  Ranked Version 1 [Result]
        else by             Ranked Version 2 [Result]
        …
        else by             Ranked Version n [Result]
        else raise failure exception
return Result
```

Fig. 6. Consensuse Recovery block technique algorithm

When two or more correct answers exist for the same problem and the same input, we have multiple correct results (MCR). NVP in general and voting-type decision algorithms in particular, are not appropriate for situations in which MCR may occur. It is claimed that the CRB technique reduces the importance of the AT used in the RcB. CRB is Also able to handle cases in which NVP would not be appropriate because of MCR.

3. Acceptance Test

Acceptance Test (AT) is the most basic approach to self-checking software (Fig. 7), which typically is used with the RcB, CRB and DRB techniques. The AT is used to verify the acceptance of the systems behavior based on the assertion on the anticipated system state.

As shown in Fig. 7, a value of TRUE or FALSE is returned. The AT needs to be simple, effective, and highly reliable in order to: (1) decrease the chance of additional design faults, (2) keep run-time overhead reasonable, (3) ensure detection of the anticipated faults and (4) ensure that a non-faulty behavior would not incorrectly be detected.
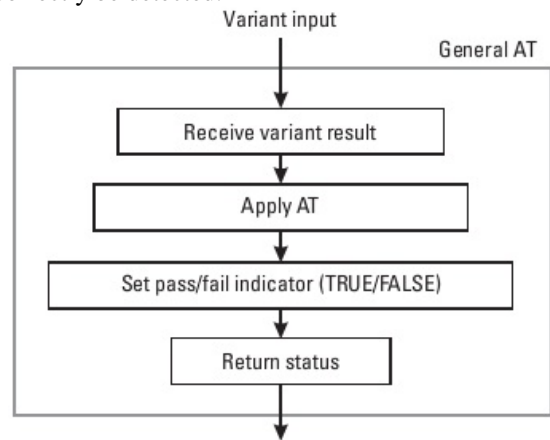
Fig. 7. Acceptance test functionality.

ATs can thus be difficult in development depending on their specifications. Also, the form of an AT depends on its application. The coverage of an AT is an indicator of its complexity, where an increase in coverage generally requires a more complicated implementation of the test. Increasing the complexity leads to increasing the time of programs execution and fault manifestations [3,7].

4. Satellite Motion System

In this section the satellite motion system, which is used in scientific computing, is introduced as a case study. The calculation of satellite motion is the most critical part of the satellite control system; so, errors in this part lead to failure of entire system. The geodetic satellites have two major missions: (1) positioning in geodesy or (2) to be used as a sensor for measuring the external gravity field of the Earth. In order to increase the reliability of this part, the fault-tolerant software techniques were utilized. Satellite motion equation is represent in Eq.(1)[8]. The analytical solution of this differential equation leads to the Kepler orbit [9].

$$\ddot{\vec{r}} = -\frac{GM}{\left|\vec{r}^3\right|}\vec{r} + K$$

(1)

The satellite motion equation is a second order vector differential equation; therefore it has to be converted to a first order differential equation that is represent in Eq. (2) [8].

$$\ddot{\vec{r}} = -\frac{GM}{|\vec{r}^3|}\vec{r} + K \rightarrow \begin{cases} \ddot{x} = -\dfrac{GM}{|\vec{r}|^3}\vec{x} + K_x \\[2mm] \ddot{y} = -\dfrac{GM}{|\vec{r}|^3}\vec{y} + K_y \Rightarrow \\[2mm] \ddot{z} = -\dfrac{GM}{|\vec{r}|^3}\vec{z} + K_z \end{cases}$$

$$\Rightarrow \begin{cases} v_x = \dot{x} \\[1mm] v_y = \dot{y} \\[1mm] v_z = \dot{z} \\[1mm] \dot{v}_x = -\dfrac{GM}{|\vec{r}|^3}x + K_x \\[3mm] \dot{v}_y = -\dfrac{GM}{|\vec{r}|^3}y + K_y \\[3mm] \dot{v}_z = -\dfrac{GM}{|\vec{r}|^3}z + K_z \end{cases}$$

(2)

Where, r is the position vector, GM is the product of gravitational constant and Earth's mass, k is the effects of all the perturbing forces on a satellite. Since the equation is a second order three-dimensional differential equation, it could be solved numerically using methods such as Runge-Kutta, Adams-Bashforth and Adams-Moulton. In this paper, various implementations of these methods are used as different versions of fault-tolerant techniques.

Ruge-Kutta, Adams-Bashforth and Adams-Moulton are the most common methods for solving first order differential equations numerically. Runge-Kutta (Eq .(3),(4) and (5)) solves these equations in single-phase, while Adams-Bashforth (Eq. (6) and (7)) and Adams-Moulton (Eq. (6) and (8)) solve it in multi-phase.

$$y' = f(x, y)$$

(3)

$$\begin{cases} k1 = hf(x_n, y_n) \\[2mm] k2 = hf(x_n + \dfrac{h}{2}, y_n + \dfrac{k1}{2}) \\[2mm] k3 = hf(x_n + \dfrac{h}{2}, y_n + \dfrac{k2}{2}) \\[2mm] k4 = hf(x_n + h, y_n + k3) \end{cases}$$

(4)

$$y_{n+1} = y_n + \frac{h}{6}(k1 + 2k2 + 2k3 + k4)$$

(5)

$$\begin{cases} y'(t) = f(y, t) \\ y(t_0) = y_0 \end{cases}$$

(6)

$$y_n = y_{n+1} + h\sum_{i=0}^{n-1}\xi_i^p f(t - (1+i)h, y_i)$$

(7)

$$y_n^c = y_{n-1} + h\sum_{i=0}^{n-1}\xi_i^c f(t - ih, y_{i+1})a$$

(8)

5. Multi-Core Architecture Usage

In a single-core platform, only one thread is running at a certain time point. But In a multi-core platform, there can be several threads which are running on different cores at the same time. So in the multi-core architecture, threads which are created to run the program, really run in parallel on a multi-core platform. Therefore synchronization issues and the cost for communication among cores are discussed. If the extra cost is quite considerable compared to the normal single core execution cost , such applications are not suitable for the multi-core architecture [9].

A software system is composed of a series of software key and non-key units (Fig. 8). Each software system includes critical and important parts in which occurrence of error leads to the system failure whose cost cannot be compensated. These critical and important parts are called software key units and other sections are non-key units[2].
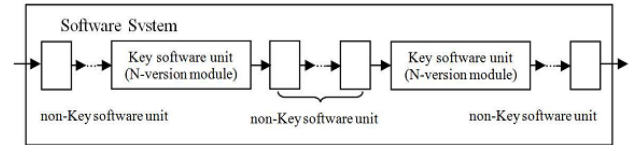
Fig. 8. non-Key software unit and key software unit

One way to increase fault tolerance is using different versions and deployment of fault tolerance techniques. But since the development of different versions of the entire system is very costly, several different versions that have different implementations are developed only for software key units. Since the key units have several versions which lead to increase of the execution time, we use multi-core architecture features to reduce time and run the versions on different cores in parallel. This approach reduces execution time and thus increases the performance. In comparison with the high cost of the sequential program, the cost of synchronization and communication between the cores is negligible [2].

6. Implementation and Results of Multi-Core Usage

The effect of multi-core architecture on increasing performance of the NVP technique has been discussed by Yang et al [10]. In this paper we discuss the effect of multi-core architecture on techniques derived from the NVP, DRB, CRB and improved consensus recovery block. In this paper, fault-tolerance techniques have been used to increase reliability; so, different implementations of numerical methods for solving differential equations of the satellite motion were used as different versions in fault tolerance techniques. Accordingly, Runge-Kutta, Adams-Bashforth and Adams-Moulton methods are implemented as different versions.

In other words, in each technique we execute different versions on single and multi-core architecture and then

compare execution times on the single core with the multi-core. Finally, we offer a new technique to reach a higher performance where the execution times of techniques are significantly decreased using the multi-core architecture. As shown in Fig. 9, the speedup rate of the NVP technique for dual and quad core processors is 1.73 and 2.42 respectively. Because the reliability on this technique is low the NVP-TB-AT Technique is used instead. The speedup rate of this technique is 1.70 and 2.06 for dual and quad core processors respectively. The effect of multi-core architecture on performance of the RcB technique is shown in Fig. 10.

Fig. 9. Execution time of NVP technique and derived technique

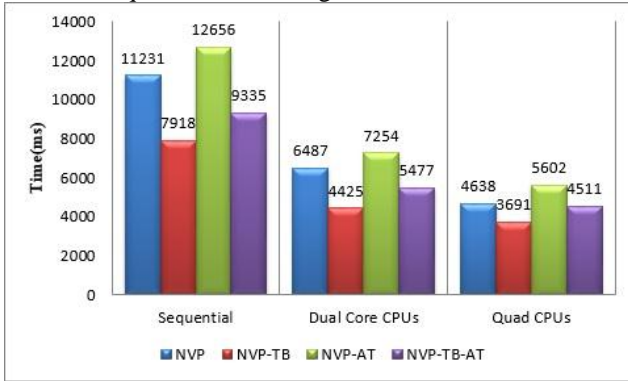The RcB technique execution time on single core, dual core and quad core are 11266, 6413 and 4718 respectively. In single core architecture, all versions are executed sequentially; so the execution time is longer than other ones. For example, in our implementation the execution time of each version is equal to 1945, 2356 and 1872 respectively. This means that the execution time of RcB technique on single core is about sum of all these times. In order to apply advantage of parallelism, we can use distributed version of this technique named Distributed Recovery Block (DRB). The DRB technique has 1.76 and 2.39 speedup rate using dual and quad core processors. Shown in Fig. 10, the execution time improvement for quad core architecture is more than dual core architecture in the case of parallelism. In other words by increasing the number of cores, an improvement of the performance is expected.
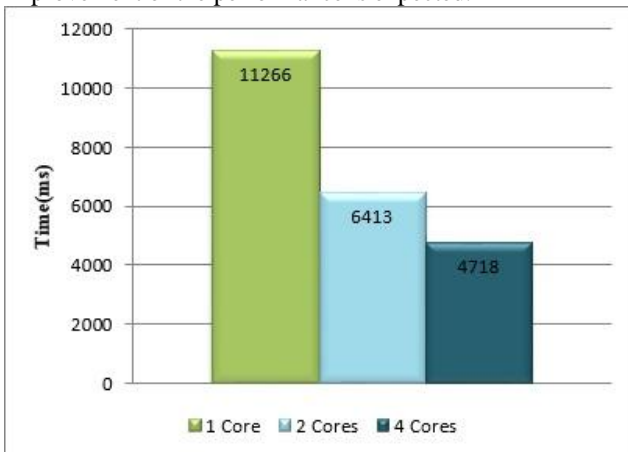

Fig. 10. Efect of multi-core architecture on performance of recovery block technique

7. Suggested Technique (Improved Consensus Recovery Block)

while using NVP-TB-AT, if the result of two faster versions were equal, one of them would be announced as the correct result and no acceptance test is performed on the results [5]. So if there is an error in the system that causes the result of two faster versions be similar and wrong, probability of the overall system failure increases using this technique. Thus this technique is less reliable than RcB technique, because in RcB technique the result goes to the acceptance test module in any conditions to be returned as a correct result. Also, if a program had several correct answers, the NVP-TB-AT technique might face failure. If both faster versions produce correct but different results, the voter waits for the slowest version and judges between results of two faster versions and result of slowest version using the decision mechanism. If the lowest version has a correct but a different result than results of faster versions, the voter cannot decide and system will face failure. But, if the RcB technique is used and the program has several correct results, system does not fail because the AT is applied to every version and so the correct result will be determined. Order of this technique is shown by Eq. (9) and (10).

$$
\begin{cases}
Versions = V_1, V_2, \dots, V_n \\
V = Nmber\ of\ Versions \\
C = Number\ of\ Cores \\
Order\ of\ Versions = f(V_1), f(V_2), \dots, f(V_n) = F_1, F_2, \dots, F_n \\
f(V) = The\ Slowest\ Version \\
S = \dfrac{V}{C} \\
Q(V) = F_1, F_2, \dots, F_n
\end{cases} \quad (9)
$$

$$ RcB - Order = O(Q(V)) $$

$$
NVP - Order =
\begin{cases}
O\left(\dfrac{Q(V)}{C}\right) & if\ C \le V \\
O\left(\dfrac{Q(V)}{V}\right) & if\ C > V
\end{cases} \quad (10)
$$

$$ DRB - Order = O(S \times f(V)) $$

$$ CRB - Order = O((NVP - Order) + (RcB - Order)) $$

$$ ICRB - Order = O((NVP - Order) + (CRB - Order)) $$

As mentioned in Section 2, different versions of RcB technique are executed consecutively. Accordingly, the RcB technique order is calculated by sum of all versions time order. In the NVP technique, time order is related to the number of versions and available cores because of running versions simultaneously. In other words, if available cores are more than the number of versions, increasing the number of cores will be ineffective on decreasing time order. On the other hand, while the available cores are equal to or less than the number of versions, increasing the number of cores leads to decrease of time order.

In the DRB technique, the execution steps of versions are computed based on relationship between the number of versions and nodes (primary and shadow nodes). This means that the arrangement for running versions considers that all versions can be performed by minimum steps. Moreover, according to concurrent execution, time order of this technique always depends on the slowest version. So, the DRB technique time order is determined by product of the number of cases in which all versions are executed and time order of the slowest version.

Since the CRB technique is a merger of the NVP and RcB techniques, the proposed technique is a combination of NVP and DRB techniques and the time order of these two techniques are computed using sum of constituent techniques time order.

On the other hand, the performance of the RcB technique is largely dependent on the performance of acceptance test. While in many cases, creation of the acceptance test module is very difficult, the CRB technique decreases the importance of acceptance test more than the RcB one. Also, the NVP technique will not be able to produce the final result when the problem has several correct answers. So, the RcB and NVP techniques have drawbacks in some cases which the CRB has resolved by combining two techniques discussed above.

According to superiority of CRB technique over other techniques, we concentrate on it and in order to improve its performance, we have proposed a technique which is similar to CRB technique and called Improved Consensus Recovery Block. In execution of CRB, first the NVP section tries to produce the correct result. If decision module was able to produce the result, the technique terminates. Otherwise, the second section namely recovery block will execute to produce the correct result. Since the execution of recovery block is sequentially, the execution time is increased. The recovery block does not use multi-core facility and therefore does not take advantage of parallel processing. In this paper, in order to take full advantage of multi-core facilities and reduce the execution time of the CRB technique, we try to use Distributed Recovery Block (DRB) instead of RcB.

Fig. 11 shows the proposed algorithm where the first versions are executed simultaneously through NVP technique and their result is given to a voter. If the voter can produce a correct result, it returns the result. Otherwise, different versions are executed through DRB technique.

```
Run Ranked Version 1, Ranked Version 2, …, Ranked Version n
If (Decision Mechanism (Result 1, Result 2, …, Result n ) )
          return Result
else
     run          RB1 on Node 1 (Initial Primary) ,
                       RB2 on Node 2 (Initial Shadow)
     ensure    AT on Node 1 or Node 2
     by           Primary on Node 1 or Alternate on Node 2
     else by     Alternate on Node 1 or Primary on Node 2
else failure exception
```

Fig. 11. Improved consensus recovery block technique algorithm

Influence of the multi-core architecture on performance of the CRB technique is shown in Fig. 12. Different implementations of numerical methods for solving differential equations of satellite motion were used as different versions which are required in CRB technique. As Fig. 12 shows, the CRB execution time on dual-core and quad-core architectures is 19106 and 16044 respectively, while Improved Consensus Recovery Block execution time on dual-core and quad-core architectures is 12637 and 10124 respectively. So Improved CRB decreases total execution time. In other words, the speedup rate of Improved CRB in comparison with CRB for dual-core and quad-core architectures is 1.51 and 1.58 respectively. Execution of the NVP section is same in CRB and Improved CRB techniques but the difference is in the recovery block section because the CRB executes the recovery block section sequentially.

$$Speed-up = \frac{T(1)}{T(P)} \tag{11}$$

Also, the Improved CRB technique Speed-up for 2, 4 and 8 Cores cases are represented in the Table 1, calculated using Eq.(11)[11] (Prefers to the number of cores and T(P) is the execution time using P cores).

Table 1. Speed-up of Improved Consensus Recovery Block Technique

Statuses	Speed up
2 Cores	1.78
4 Cores	2.22
8 Cores	2.29

Important point of this technique is the close relation between speed-up and both the number of versions and available cores., if the number of available cores is greater than the number of versions, increasing the number of cores will be ineffective on Speed-up improvement. Otherwise, increasing the number of cores is effective on speed-up.

In the worst case, namely the case in which last version performs the acceptance test successfully, the execution time will be equal to the total time of running all versions. However, in the Improved CRB, the recovery block section is executed distributedly and so its execution time is equal to execution time of the longest version.
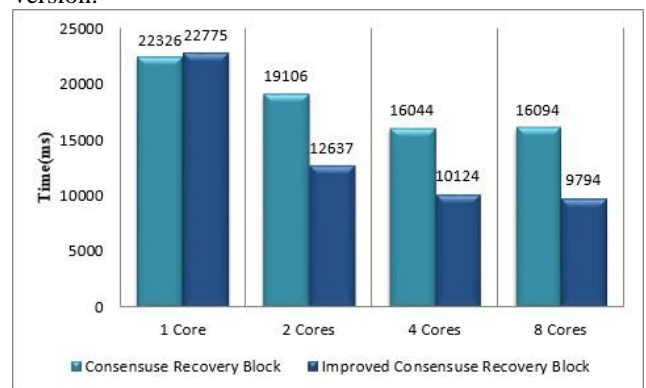

Fig. 12. Influence of multi-core architecture on performance of consensus recovery block technique

According to Fig. 10, execution time of the DRB technique in quad core architecture is less than execution time of CRB technique. But since the CRB does not have problems of the DRB technique, it is more suitable in many cases. In this paper, we showed that the CRB execution time can also be decreased.

8. Conclusions

Among different software fault tolerance techniques the Consensus Recovery Block (CRB) has more reliability over other ones in some cases and also it does not have problems of other techniques. To increase performance of this technique, we proposed one technique which is called Improved CRB technique in which the reliability is like the CRB and because of using distribution concepts, it has more performance. According to capability of multi-core architecture for supporting parallel processing, this architecture has been used to decrease the execution time and thus increasing performance of the fault-tolerance techniques. As a result, we showed that the Improved CRB technique is more suitable over other techniques from view of the reliability and performance properties.

Because the satellite motion computation is the most critical part of the system, in this paper we have used this subsystem as a case study and software fault tolerance techniques were used to solve the numerical differential equation of satellite motion in order to increase the reliability. To this end, different implementations of the numerical differential equation of the satellite motion methods were employed as different versions which are required in software fault tolerance techniques. Then, to determine the increase rate of the performance, we compared the execution time for single core architecture in the sequential mode and for multi-core one in the concurrent mode in different fault tolerance techniques.

The NVP-TB-AT technique, which has more performance and reliability over other derived NVP techniques, the execution time in case of sequential mode at single core architecture was 9335 while the execution time in case of the parallel mode at dual-core and quad-core architecture was 5477 and 4511 respectively. So, the speedup rate for dual-core and quad-core architectures is 1.70 and 2.06 respectively. Moreover, the execution time of recovery block technique on single-core, dual-core and quad-core is 22.04, 16.14 and 12.14 respectively.

Since high reliability is critical in the satellite motion computation system, we use the Consensus Recovery Block technique which has high reliability but its problem is high execution time. This problem was solved by proposing an Improved Consensus Recovery Block technique.

According to our experiments, the best execution time of Improved CRB is at quad-core architecture and it is equal to 10124, while the execution time of CRB is 16044 at quad core architecture. These two techniques have similar reliability but their performance rate is different. In other words, Consensus Recovery Block does not use distribution and concurrency mechanisms, therefore it cannot use advantages of concurrency in multi core architecture. The proposed technique has high performance because of taking advantage of distribution mechanism and using concurrency in multi core architecture.

Therefore according to the obtained results, using Improved Recovery Block technique and the multi core architecture simultaneously increases the reliability and performance in a fault tolerant software.

References

[1] A. Avizienis and J. P. J. Kelly, "Fault tolerance by design diversity- Concepts and experiments," *IEEE Computer*, vol. 17, pp. 67-80, 1984.

[2] L. Yang, L. Yu, J. Tang, L. Wang, J. Zhao, and X. Li, "McC++/Java: Enabling Multi-core Based Monitoring and Fault Tolerance in C++/Java," in *15th IEEE International Conference on Engineering of Complex Computer Systems (ICECCS)*, 2010, pp. 255-256.

[3] L. L. Pullum, *Software fault tolerance techniques and implementation*: Artech House Publishers, 2001.

[4] A. T. Tai, J. F. Meyer, and A. Avizienis, "Performability enhancement of fault-tolerant software," *Reliability, IEEE Transactions on*, vol. 42, pp. 227-237, 1993.

[5] A. T. Tai, J. F. Meyer, and A. Avizienis, *Software performability: From concepts to applications*: Kluwer Academic Publishers, 1996.

[6] K. H. Kim, "The Distributed Recovery Block Scheme," *M. R. Lyu(ed.), Software Fault Tolerance*, pp. 192-198, 1995.

[7] I. Koren and C. M. Krishna, *Fault-tolerant systems:* Morgan Kaufmann, 2007.

[8] M. Eshagh and M. Najafi Alamdari, "Comparison of numerical Integration methods in orbit determination of low earth orbiting satellites," *Journal of The Earth and Space Physics*, vol. 32, pp. 41-57, 2006.

[9] S. Akhter and J. Roberts, *Multi-Core Programming* vol. 33: Intel Press, 2006.

[10] L. Yang, Z. Cui, and X. Li, "A case study for fault tolerance oriented programming in multi-core architecture," in *11th IEEE International Conference on High Performance Computing and Communications, HPCC '09.* , 2009, pp. 630-635.

[11] B. Parhami, *Introduction to parallel processing: algorithms and architectures* vol. 1: Springer, 1999.

Hoda Banki is M.Sc. student at Kashan University in software engineering. She received B.Sc. degree in software engineering from Islamic Azad University Central Tehran Branch (IAUCTB) in 2008. Her main research interests are high performance computing, distributed systems, quantitative evaluation of software architecture and design based on software architecture styles.

Seyed Morteza Babamir received BS degree in Software Engineering from Ferdowsi University of Meshhad and MS and PhD degrees in Software Engineering from Tarbiat Modares University in 2002 and 2007 respectively. He was a researcher at Iran Aircraft Industries, Tehran City, Iran, from 1987 to 1993, head of Computer Center in University of Kashan, Kashan, Iran, from 1997 to 1999 and haed of Computer Engineering Department in University of Kashan from 2002 to 2005. Since 2007, he has been an associate professor of Department of Computer Engineering in University of Kashan, Kashan, Iran. He authored one book in Software Testing, four book chapters, fourteen journal papers and more than forty international and internal conference papers (http://ce.kashanu.ac.ir/babamir/Publication.htm). He is managing director of Soft Computing Journal published by supporting University of Kashan, Kashan, Iran. He is a member of the ACM.

Azam Farokh is M.S. student at Kashan University in software engineering. She received B.S. degree in software engineering from Arak University in 2009. Her research interests are including Software Engineering, high performance computing, Distributed Systems, Fault Tolernat Systems and software architecture. Her current research project is Evaluation of the appropriate style for Adaptive software architecture.

Mohammad Mehdi Morovati is M.Sc. student at Kashan University in software engineering. He received B.Sc. degree in software engineering in 2008 from college of Bahonar. His research interests include the field of Software Engineering and Artificial Intelligence and to date his focus has spanned the areas of Distributed Software Systems, Fault Tolerance Software Systems, High Performance Computing and Self-adaptive Software Systems.

Design of Fall Detection System: A Dynamic Pattern Approach with Fuzzy Logic and Motion Estimation

Khosro Rezaee*
Department of Electrical and Computer Engineering, Hakim Sabzevari University, Sabzevar, Iran
kh.rezaee@hsu.ac.ir
Javad Haddadnia
Department of Electrical and Computer Engineering, Hakim Sabzevari University, Sabzevar, Iran
haddadnia@hsu.ac.ir

Abstract

Every year thousands of the elderly suffer serious damages such as articular fractures, broken bones and even death due to their fall. Automatic detection of the abnormal walking in people, especially such accidents as the falls in the elderly, based on image processing techniques and computer vision can help develop an efficient system that its implementation in various contexts enables us to monitor people's movements. This paper proposes a new algorithm, which drawing on fuzzy rules in classification of movements as well as the implementation of the motion estimation, allows the rapid processing of the input data. At the testing stage, a large number of video frames received from CASIA, CAVAIR databases and the samples of the elderly's falls in Sabzevar's Mother Nursing Home containing the falls of the elderly were used. The results show that the mean absolute percent error (MAPE), root-mean-square deviation (RMSD) and standard deviation error (SDE) were at an acceptable level. The main shortcoming of other systems is that the elderly need to wear bulky clothes and in case they forget to do so, they will not be able to declare their situation at the time of the fall. Compared to the similar techniques, the implementation of the proposed system in nursing homes and residential areas allow the real time and intelligent monitoring of the people.

Keywords: Video Processing; Gaussian Mixture Model; HSV Conversion; the Elderly's Falls; Fuzzy Inference System; Motion Estimation.

1. Introduction

Today, many countries are faced with the growing population of the elderly each year. In 2000, the elderly aged above 65 constituted one-eighth of the world's population, i.e. a population equivalent to 750 million people [1]. Based on demographics released in 2010, it is estimated that in 2035, one-third of Europe's population will be above 65 years old [2]. Iran is one of the countries with young population and in near future, it has to deal with an aging population. Falls and loss of balance is a common threat to the health of the elderly. It can affect the quality of life, increase maintenance costs, and lead to adverse physical, psychological and social conditions, or even death [3]. Studies show that 25% to 47% of elderly suffer from falls once or more and this figure adds up to 50% among the elderly who live in health care centers. Since this accident can jeopardize the performance and independence of the elderly, the identification of people who are at risk of falling is of paramount importance [5]. Therefore, the first step in the prevention of this incident is to alleviate the side effects of falling [6]. If the elderly are not able to inform people in case of their fall, it might aggravate the damages of this incident and in some cases lead to the loss of their life. Therefore, a smart and efficient system to detect falls of elderly people seems essential. The techniques that have been proposed to date to signify people's falls can be classified into three general categories:

- Sensor networks and wearing sensors.
- The use of gyroscopes, accelerometer and devices for detecting the vibrations caused by falls.
- Monitoring the dynamic state based on video analysis.

In the system designed by Alexander et al. [7] sensor network techniques have been used for monitoring and online surveillance of the elderly. Another technique is employing wireless sensor network and alar system in which the elderly use a button to declare their situation in case of suffering a fall. The main shortcoming of this system is that the elderly need to wear bulky clothes and in case they forget to do so, they will not be able to declare their situation at the time of the fall.

Furthermore, this technique will be inoperable in case the person loses his/her consciousness after the fall. Vibration analysis instruments, gyroscope, status belts and pressure gauge board are other methods designed according to individuals' manner of movement. In 2008, Bourke et al. [9] created a secure threshold for fall detection algorithms which used a biaxial gyroscope. The simultaneous combination of the accelerometer system of the elderly's movement and the estimate of the movement's direction was also proposed by Nyan [10]. The vibration analysis system is also used in detecting the fall of the elderly or the disabled. Among all current systems, the real-time systems which detect the fall of people based on analysis of video images have the highest

---

efficiency and accuracy [11]. As to the designing of video surveillance algorithm, Naseimento [12-13] proposed methods based on the analysis of machine vision in detecting changes in individuals' position. In 2012, Liao and Huang [14] detected slips and falls of people based on Bayesian networks. Each of the current systems has strengths and weaknesses with regard to their detection. Low accuracy, low processing speed, lack of real-time response to the events in some of the above cases and high levels of positive error are among the weaknesses of such systems.

2. Methodology

The method proposed for detection of the elderly's falls in this paper draw mainly on video processing techniques to detect the target area. The algorithm has been shown in in Fig. 1 and the main body of the system will be introduced in following sections accordingly.
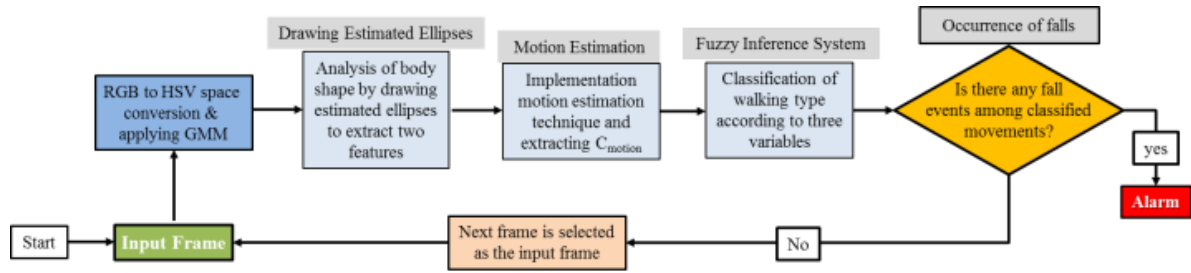
2.1 Conversion from RGB to HSV space

In many machine vision and image processing algorithms, the intensity of disproportionately high or low light, such as shades in separating a special part of the image, produces error. The color space, which is the result of the removal of unwanted effects of light, is the conversion to HSV space. Using the features of color space in HSV environment can reduce the complexities between the image surface and the intensity of unwanted light which causes errors. In calculation of H section, it is assumed that *M=max (R,G,B), m=min (R,G,B)* and *d=M-m*. The values of r, g and b are also calculated according to *r= (M-R)/d, g= (M-G)/d* and *b= (M-B)/d*. The main function of frame conversion from RGB into HSV space is minimizing the effects of the individual's shadows in images, which is the major cause of errors in mode separation.

Fig. 1. Proposed algorithm structure

2.2 Adaptive gaussian mixture model (AGMM)

Gaussian Mixture Model (GMM) is a parameter of a probability density function that specifies the weighted sum of Gaussian component densities. This model uses fixation technique to maximize the likelihood or probability for some of the parameters and its function is similar to K-means algorithm. A Pixel *I* at position x and time *t* is modeled as a mixture of K-Gaussian distributions.

The current pixel value in the probability distribution is calculated according to (1):

$$P(I_{t,x}) = \sum_{i=1}^{K} W_{t-1,x,i} * \eta(I_{t,x}, \mu_{t-1,x,i}, \sigma_{t-1,x,i}^2) \qquad (1)$$

In this equation, the parameters $W_{t-1,x,i}$, $\mu_{t-1,x,i}$ and $\sigma_{t-1,x,i}^2$ are weight, mean and variance of the i_{th} Gaussian model in the mixture at time *t-1* respectively and also η is a Gaussian probability density function that is obtained as (2):

$$\eta(I, \mu, \sigma^2) = \frac{1}{\sqrt{2\pi\sigma^2}} \exp(-\frac{(I-\mu)^2}{2\sigma^2}) \qquad (2)$$

The parameter initialization of the weight, the mean and the covariance matrix will be performed using updating producer of k-means algorithm. In this model, the parameters $W_{t-1,x,i}$, $\mu_{t-1,x,i}$ and $\sigma_{t-1,x,i}^2$ are updated based on the new pixel $I_{t,x}$ and the covariance matrix is calculated (3) due to the assumption of independent color components (R, G and B):

$$\sum_{t,x,i} = \sigma_{t,x,i} \qquad (3)$$

If $I_{t,x}$ is a standard Gaussian, the current pixel called matched or adapted pixel.

$$\left| I_{t,x} - \mu_{t-1,x,i} \right| \leq T_\sigma \sigma_{t-1,x,i} \qquad (4)$$

Matched pixels can be found using this approach and in overall if one of the K Gaussian is adapted, the adapted Gaussian is updated as (5) and (6):

$$\mu_{t,x,i} = (1-\rho)\mu_{t-1,x,i} + \rho(I_{t,x}) \qquad (5)$$

$$\sigma_{t,x,i}^2 = (1-\rho)\sigma_{t-1,x,i}^2 + \rho(I_{t,x} - \mu_{t,x,i})^T (I_{t,x} - \mu_{t,x,i}) \qquad (6)$$

In these equations, RAO is defined as a learning rate which changes the converge fast of μ and σ^2 so is combined by known parameters in (7):

$$\rho = \alpha\eta(I_{t,x} | \mu_{t-1,x,i}, \sigma_{t-1,x,i}^2) \qquad (7)$$

Similarly, the weights are updated according to the following procedure:

$$W_{t,x,i} = (1-\alpha)W_{t-1,x,i} + \alpha(M_{t,i}) \qquad (8)$$

In which $M_{t,i}$=1 is set for the adapted Gaussian and $M_{t,i}$=0 for the others. The learning rate α is used to update the weight and its value ranges between 0 and 1. If none of the K Gaussian component adapts the current pixel value, the least weighted component is replaced by a distribution with the current value as its mean, a high variance, and a low value of weight parameter is chosen as (9) and (10) and finally the weights are normalized as (11) so that $\sum_{i=1}^{K} W_{t,x,i} = 1$:

$$k = \arg\min_{i=1,\ldots K} W_{t-1,x,i} \qquad (9)$$

$$\mu_{t,x,k} = I_{t,x}, \sigma^2_{t,x,k} = \sigma^2_0, W_{t,x,k} = W_0 \qquad (10)$$

$$W_{t,x,i} = W_{t,x,i}(\sum_{i=1}^{K} W_{t,x,i})^{-1} \qquad (11)$$

The number of distribution K is estimated according to the w_k divided σ_k merit function and the first distribution of (B) is used as a foreground model. B function is calculated according to equation (12) sufficiency:

$$B = \arg\min_b(\sum_{i=1}^{b} W_i > T) \qquad (12)$$

In which T is the lowest decimal value in the foreground model. During the conversion, the foreground and background are separated. If a pixel I do not matches with any one of the background component, then the pixel is marked as foreground. Fig. 2 shows a set of frames taken from a video sequence as well as the application of conversion to HSV space and Gaussian mixture model.
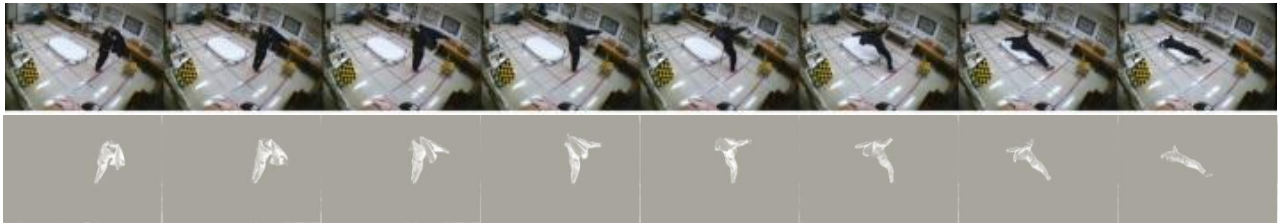

Fig. 2. The person falls on the bed and GMM is applied to separate the moving part of the image in 40 frames with 5 step.

2.3 The anatomical changes of human body during a fall

After separation of the foreground and background of the image, the location and position of the person is identified. The main advantage of this process is the identification of the person's posture relative to the horizontal and vertical axes. After the removal of the additional image pixels and by defining an estimated oval that specifies the position of the person, information about the shape, form and direction of the person's movement can be obtained. In two-dimensional coordinate system, the estimated oval is made of (x, y) center, φ direction and

d1 and d2 diameters. When a change in the manner of movement is made, the analysis of two indexes is of paramount importance.

- Standard deviation of the movement direction (η_φ) in the estimated oval.
- Calculating the ratio of d_1 and d_2 as well as standard deviation $\eta_{d1/d2}$.

In Fig. 4 the estimated oval technique is applied on the sample frames (Fig. 3). In this Figure, a set of 9 frames has been shown in which an estimated oval based on the formal mold of a person's body has been depicted.

Fig. 3. Images from left to the right, 135, 140, 145, 150, 155, 160, 165 and 170 frames, and the change of oval based on variation in one's posture has been depicted.

3. Motion Estimation

The important features are extracted from motion estimation that is suitable tools to analysis of motion. Intelligent drawing of estimated ellipse will due to elicit diagonals of ovals and direction of motions. Also motion estimation includes:

A. Motion Vector
The direction of motion based on (13):

$$\delta_j = \frac{1}{I_j}(\sum_{i(x)=1}^{I_j} \delta_{i(x)}, \sum_{i(y)=1}^{I_j} \delta_{i(y)}) \qquad (13)$$

Where $\delta_{i(x)}$ and $\delta_{i(y)}$ are horizontal and vertical components (for estimated j^{th} ellipse) in i^{th} frame. I is interested area which is segmented from body shape.

B. The Speed of Motion
The speed of motion is calculated by using Euclidian norm between (x_t, y_t) and (x_{t+1}, y_{t+1}).

C. Motion History Image (MHI)
The process of moving in successive frames of a video sequence can be considered as a type of a memory. The person's motion history in the combined image or images, which defines the precedent of the person's movement, is one of the techniques used for displaying the process of movement in the elderly, which according to the binary sequence of the motion area of the person, is modeled based on $D (Pixx, Pixy, t)$ taken from the sequence of the main image $I (Pixx, Pixy, t)$.

Each pixel in the images representing the precedent of individual motion by P_{MMI} is shown according to equation

(14) which is, in fact, the temporary memory of movement in each point that occurs in time interval T ($1 \pounds T \pounds N$) in which N is the number of sample frames in the input video sequence.

$$P_{MMI} = \begin{cases} T & D(Pix_x, Pix_y, t-1) \\ \max(0, P_{MMI}((Pix_x, Pix_y, t-1))-1) & otherwise \end{cases} \quad (14)$$

In the frames showing the previous movements, the pixels with higher brightness change show greater motion. To quantify the person's movement, the C_{motion} coefficient is estimated according to motion in frames which is recorded every 500ms. This coefficient is calculated according (15).

$$C_{motion} = \frac{Pix_{CuFrames}}{Pix_{CuFrames} + Pix_{OtherLevels}} \quad (15)$$

This equation is expressed based on pixels belong current frame and other pixels with lower values which is belong on pervious motions in [0-1] range. The motion history image algorithm applied on set of frames of sample clip in Fig. 4.
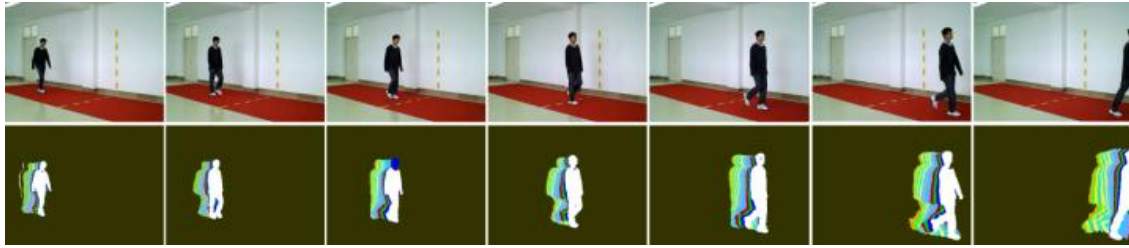

Fig. 4. Motion History Images (left to right and buttom column) for 95 to 170 frames, 95 to 110 frames, 105 to 120, 115-130, 125-140, 135-150, 145-160, 155-170 frames of a sample video sequence or 132 video frames.

4. Motion Classification Based on Fuzzy Logic Motion Estimation

Fuzzy logic system is effective technique which is based on logical reasoning and uses the concept of degrees awarded to each member or membership function. Fuzzy logic gives an accurate expression of the correct Boolean propositions. In classical logic sets the membership function $u(x)$ of an element x belonging to a set A could take only two values: 1 and 0. In contrast to classical logic sets the membership function of a fuzzy set is in form of a curve which displays how each point of space is mapped to a degree of membership, in other hand, $u_A(x) \in [0,1]$. The proposed fuzzy inference system is composed of three steps that include Fuzzification, Fuzzy rules and inference system and De-fuzzification steps.

4.1 Fuzzification

In the process of fuzzification, membership functions defined on input variables are applied to their actual values so that the degree of truth for each rule premise can be determined. Fuzzy statements in the antecedent are resolved to a degree of membership between 0 and 1 and also membership functions take different shape. We use A trapezoidal membership function in this paper in which is specified by four parameters as *A=trapezoid(x,a,b,c,d)*. This membership function has a flat top and really is just a truncated triangle curve. These straight line membership functions have the advantage of simplicity. This function is described as:

$$A = \begin{cases} 0 & x \le a \\ (x-a)/(b-a) & x \in (a,b) \\ 1 & x \in (b,c) \\ (d-x)/(d-c) & x \in (c,d) \end{cases} \quad (16)$$

Three member functions for each input are shown in Fig. 5.

4.2 Fuzzy inferencing

To assay the severance of the rule antecedents, we use the *OR* fuzzy operation. Typically, fuzzy expert systems make use of the classical fuzzy operation union:

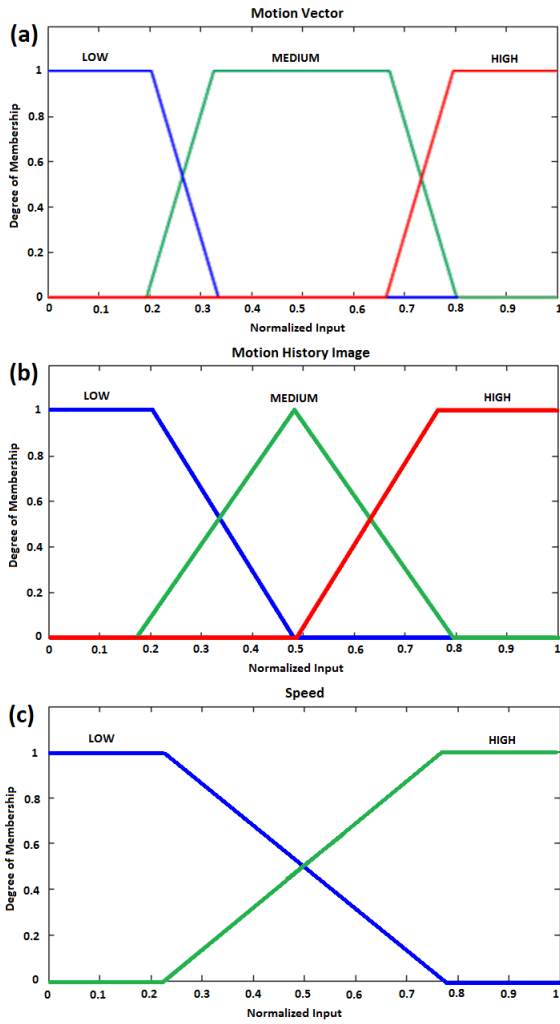$$\mu_{A \cup B}(x) = \max [\mu_A(x), \mu_B(x)] \quad (17)$$

Fig. 5. Inputs of fuzzy model, (a) relative motion vector, (b) relative MHI, and (c) speed.

Similarly, in order to assay the conjunction of the rule antecedents, we apply the *AND* fuzzy operation intersection:

$$\mu_{A \cap B}(x) = \min [\mu_A(x), \mu_B(x)] \qquad (18)$$

Three input variables, which were introduced in the previous section, are directly involved in determining the normal walking of the elderly. Two output variables were also used to indicate its value in decision-making classification of the motion. Five sets of *IF-THEN* fuzzy rules have been shown in Table 1 using an inference system along with a trapezoidal function as the membership functions. The output of the system includes the classification of the normal and abnormal movement's modes, which has been divided into six different intervals. There are three inputs variables *(X₁, X₂, and X₃)* and two outputs *(Y₁, Y₂)* in this inference system.

Table 1. A representation of the rules extracted from fuzzy system

Rules		X_1	X_2	X_3		Y_1	Y_2
1		L	L	L		1	0
2		L	L	M		1	0
3		L	L	H		1	0
4		L	H	L		1	0
5		L	H	M		1	0
6		L	H	H		0	1
7		M	L	L		1	0
8		M	L	M		1	0
9	*If*	M	L	H	*Then*	1	0
10		M	H	L		1	0
11		M	H	M		1	0
12		M	H	H		0	1
13		H	L	L		1	0
14		H	L	M		1	0
15		H	L	H		1	0
16		H	H	L		1	0
17		H	H	M		0	1
18		H	H	H		0	1

4.3 De- Fuzzification

In the final phase, the motion classification based on fuzzy logic is proposed to distinguish the normal or abnormal walking. The last step in the fuzzy inference process is de-fuzzification that helps us to evaluate the rules, but the final output of a fuzzy system has to be a crisp number. The input for the de-fuzzification procedure is the accumulate output fuzzy set and the output is a single number. We have several de-fuzzification techniques, but the centroid method finds the point where a vertical line would slice the accumulate set into two equal masses. Mathematically this center of gravity (*COG*) can be defined as:

$$COG = \frac{\int_a^b \mu_A(x)x\,dx}{\int_a^b \mu_A(x)\,dx} \qquad (19)$$

A logical appraise can be obtained by calculating it over a sample of points.

5. Results and Discussion

In three steps, the detection process of a fall in video images was carried out. These three steps were:
- Quantification of movements and modeling accordingly.

When C_{motion} changes from the defined threshold, which has been obtained according to the statistical calculations of video images, the movements similar to the occurrence of a fall can be detected.
- Analysis of the body shape and form in the binary frame

One of the main parameters which will undergo tremendous changes is η_φ or standard deviation in the direction of motion. In average, of 96 tested video sequences, η_φ was about 15 degree and the ratio of $\eta_{d1/d2}$ was 0/9.
- The inactivity of the elderly after the fall.

The parameters that might change after a fall or during inactivity of the person are expressed as follow:

- o C_{motion} < 5%
- o Standard deviations η_x and η_y which are both smaller than 2.
- o Standard deviations in the estimated oval equations, which under conditions η_{d1}<2, η_{d2}<2 and η_{φ}<15° shows the inactivity or stillness of the elderly after suffering from a fall.

To evaluate the performance of the proposed system, the behavioral model of detection algorithm is simulated based on the criteria of valuation where the outputs have been compared to reality. Also, the model of inferred motion is verified using actual measured values as inputs.

The system was implemented on set of video sequences taken from CASIA, CAVAIR databases [15-16] and the samples of the elderly's falls in Sabzevar's Mother Nursing Home containing the occurrence of the falls, abnormal gate and normal gate in Iran. All sequences were randomly converted into 4 categories of Movie with these details: AVI format, 120×160 pixels resolution and 15 fps.

To examine the performance of developed models, various criteria are used to calculate errors. In the next equations, F_k shows the real value of the variable being modeled or forcasted (observed data), and A_k is the real mean value of the variable and N is the number of test observations [17]. In Fig. 6, the performance of proposed system is dedicated for original walking and predicted posture of walking in sample time.
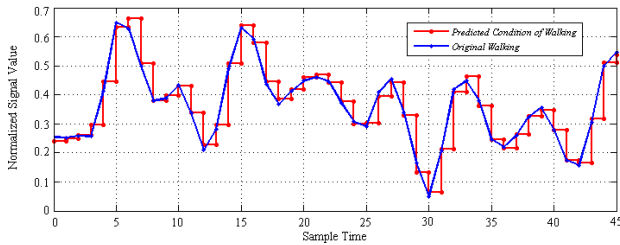

Fig. 6 Results for fuzzy predictor for various posture of walking among normal walking and abnormal walking like falling

The *MAPE* (Mean Absolute Percent Error) proposes the size of the error in percentage terms. It is calculated as the average of the unsigned percentage error, as shown in the (20):

$$MAPE = \frac{1}{N}\sum_{k=1}^{N}\frac{|F_k - A_k|}{A_k} \qquad (20)$$

The root-mean-square deviation (*RMSD*) is a frequently used measure of the differences between values predicted by a model or an estimator and the values actually observed [17]. Basically, the *RMSD* represents the sample standard deviation of the differences between predicted values and observed values as (21).

$$RMSD = \sqrt{\frac{1}{N}\sum_{k=1}^{N}(F_k - A_k)^2} \qquad (21)$$

Standard deviation error (*SDE*), according to (22), indicates the persistent error even after calibration of the model.

$$SDE = \sqrt{\frac{1}{N}\sum_{k=1}^{N}(\frac{|F_k - A_k|}{A_k} - \frac{MAPE}{100})^2} \qquad (22)$$

Errors in modeling with considering *MAPE*, *RMSD* and *SDE* are summarized in Table 2 so that the error rate is minimal and the proposed algorithm not only has the capability to classify, but fuzzy system can also act as a good walking predictor. In this table, the threshold of falling is assigned for different postures and different angles of walking. Accelerometers and vibration analysis systems are facing with the sensitivity between 90%-95% and specificity higher than 95%. While the sensitivity and specificity of the algorithm based on machine vision is respectively 85-95% and 90%-100% [18-24].

Table 2. The received video sequences, calculation of MAPE, RMSD, SDE and Precision of the proposed algorithm

	Input Parameters			Error Criteria			
	On MV parameter	On MHI parameter	On Speed parameter	MAPE (%)	RMSD	SDE	Precision (%)
Threshold Value	0.2	-	-	3.5708	0.0128	0.0379	96.42
	0.27	-	-	4.8461	0.0172	0.0510	95.15
	0.34	-	-	5.5545	0.0197	0.0583	94.44
	0.67	-	-	5.9079	0.0637	0.1406	94.09
	0.74	-	-	6.3717	0.0645	0.1425	93.62
	0.8	-	-	7.0675	0.0657	0.1459	92.93
	0.27	0.35	-	6.8614	0.0601	0.1332	93.13
	0.74	0.35	-	7.9326	0.0595	0.1336	92.06
	0.27	0.65	-	8.6511	0.0594	0.1346	91.34
	0.74	0.65	-	9.3696	0.0594	0.1361	90.63
	0.27	0.35	0.5	8.3842	0.0682	0.1532	91.61
	0.74	0.35	0.5	9.0926	0.0695	0.1570	90.90
	0.27	0.65	0.5	10.0881	0.0596	0.1382	89.91
	0.74	0.65	0.5	10.5671	0.0597	0.1400	89.43
Mean Value	*If* T=0.35			4.4210	0.0157	0.0466	95.57
	If T=0.5			7.5382	0.0267	0.0788	92.46
	If T=0.65			10.0887	0.0357	0.1053	89.91

Therefore, systems based on machine vision techniques in terms of accuracy and sensitivity is competitive in performance compared to other techniques such as sensor network and accelerometers and vibration analysis systems. Unlike other techniques, the method of video processing has the advantage which is doing intelligent monitoring of the elderly person and is comfortable wearing heavy clothing.

6. Conclusions

Based on the analysis of video sequences, using machine vision and fuzzy logic, the proposed system detects the occurrence of the falls with higher precision and lower SDE. The practical results and final simulation of the algorithm showed that the system, though using a single camera to capture the movements of the elderly, produced higher sensitivity and specificity compared to similar methods. 93% accuracy, low mean absolute percent error (MAPE) and high detection rate have dramatically increased the reliability of the system performance. The accurate prediction of the fall of the elderly based on the analysis of video images will be among the future researches of the author. It would be based upon motion equations and biomechanics joints of the elderly.

References

[1] Newton, R.A. "Standing balance abilities of elderly subjects under altered visual and support surface conditions", Physical therapy Canada, Vol. 47, No. 1, 1995, pp. 25-29.

[2] Ambient Assisted Living Joint Programme (2008), available from http://www.aal-europe.eu.

[3] Fife, T.D., Zwerling, L., Socotch, T., Jacobson, K., Bell, T., Beykirch, K. "Compassion of Static and Dynamic Posture Graphy in Young and Older Normal People", Journal of American Geriatric Society, Vol. 42, No. 4, 2000, pp. 405-412.

[4] Wegner, L., Kisner, C., Nichols, D. "Static and Dynamic Balance Response in Persons with Bilateral Knee Osteoartherritis", Journal of Orthopaedic and Sports Physical Therapy, Vol. 25, No. 1, 1997, pp. 13-18.

[5] Atwater, S.L., Crawe, T.K., Deitz, J.C., Richardson, P.K. "Inter Rater and Test-Restart Reliability of Two Predictive Balance Tests", Physical Therapy, Vol. 70, No. 2, pp. 79-87.

[6] Satterfied, K.S. "Balance Testing Helps Identify Elderly at Risk of Multiple Falls", American Otological Society, May 2001.

[7] DirectAlert (2010). Wireless emergency response system. URL: http://www.directalert.ca/emergency/help-button.php.

[8] Alexander, G.L., Rantz, M., Skubic, M., Aud, M.A., Wakefield, B., Florea, E., Paul, A. "Sensor systems for monitoring functional status in assisted living facility residents", Research in Gerontological Nursing, Vol. 1 No. 4, 2008, pp. 238-244.

[9] Bourke, A.K., Lyons, G.M. "A threshold-based fall-detection algorithm using a bi-axial gyroscope sensor", Medical Engineering and Physics, Vol. 30, No. 1, 2008, pp. 84–90.

[10] Nyan, M., Tay, F.E., Murugasu, E. "A wearable system for pre-impact fall detection", Journal of Biomechanics, Vol. 41, No. 16, 2008, pp. 3475–3481.

[11] Rezaee, K., Haddadnia, J., Delbari, A., Madanian. M. "Predicting and Monitoring of the Elderly Falls Based on Modeling of the Motion Patterns Obtained from Video Sequences", Iranian Journal of Aging, Vol. 8, No. 28, 2014, pp. 15-21.

[12] Nascimento, J.C., Marques, J.S. "Performance evaluation of object detection algorithms for video surveillance", IEEE Transactions on Multimedia, Vol. 8, No. 4, 2006 pp. 761–74.

[13] Rezaee, K., Haddadnia, J., Delbari, A. "Intelligent Detection of the Falls in the Elderly Using Fuzzy Inference System and Video-based Motion Estimation Method", The 8th Iranian Conference on Machine Vision and Image Processing, 2013.

[14] Liao, Y.T., Huang, C.L., Hsu S.H. "Slip and fall event detection using Bayesian Belief Network", Pattern Recognition, Vol. 45, No.1, 2012, pp. 24–32.

[15] Yu, S., Tan, D., Tan, T. "A framework for evaluating the effect of view angle, clothing and carrying condition on gait recognition", in: Proc. of IEEE International Conference on Pattern Recognition, Vol. 4, Hong Kong, China, 2006, pp.441–444.

[16] Auvinet, E., Rougier, C., Meunier, J., St-Arnaud, A., Rousseau, J. "Multiple cameras fall dataset", Technical report 1350, DIRO - Université de Montréal, July 2010.

[17] Hyndman, Rob J., Koehler, Anne B. "Another look at measures of forecast accuracy". International Journal of Forecasting, Vol. 22, No. 4, 2006, pp. 679–688.

[18] Tyrer, H.W., Alwan, M., Demiris, G., He, Z. "Technology for successful ageing", Proceedings of the 28th IEEE Annual International Conference, 2006.

[19] Zhang, T., Wang, J., Liu, P., Hou, J. "Fall Detection by Embedding an Accelerometer in Cellphone and Using KFD Algorithm", International Journal of Computer Science and Network Security. Vol. 6, No. 10, 2006, pp. 277-284.

[20] Rougier, J., Meunier, J., St-Arnaud, A., Rousseau, J. "Fall detection from human shape and Motion history using video surveillance", In: International on Advanced Information Networking and Applications Workshops, 21-23 May 2007, pp. 875-880.

[21] Vishwakarma, V., Mandal, C.A., Sural, S. "Automatic detection of human fall in video", In: International Conference on Pattern Recognition and Machine Intelligence, 2007, pp. 616–23.

[22] Tao, J., Turjo, M., Wong M-F, Wang, M., Tan, Y-P. "Fall incidents detection for intelligent video surveillance", In: Proceedings of the Fifth International Conference On Information, Communications and Signal Conference Processing, 2005, pp.1590–4.

[23] Shieh, W.Y., Huang, J.C. "Falling-incident detection and throughput Enhancement in a multi-camera video-surveillance system", Medical Engineering & Physics, Vol. 10, No. 16, 2011, pp. 28-38.

[24] Rezaee Kh., Ghezelbash M.R., Haddadnia J., Delbari A. "An Intelligent Surveillance System for Falling Elderly Detection Based on Video Sequences", 19th Iranian Conference of Biomedical Engineering (ICBME), Tehran, Iran, 20-21 December 2012.

Khosro Rezaee received the M.Sc. degree in 2012 in biomedical engineering from the electrical and computer engineering department of Hakim Sabzevari University, Iran, and worked in computer and biomedical Engineering. His main research interests are image processing, computer vision and image analysis for medical and immersive communications and published many papers in these categories. He is a member of ICT and IEEE community in Iran.

Javad Haddadnia received his B.Sc. degree in Electrical and Electronic Engineering with the first rank in 1993 and M.Sc. in Electronic Engineering in 1995, from Amirkabir University of Technology, Tehran, Iran, respectively. He is currently a associate professor in the Electrical Engineering Department of Hakim Sabzevari University of Technology, Sabzevar, Iran. His research interests include neural network, digital image processing, computer vision, face detection and recognition. He has published several papers in the above area. He has served as a visiting research scholar at the University of Windsor, Canada during 2001–2002. He is a member of SPIE, CIPPR and IEICE.

Fast Automatic Face Recognition from Single Image per Person Using GAW-KNN

Hasan Farsi*

Department of Electrical and Computer Engineering, University of Birjand, Birjand, Iran
hfarsi@birjand.ac.ir

Mohammad Hasheminejad

Department of Electrical and Computer Engineering, University of Birjand, Birjand, Iran
mhashemi @birjand.ac.ir

Abstract

Real time face recognition systems have several limitations such as collecting features. One training sample per target means less feature extraction techniques are available to use. To obtain an acceptable accuracy, most of face recognition algorithms need more than one training sample per target. In these applications, accuracy of recognition dramatically reduces for the case of one training sample per target face image because of head rotation and variation in illumination state. In this paper, a new hybrid face recognition method by using single image per person is proposed, which is robust against illumination variations. To achieve robustness against head variations, a rotation detection and compensation stage is added. This method is called Weighted Graphs and PCA (WGPCA). It uses harmony of face components to extract and normalize features, and genetic algorithm with a training set is used to learn the most useful features and real-valued weights associated to individual attributes in the features. The k-nearest neighbor algorithm is applied to classify new faces based on their weighted features from the templates of the training set. Each template contains the corrected distances (Graphs) of different points on the face components and the results of Principal Component Analysis (PCA) applied to the output of face detection rectangle. The proposed hybrid algorithm is trained using MATLAB software to determine best features and their associated weights and is then implemented by using delphi XE2 programming environment to recognize faces in real time. The main advantage of this algorithm is the capability of recognizing the face by only one picture in real time. The obtained results of the proposed technique on FERET database show that the accuracy and effectiveness of the proposed algorithm.

Keywords: EBGM; Face Recognition; PCA; Weighted Feature; WGPCA.

1. Introduction

There has been a great deal of progress in face detection methods. This field has been concerned researchers of several disciplines such as image processing, pattern recognition, computer vision, neural network and computer graphic [1] because of its high accuracy and low intrusiveness [2]. The performance of the most face recognition algorithms can be seriously affected by the limited number of training sample per person [2].

There are two major steps in face recognition algorithms. First, it is necessary to know whether any human face is available on the image. This is called face detection step. In the second step, by means of extracted features from the image, the aforementioned face should be recognized which is called face classification step.

In the face detection step, there are number of algorithms that can detect frontal face position in an image. Learning based approaches [3] estimate the complex non-convex face and non-face from training images. In these methods, the problem is to select sufficient pattern to adequately characterize non-face space. Some other methods [4] use multiple features such as color, shape and texture to segment faces from the background. Although these methods are fast, they suffer from complex backgrounds. One of the fastest and most reliable algorithms used in this step is HAAR-like algorithm which is used to reliably detect objects in real time. HAAR-like features were introduced by Viola et al [5] and are successfully used in much object detection and face detection methods [6]. The goal of face detection is to specify existence of face in an image that is a frame obtained from a surveillance camera or an individual stored image and if exists, accurately determination of face position in the image.

Face recognition refers to an automatic method that identifies an individual face image and pre-trained templates on a database. Face recognition techniques can be divided into three main categories. The earliest methods are local feature-based matching methods [7, 8]. These approaches are based on detection of individual facial features such as eyes and nose, and comparing to the corresponding features stored in the database. Elastic Bunch Graph Matching (EBGM) and its variations are included in this category. In EBGM local information extracted with Gabor filters is used for discrimination. Second category is holistic feature-based matching

methods [9,10]. These methods are centered on using the whole face region as raw input for face recognition system. Principal Component Analysis (PCA), Linear Discriminate Analysis (LDA), Independent Components Analysis (ICA), Fisher's Linear Discriminate (FLD) and their variations are examples of this category. The last one is hybrid matching method that uses both local and holistic features [11].

After extracting facial features form input face image the image is classified as one of predefined target faces. In this stage classification is performed using neural network, statistical methods or any other pattern recognition methods. It has been shown that hybridizing genetic algorithm (GA) and a K-Nearest Neighbor (KNN) classification, as a statistical method, can be used in classification [12]. This method improves the performance of the k-nearest neighbor algorithm and can be used in optimization problems. In the presented method 82 points are extracted from face using Active Shape Model (ASM) and some feature vectors obtained from PCA. Since there is 3321 distances between 82 points, these distances and PCA vectors are stored as template for targets. GA is used to determine weights related to each feature.

It is not a simple matter to find an optimal vector of attribute weightings. In this paper we show how to use a GA-WKNN and human face component harmony in face recognition.

This paper is organized as follows: In section 2 the k-nearest neighbors with genetic algorithm is presented. In section 3 the proposed full automated hybrid face recognizer is introduced in details. Experimental results and a comparison of existing and the proposed methods are given in section 4 and a conclusion is drawn in the last section.

2. The K-nearest Neighbours Classification and Genetic Algorithm

The Nearest Neighbor (minimum distance) classification algorithm (NN) is based on the idea that, given a data set of classified examples, an unclassified individual should belong to the same class as its nearest neighbor in the data set [13]. The measurement of proximity, or similarity, between two individuals is given by equation (1).

$$d_{ij} = \left\{ \sum_{a=1}^{n} \left(x_{ia} - x_{ja} \right)^2 \right\}^{\frac{1}{2}} \tag{1}$$

Where x_{ia}, is value of the ath attribute for the ith datum. In K-NN, a new instance is classified by looking at its nearest neighbors. Then the unclassified individual is assigned to the class of the majority of its k closest neighbors. This algorithm is simple, quick, and effective. It corresponds to incorrect results, however, in the case of face recognition because portion of features that are significant in the classification process is small with respect to the number of less important features. Given a vector of features, the KNN treats each feature as equal in

the classification process. So, it is necessary to use Weighted KNN (WKNN) instead.

Assigning proper weights to the extracted features modifies the importance of features to reflect its relevance in recognition. Muscular structure of human face results in variations in face components positions and shape also illumination conditions, position of face according to the camera and many other factors makes the aforementioned variety of importance.

Genetic algorithm is a heuristic algorithm used in optimization and machine learning inspired from processes of biological evaluation. John Holland created the genetic algorithm field [14]. GA can efficiently solve the large parameter optimization problems and is used to find an optimal solution for the problems. Since genetic algorithm do not relay on problem specific knowledge, it can be used to find solutions that is difficult to find by classic mathematics. Chromosomes represent solutions within the genetic algorithm. Chromosomes are grouped into population (set of solutions) on which the genetic algorithm operates. In each step (generation), the genetic algorithm selects chromosomes from a population (selection is usually based on the fitness value of the chromosome) and combines them to produce new chromosomes. These offspring chromosomes form a new population (or replace some of the chromosomes in the existing population) in the hope that the new population will be better than the previous ones. Populations keep track of the worst and the best chromosomes, and stores additional statistical information which can be used by the genetic algorithm to determine the stop criteria. In the case of determining face features weighting, we have about 4000 face features that should be evaluated. Because weights are real values and there is large number of features, the search area for optimal values is infinite and it is impossible to find optimal values by classic mathematics. The only option is use of heuristics algorithms, and we use GA.

3. Proposed Algorithm

As mentioned all face recognition algorithms consist of two different steps, face detection and face classification. In face classification step, first some useful features should be extracted from the image by an accurate image analyzing technique and then image should be classified according to extracted features from the primary image.

3.1 Face detection

There are number of algorithms that can detect frontal face position in an image. In this section HAAR-like feature is used in Adaboost algorithm to reliably detect faces in real time. This approach is used because of its speed and accuracy. This technique is based on the idea of wavelet template that defines shape of a template in terms of wavelet coefficients of the image. With a scaling factor of 1.1, as recommended in [15], the input image is scanned

across location and scale. According to AdaBoost algorithm [3] a set of weak binary classifiers is learned by a training set. Each classifier is a function composed of a rectangular sum followed by a threshold. The features consist of boxes of different sizes and locations.

3.2 Local and holistic feature extraction

In this article, the recognition system has only one picture of the target face that it should gain the maximum use of the picture to be robust to head rotation and illumination variations. Therefore, integration of global and local features is implemented to achieve maximum use of the training set.

3.2.1 Local features

In this stage, face features are extracted from the output square region in face detection block. Facial ground truth is found according to Active Shape Model (ASM) algorithm as local features. ASM is a powerful tool for shape localization problems. In ASM, a set of points are assumed to be a flexible model of image structure whose shape can vary. A set of points are aligned automatically to minimize the variance in distance between equivalent points [16]. To achieve higher speed and accuracy, the algorithm search area for each component is restricted. As shown in Fig.1, the location of 82 points is specified in input face image.

According to our work on FERET [17], ORL [18] and face94, face95, face96 and grimace databases [19], every facial component has a region and a harmony exists about place and size of these components.

Fig. 1. Of Point Extraction Results from FERET and Face94 Databases

The first component that will be found is eye. Because of kind of HAAR-like template, we use eyes which are around the height middle of the face boundary square. In worst case, pupil was about $\pm 1/10$ far from middle of the height. So, for assurance we consider it to be $\pm 1/5$. Therefore, if upper right corner of the square would be center of coordinates, with respect to the pupil and eye width, vertical search region for eyes would be [2/5w 3/5w], where w denotes length of the extracted face boundary square. Different components should be sequentially analyzed.

Table 1: Proposed search boundary for each facial component

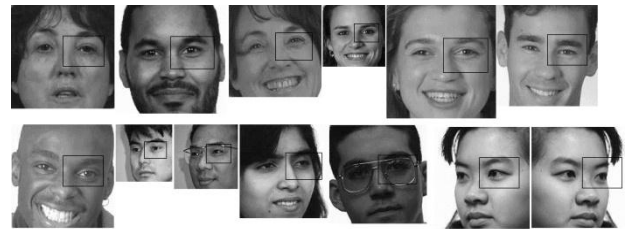| Graph name	X		Y	
Left eye	$\frac{1}{2}$w	$\frac{9}{10}$w	$\frac{3}{10}$w	$\frac{3}{5}$w
Right eye	$\frac{1}{10}$w	$\frac{1}{2}$w	$\frac{3}{10}$w	$\frac{3}{5}$w
Left eyebrow	$\frac{1}{2}$w	$\frac{9}{10}$w	$ule^1 - \frac{1}{5}$w	Min(licy[2], locy[3])
Right eyebrow	$\frac{1}{10}$w	$\frac{9}{10}$w	$ure^4 - \frac{1}{5}$w	Min(ricy[5], rocy[6])
Between eyebrows	$= \frac{rbi^7 + lbi^8}{2}$			
Nose	$\frac{1}{4}$w	$\frac{1}{2}$w	bey[9]	uply[10]
Left wrinkle	leox[11]	leix[12]	locy	licy
Right wrinkle	reox[13]	reix[14]	rocy	ricy
Lower jaw boundary	0	w	$-\frac{w}{2}$	oey[15]
Nose tip	$\frac{w}{4}$	$3\frac{w}{4}$	bey	uply

Fig. 2. Search Area for Left Eye Model inside the Result of HAAR-like Detection.

We extract the points from the following components: eyes, eyebrows, nose, under eyes wrinkles, lips, lower jaw boundary and finally individual points such as point between eyebrows (middle of inner points of eyebrows to find rotation radius), concavity at the upper part of nose, nose tip and middle of nose holes. TABLE I shows search boundary for each component. The other points are inside one of models.

As shown in Fig.2, for all tested facial images in FERET database, left eye is inside its corresponding proposed region. These images have been chosen from those of different size and rotation state.

Rotation of head around vertical axis changes distances between points, especially horizontal ones. To eliminate this effect, a distance correction stage is applied. With respect to the place of nose tip and eyes, and eyes versus mid line, degree of rotation of head around vertical axis is found and corrected.

---

[1] y of upper point found on left eye
[2] y of left eye inner corner
[3] y of left eye outer corner
[4] y of upper point found on right eye
[5] y of right eye inner corner
[6] y of right eye outer corner
[7] found coordinate of right eyebrow inner point
[8] found coordinate of left eyebrow inner point
[9] y of point between eyebrow
[10] Maximum y of lip model
[11] x of left eye outer corner
[12] x of left eye inner corner
[13] x of right eye outer corner
[14] x of right eye inner corner
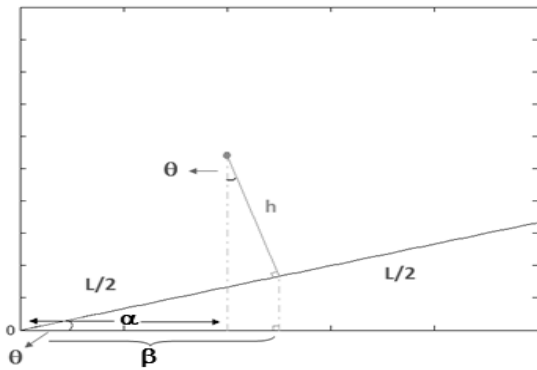[15] minimum of outer eye point on y axis

Fig. 3. Top View of Face, his distance between nose tip and a vertical plane passing center of eyes points.

In a front view of face, projection of face on the x-y plane and for a face perpendicular to camera in most cases, as shown in Fig.3, horizontal position (x) of nose tip is in the middle of left and right eye, on the x axis, but in a rotated face this is changed and x of nose tip is equal to a instead of L/2 and L is being seen as L×Cos(q). Real values can be calculated from a, b and h using equation (2).

$$L = \frac{\beta}{Cos\left(arcsin\left(\frac{\beta-\alpha}{h}\right)\right)} \qquad (2)$$

For a real time automatic face recognition system, calculations can be reduced by means of a lookup table to correct important distances rapidly.

3.2.2 Holistic features

Holistic features represent a global appearance of sample. Principal Component Analysis (PCA) is a holistic feature that is widely used in face recognition. PCA is a statistical method for reducing dimension of data set while retaining the majority of the variation present in a dataset.

Recent works on face recognition have introduced linear and nonlinear dimensionality reduction techniques based on PCA. KPCA (kernel PCA), 2DPCA, B2DPCA are examples of these techniques. PCA identifies the linear combinations of variables and ignore the high order correlation value [9].

3.2.3 Specifying feature weights

Both holistic and local facial features of target and input data are compared using KNN algorithm. To improve the effectiveness of KNN approach, GA is used to select important features [20]. This decreases process time that is important in real time recognition. It has been shown that specifying proper weights increases the efficiency for every feature [12]. This stage is performed once by the researcher and there is no need for weight determination in the real time recognition application. The real time application just loads predetermined weights at startup and performs real time process. Determination of effective weights for a WKNN face recognition algorithm with more than 3000 feature vector is a hard optimization problem with an infinite search space. Since 82 points are extracted from the facial image, there is 82*(82-1)/2=3321 distances between these points

which should be analyzed for every target. Every gene can have infinite number of real values between 0 and one. The comparison should be performed for every target and for every generation.

Solving this problem is impossible with classic mathematics. In GA-WKNN process chromosomes are vectors of real valued weights between 0 and 1.

Therefore optimization problem shown in (3) should be solved.

$$\min_w \sum_{n=1}^{N} w_m \cdot |x_{nm} - v_{nm}| \qquad (3)$$

Subject to $w_m \geq 0$

Where w_m is weight for m^{th} feature, x_{nm} is m^{th} feature for n^{th} target and v_{nm} is m^{th} feature for an input face image that its correct target is x_n.

3.3 Face classification

Face classification is the problem of identifying to which of a set of categories (sub-populations) a new observation belongs. In the training stage both features will be extracted normalized and stored in a database. In the test stage features of receiving new input is compared to the stored templates with respect to predetermined weights and classified to a category that has minimum weighted Euclidean distance from the input feature vector. There may be an input face image that does not belong to any of the stored categories.

Therefore, in order to prevent misclassification a threshold is assumed to categorize input face images that are not similar enough to the selected target, as an unknown face. Fig.4 depicts the block diagram of the face recognition system. This diagram consists of three main parts, Train, test and weight determination which is implemented once and not included in the real time face recognition.

In the training process position of target face is first determined. Found face region is then sent to perform local and global feature extraction. Normalization process is needed before PCA feature extraction and after distance calculation to reduce face image variability due to lighting and size.
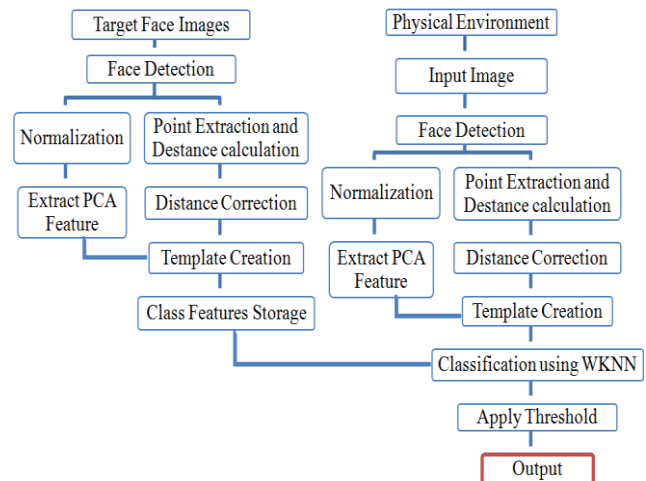

Fig. 4. The Block Diagram of the Proposed Face Recognition System

Image is rescaled to 128×128 pixels and histogram equalization is performed before PCA and distances are normalized with respect to the detected square region.

In the test stage the same process is done and resulting template is compared to the stored target templates

Weight determination process is performed once and it is not included in recognition process.

4. Simulation Results and Discussion

4.1 Weight determination

As mentioned before, weight determination is performed once, and is not included in the real time process. Since process speed is not an issue in the weight determination, in this stage we used MATLAB optimization toolbox. To gain the accuracy of optimization toolbox, we first extract templates from training faces using an application developed in Delphi programming environment. This application uses OpenCV library [15] in face detection phase. Using the extracted templates, genetic algorithm has been implemented with 200 iterations, 20 population, 20 targets and 111 training samples. It takes 138 minutes with a core i7 2.2GHz system to find optimum weights and increase recognition rate from 84.6% to 93.7% of correct classifications. For every class only one fa picture is used as a known sample. Fig. 5 shows the convergence of population to the optimum weights for this experiment. In this and next experiment the important matter is finding proper weighting and the code is not optimized in the case of speed.

In a second experiment, we use a computer sever with 16 CPU of 2.9 GHz and Matlab 2010a optimization toolbox on windows server 2008. Using the aforementioned templates, 502 samples in 197 categories were tested with 500 iterations and population of 30. It took about 26 hours to reach 94% of accuracy. The convergence has been shown in Fig. 6.
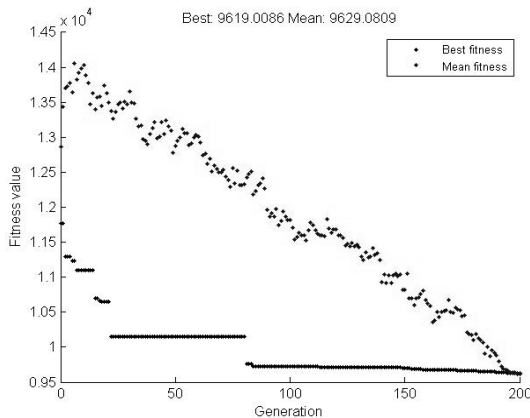

Fig. 5. First GA Experiment: with a 20 target database and 111 samples best weights has been determined for best classification results.

In both experiments equation (4) was used as fitness function.

$$Cost = 500 \times NMC + \sum_{i=1}^{k} d_i \qquad (4)$$

Where NMC is number of misclassifications, di is distance of the ith sample from correct target and k is number of samples. A typical distance between target and probe image was about 50. Therefore, we should regulate the cost function with respect to that distance. As mentioned, we considered the number of misclassifications which is more important than the distance. We have empirically used the coefficient of 500 in the equation to consider the importance. Due to adaption of the genetic algorithm, little changes in the coefficient do not have any effect on the final results.
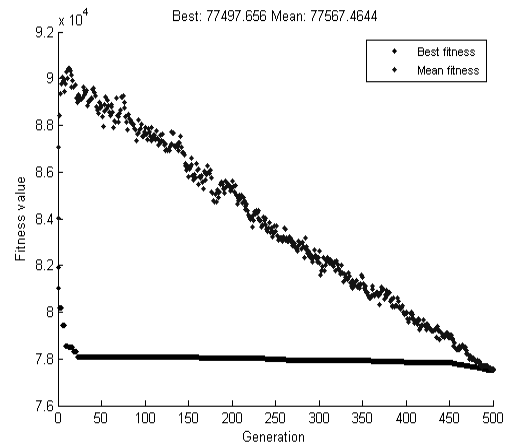

Fig. 6. Second GA Experiment: with a 197 target database and 502 samples best weights has been determined for best classification results.

4.2 Classification results

After obtaining optimal weights, classification is applied to FERET database with 699 stored targets. One image of fa series is chosen as target and other fa, fb, hl, hr, ql, qr, ra, rb, rc, rd, re has been tested separately. As we may not expect to recognize a 90 degree rotated face from a frontal face image (an example of the situation is shown in Fig. 7), recognition percentage is very low in this situation. Frontal facial image in different illumination, hair styleand clothing can be recognized with a high correct decision percentage using the proposed method, and recognition percentage is reduced in series other than fa and fb. Table (2) shows detection and recognition results for different series. An example of some FERET image series has been shown in Fig. 8.

4.3 Method comparison

Most of recent works on face recognition have implemented more than one image per person as training set [21,22]. Q. Gao Et. Al. [23] proposed novel subspace method called sequentialrow–column independent component analysis (RC-ICA) for face recognition and implemented experiments 400 gray level frontal view from 200 persons from FERET database. One fa was used as training and an fb image as probe for each person. PCA, 2D-PCA, BDPCA, W-BDPCA, ICA, EICA and the proposed row-ICA and RC-ICA methods are used for feature extraction, and then a nearest neighbor classifier is employed for classification. Fig.9 shows experimental

result of the experiment in addition to our proposed hybrid WGPCA method. Results clarify that our proposed method outperforms all those methods in spite of more target classes and more variation of probe face images.

Movellanet. al. [24] reported face recognition results using PCA and ICA for three different conditions of same day different expression, different day similar expression and different day different expression. Most of correct recognition percentage was under 90%. In these experiment best results is obtained in same environmental condition and deferent facial expression that is about 90% of correct classification.

Fig. 7. Left picture shows one of re faces and right picture shows one of fa faces as it is clear from their names.

Table 2: Detection and recognition results for different series of feret database with 699 target classes having one fa series facial image per class

Series name	Detection	Recognition
fa	99.72%	97.40%
fb	99.76%	94.10%
hl	33.57%	8%
hr	38.62%	9.40%
ql	77.90%	35.82%
qr	94.20%	54.25%
ra	42.34%	8.51%
rb	91.89%	54.90%
rc	99.06%	66.82%
rd	61.76%	12.70%
re	18.62%	0%

As it is shown in Fig.10, 94.1% of correct decisions over different day, expression, lighting and size is better than all results of the report.

5. Timing profile

For the final experiment, we designed a full automatic application using Delphi XE2 programming environment and the proposed algorithm. Completely apart from the weight determination stage, speed is a critical issue in the current experiment. Therefore, we developed a standalone application that automatically detects and recognizes faces as a known target or an unknown face. This stage does not need to use MATLAB or any of its toolboxes. The only connection between this real time application and previous mentioned parts is weighting vector which is found using MATLAB optimization toolbox, and used in real time application. Table 3 shows the timing profile of the final recognizer application. As depicted in table 3, if normal HAAR-Like algorithm is applied without considering possible head rotation around roll [1] axis it took up 194ms to train a new class and about 194ms to

---

[1] Axis perpendicular to frontal view plane of face

extract features and compare an input face image to 50 predefined classes using core 2dou 2.4 with 2Gof RAM computer system. Using a multi-threaded application some of items in the timing profile such as distance calculations and PCA can be executed in parallel. This will significantly reduce the process time.

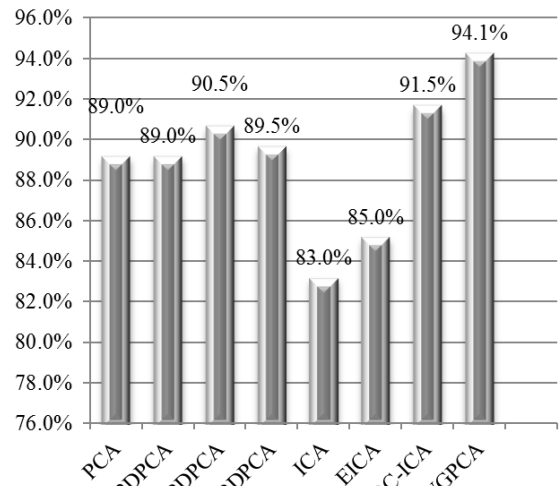Fig. 8. An Example for some FERETImage Series

Fig. 9. Comparison of WGPCA with Other Methods Using fa and fb FERET Series
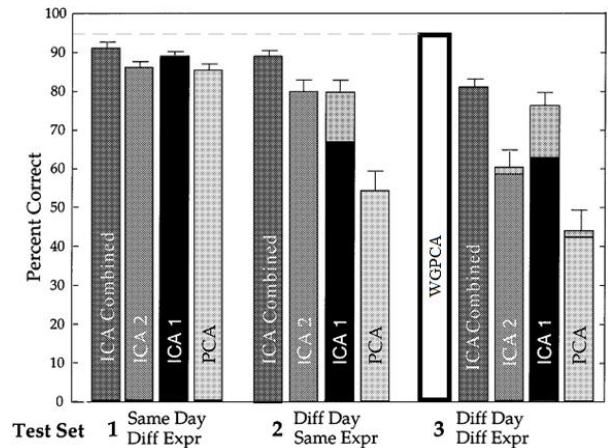

Fig. 10. Face Recognition Performance of WGPCA and Reported Results of Movellanet. Al.

Table 3 timing profile of the recognizer application

	Task	Time(ms)
1	Light and contrast normalization	1
2	HAAR-Like	36
3	HAAR-Like with rotation	222
4	Point extraction	138
5	Distance measure and multiplication to weights	5
6	Calculating head rotation and distance correction	2
6	PCA	10
7	Array saving	1
8	comparison to 50 target templates using KNN	1

6. Conclusions

This research shows the influence of using multi-core architecture to reduce the execution time and thus increase performance of some software fault tolerance techniques. According to superiority of N-version Programming and Consensus Recovery Block techniques in comparison with other software fault tolerance techniques, implementations were performed based on these two methods. Finally, the comparison between the two methods listed above showed that the Consensus Recovery Block is more reliable. Therefore, in order to improve the performance of this technique, we propose a technique named Improved Consensus Recovery Block technique. In this research, satellite motion system which known as a scientific computing system is consider as a base for our experiments. Because of existing any error in calculation of system may result in defeat in system totally, it shouldn't contains any error. Also the execution time of system must be acceptable. In our proposed technique, not only performance is higher than the performance of consensus recovery block technique, but also the reliability of our proposed technique is equal to the reliability of consensus recovery block technique. The improvement of performance is based on multi-core architecture where each version of software key units is executed by one core. As a result, by parallel execution of versions, execution time is reduced and performance is improved.

References

[1] A. Parsi, M. Salehi, A. Doostmohammadi, "Swap Training: A Genetic Algorithm Based Feature Selection Method Applied on Face Recognition System," World of Computer Science and Information Technology Journal, pp. 125-130, 2012.

[2] X. Tan, S. Chen, Z. Zhou, F. Zhang, "Face recognition from a single image per person: A survey," The journal of pattern recognition society, pp. 1725-1745, 2006.

[3] S. H. Lin, S.Y. Kung, "Face recognition/detection by probabilistic decision-based neural network", IEEE Trans. Neural Networks 8 (1), pp. 114–132, 1997.

[4] L. Liu, N. Sang, S. Yang, R. Huang, "Real-time skin color detection under rapidly changing illumination conditions," IEEE Trans. Consumer Electronics, Vol. 57, pp. 1295- 1302, 2011.

[5] P. Viola and M. Jones, "Rapid object detection using a boosted cascade of simple features," In Proc. of IEEE conference on computer vision and Pattern Recognition, pages 38-44, 1998.

[6] C. Kim, S. I. Choi, M. Turk, C. H. Choi, "A New Biased Discriminant Analysis Using Composite Vectors for Eye Detection," IEEE Trans. Systems, Man, and Cybernetics, Part B: Cybernetics, Vol. 42, pp. 1095-1106, 2012.

[7] A. J. Goldstein, L. Harmon, and A. Lesk, "Identification of human faces," Proceedings of the IEEE, pp. 748-760, 1971.

[8] L. D. Harmon, M. K. Khan, R. Lasch, and P. F. Ramig, "Machine identification of human faces," Pattern Recognition, pp. 97-110, 1981.

[9] S. Chitra, G. Balakrishnan, "A survey of face recognition on feature extraction process of dimensionality reduction techniques," Journal of Theoretical and Applied Information Technology, Vol. 36 No.1, Feb. 2012.

[10] X. Fan and B. Verma, "Selection and fusion of facial features for face recognition," Expert Systems with Applications: an International Journal, vol. 36, pp. 7157-7169, Apr. 2009.

[11] N. Hundewale "Face recognition using combined global local preserving projections and compared with various methods", International Journal of Scientific & Engineering Research, Volume 3, Issue 3, Mar. 2012.

[12] J. D. Kelly, J. L. Davis, "A hybrid genetic algorithm for classification," Learning and Knowledge Acquisition, pp. 645-650, 1991.

[13] K. Fukunaga, Introduction to Statistical Pattern Recognition, 2nd ed., Academic Press, New York, 1990.

[14] J. H. Holland (1975) Adaptation in Natural and Artificial Systems, University of Michigan Press, Ann Arbor, Michigan; re-issued by MIT Press (1992).

[15] R. Lienhart, A. Kuranov, V. Pisarevsky, "Empirical Analysis of Detection Cascades of Boosted Classifiers for Rapid Object Detection". Microprocessor Research Lab, Intel Labs. [online]. Available:http://citeseerx.ist.psu.edu/viewdoc/download?doi= 10.1.1.139.4825&rep=rep1&type=pdf

[16] L. Dang, F. Kong, "Facial feature point extraction using a new improved Active Shape Model," Image and Signal Processing (CISP), 2010 3rd International Congress, vol. 2, pp. 944-948.

[17] P. J. Phillips, H. Moon, S. Rizvi, P. Rauss, "The FERET evaluation methodology for face recognition algorithms," IEEE Trans. Pattern Analysis, pp. 1090–1103, 2000.

[18] F. Samara, A. Harter, "Parameterisation of a stochastic model for human face identification," Proceedings of Second IEEE Workshop on Applications of Computer Vision, pp. 138-142, Dec. 1994.

[19] Dr Libor Spacek Computer Vision Science Research Projects, Available: http://cswww.essex.ac.uk

[20] D. Mohamad, "Multi local feature selection using genetic algorithm for face identification," International Journal of Image Processing, vol. 1, pp. 1-10, 2008.

[21] J. Wang, J. You, Q. Li, Y. Xu, "Orthogonal discriminant vector for face recognition across pose," Pattern Recognition 45, pp. 4069–4079, 2012.

[22] I. Naseema, R. Togneri, M. Bennamoun, "Robust regression for face recognition," Pattern Recognition 45, pp. 104-118, 2012.

[23] Q. Gao, L. Zhang, D. Zhang, "Sequential row– column independent component analysis for face recognition" Neurocomputing 72, pp.1152-1159, 2009.

[24] M. S. Bartlett, J. R. Movellan, T. J. Sejnowski, "Face recognition by independent component analysis" IEEE Trans. On neural networks, vol. 13, no. 6, pp. 1450-1464, Nov. 2002.

Hasan Farsi received the B.Sc. and M.Sc. degrees from Sharif University of Technology, Tehran, Iran, in 1992 and 1995, respectively. Since 2000, he started his Ph.D in the Centre of Communications Systems Research (CCSR), University of Surrey, Guildford, UK, and received the Ph.D degree in 2004. He is interested in speech, image and video processing on wireless communications. Now, he works as associate professor in communication engineering in department of Electrical and Computer Eng., university of Birjand, Birjand, IRAN. His Email is: hfarsi@birjand.ac.ir.

Mohammad Hasheminejad received the B.Sc. degree in Bio-electrical engineering from University of Isfehan, Isfehan, Iran, in 2003. He received the M.Sc. degree in communication engineering from Maleke ashtar university of technology, Tehran, Iran, in 2008. He is currently Ph.D student in Department of Electrical and Computer Engineering, University of Birjand, Birjand, Iran. His area research interests include Image Processing and retrieval, Pattern recognition, Digital Signal Processing and Sparse representation. His email address is: mhashemi@birjand.ac.ir.